[redacted]

BNWL-1120 FF-1

2 -
5-31-69

FFTF FUEL DEPARTMENT CURRENT PRELIMINARY DATA FOR THE MONTHS OF MARCH, APRIL, MAY, 1969

By
Staff, FFTF Fuels Department

MAY 31, 1969

BATTELLE MEMORIAL INSTITUTE
PACIFIC NORTHWEST LABORATORY
RICHLAND, WASHINGTON 99352

SUBJECT	TO/MO.	LOCATION	FILES ROUTE DATE

DRAFT ISSUE DOCUMENT

[redacted]

INFORMATION CONCERNING USE OF THIS REPORT

PATENT STATUS

This document copy, since it is transmitted in advance of patent clearance, is made available in confidence solely for use in performance of work under contracts with the U. S. Atomic Energy Commission. This document is not to be published nor its contents otherwise disseminated or used for purposes other than specified above before patent approval for such release or use has been secured, upon request, from the Chief, Chicago Patent Group, U. S. Atomic Energy Commission. 9800 So. Cass Ave., Argonne, Illinois.

PRELIMINARY REPORT

This report contains information of a preliminary nature prepared in the course of work under Atomic Energy Commission Contract AT(45-1)-1830. This information is subject to correction or modification upon the collection and evaluation of additional data.

LEGAL NOTICE

This report was prepared as an account of Government sponsored work. Neither the United States, nor the Commission, nor any person acting on behalf of the Commission:

A. Makes any warranty or representation, expressed or implied, with respect to the accuracy, completeness, or usefulness of the information contained in this report, or that the use of any information, apparatus, method, or process disclosed in this report may not infringe privately owned rights; or

B. Assumes any liabilities with respect to the use of, or for damages resulting from the use of any information, apparatus, method, or process disclosed in this report.

As used in the above, "person acting on behalf of the Commission" includes any employee or contractor of the Commission, or employee of such contractor, to the extent that such employee or contractor of the Commission, or employee of such contractor prepares, disseminates, or provides access to, any information pursuant to his employment or contract with the Commission, or his employment with such contractor.

PACIFIC NORTHWEST LABORATORY
RICHLAND, WASHINGTON
operated by
BATTELLE MEMORIAL INSTITUTE
for the
UNITED STATES ATOMIC ENERGY COMMISSION UNDER CONTRACT AT(45-1)-1830

PREFACE

This document comprises a compilation of preliminary data generated during the reporting months of March, April, May, 1969. As such it includes more detail than the finally edited version appearing in BNWL-1090, FFTF Quarterly Technical Report, April, May, June, 1969.

The purpose of distributing this document is solely to provide more detailed raw data to the limited number of investigators having need for it.

AEC or Contractor personnel requiring glossy prints of photomicrographs may obtain them by writing the responsible FFTF Department Manager.

Work described herein will eventually be formally documented.

TABLE OF CONTENTS

LIST OF FIGURES

A. FUEL ELEMENT DEVELOPMENT

C. A. Burgess, Assistant Department Manager

1. Subassembly Development Section

J. W. Thornton, Manager

Prototype Debinder Furnace Operational Tests

M. D. Jackson

Stainless steel retorts in Hoskins pot furnaces are being used temporarily to remove binder from the mixed oxide pellets. The following four tests were performed to check out the Hoskins pot furnaces.

Two tests were performed by vaporizing and removing free Carbowax from a dish in the furnace chamber. An inert cover gas carried the vaporized carbowax from the chamber through a cold trap where the Carbowax was condensed and trapped. The remaining gas was exhausted out to the E-4 system.

Two tests were run using approximately 400 (200 per test) natural uranium pellets containing 3% Carbowax. The pellets were heated to 500°C and held at this temperature for ≈2 hours. The Carbowax was vaporized and carried away with a cover gas as in the previous tests using free Carbowax. The vaporized Carbowax was condensed and trapped in a cold trap. The remaining gas was exhausted to the E-4 glovebox ventilation system.

Preparation of Seven-Pin Subassembly for Sodium Component Test Loop Number Two

D. E. Blahnik, R. L. Myers

A seven-pin subassembly with duct was fabricated and delivered to the Sodium Component Test Loop #2. The purpose of the test is to provide initial identification of any fretting problems that may result from loose or broken spacer wires in FTR driver fuel subassemblies. The loop environment is flowing sodium at a velocity of 31 ft/sec and a temperature of 1150°F.

The seven-rod cluster was fabricated per drawing SK-3-13055. Figures 1 and 2 are pictures of the components including bar, cluster, duct, and transition pieces. The cluster is held inside the duct with the bar which fits through the slot in the end bracket and is welded to the duct wall. Figure 3 shows a plan of the seven-rod cluster indicating the desired condition of the wire wraps. Wires were loosened by stretching.

Calculations

For the purposes of this task, looseness was defined as the axial length in excess of that required to keep the wire tight on the surface of the fuel pin. Therefore, any looseness in the wire results in a gap between the wire and the pin. Measuring the looseness in the wire was done by calculating corresponding gap distances and then measuring the gap.

When the wire is raised from the fuel pin surface at a point, the separation of the wire from the pin occurs over approximately 5.5 inches of the fuel pin length (wire wrap 12 inch pitch). For the purposes of this calculation, separation was assumed to occur in a straight line along the fuel pin. The difference in length due to the wire wrapping around the pin was assumed negligible.

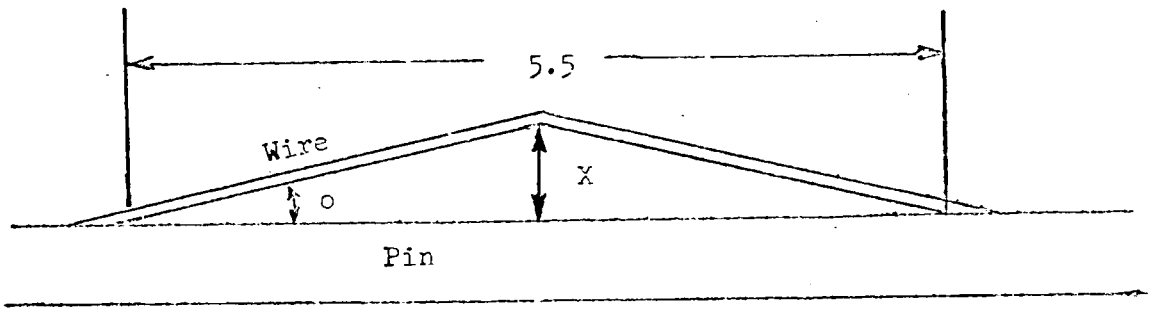

FIGURE 4 - Wire Wrap Looseness Measurement

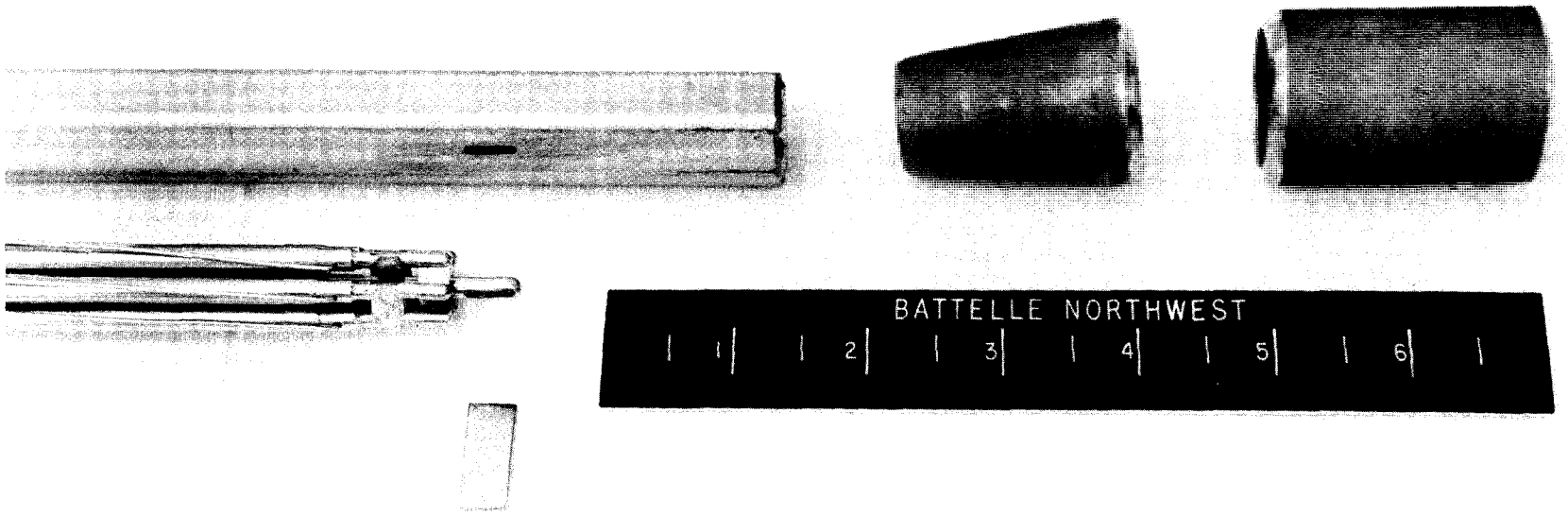

Neg 069138

FIGURE 1. Seven Rod Cluster Assembly Components

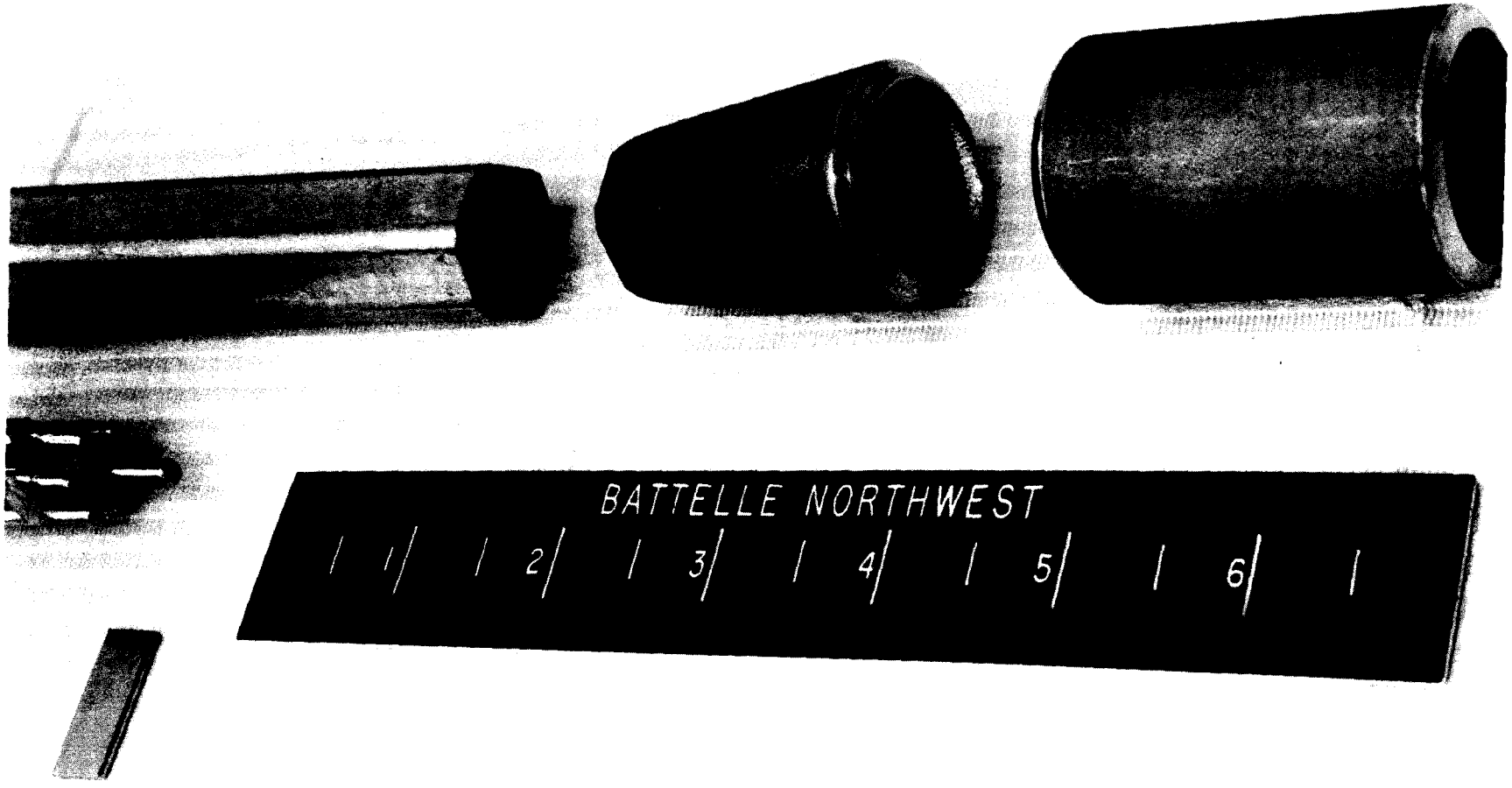

Neg 06913

FIGURE 2. Seven Rod Cluster Assembly Components

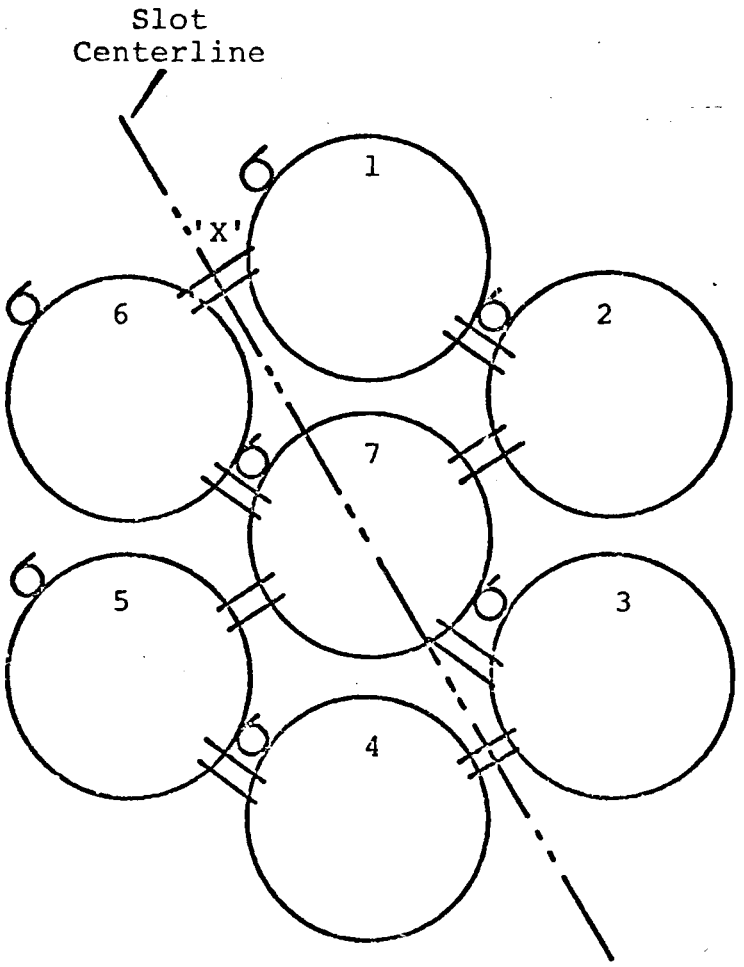

PIN	CONDITION
1	0.020 Looseness
2	0.020 Looseness
3	0.020 Looseness
4	0.030 Looseness
5	0.030 Looseness
6	0.030 Looseness
7	Wire Clipped on Inlet End

FIGURE 3
Wire Wrap Condition

Referring to the previous sketch and using looseness values of 0.020 and 0.030 inch, the corresponding gap distances (X) are 0.234 and 0.287 inch, respectively.

Wire Wrap Stretching and Measuring Techniques

A wire stretching tool as shown in Figure 5 was fabricated and used to stretch the wire wrap. The tool was designed such that the maximum radius (dimension B) would not exceed the gap distance required for the desired looseness. Even when the tool was inserted all the way under the wire, it did not stretch the wire the required amount due to the elasticity of the wire. The tool was worked back and forth along the pin at all places where the wire was on the outside of the cluster. This technique allowed the uniform stretching of the wire to the desired looseness.

After stretching the wire, the gap was measured by inserting another wire under the wire wrap and pulling with enough force to take up all the slack. Then the gap was measured with a taper gauge. This procedure was repeated several times for each pin until the desired looseness was attained. Figure 6 shows the wire wrap after loosening.

The center wire was cut where the wire was bent near the end cap weld, the most likely place for a break to occur.

Assembly into Duct

Figure 7 shows the hexagonal duct which encloses the fuel pin cluster. The duct and transition pieces were welded together using a special tool for alignment. The cross-sectional view of the duct shows dimensions, including those specified as well as those measured. The bottom, inlet end of the fuel cluster was welded to the duct at the slot shown using a 3/8 inch x 0.744 inch 304 stainless steel bar. All welds were x-rayed for full penetration prior to assembly into the loop.

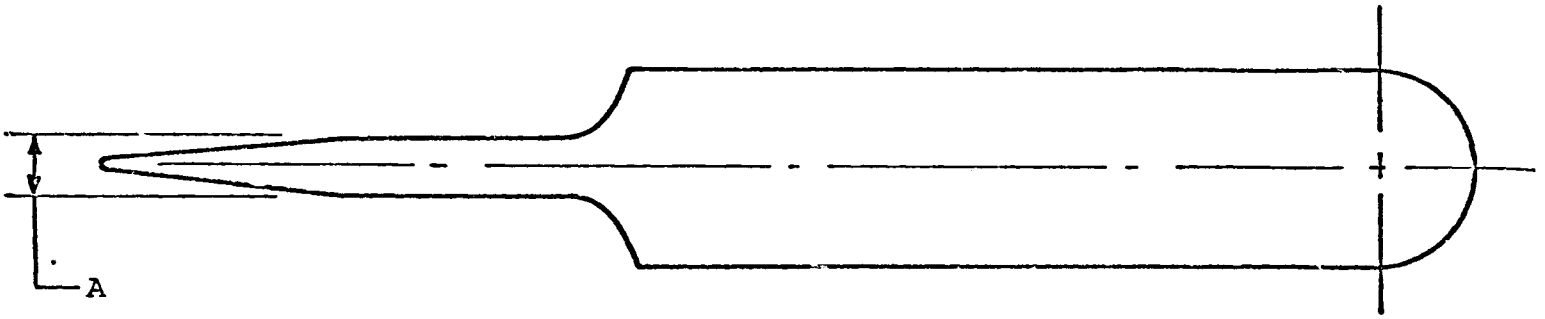

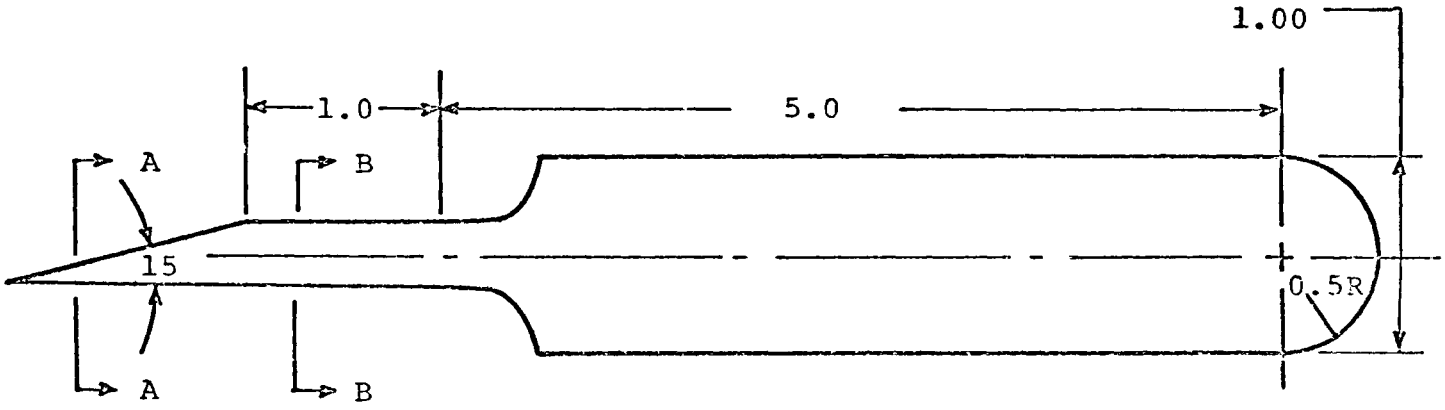

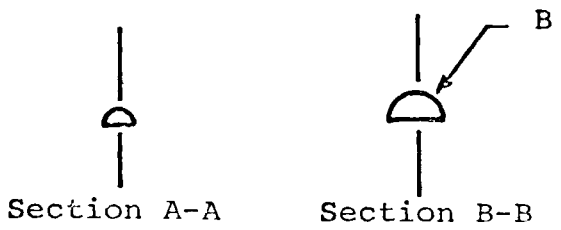

	PART 1	PART 2
A	0.468	0.574
B	0.234 R	0.287 R

FIGURE 5
Wire Wrap Stretching Tool

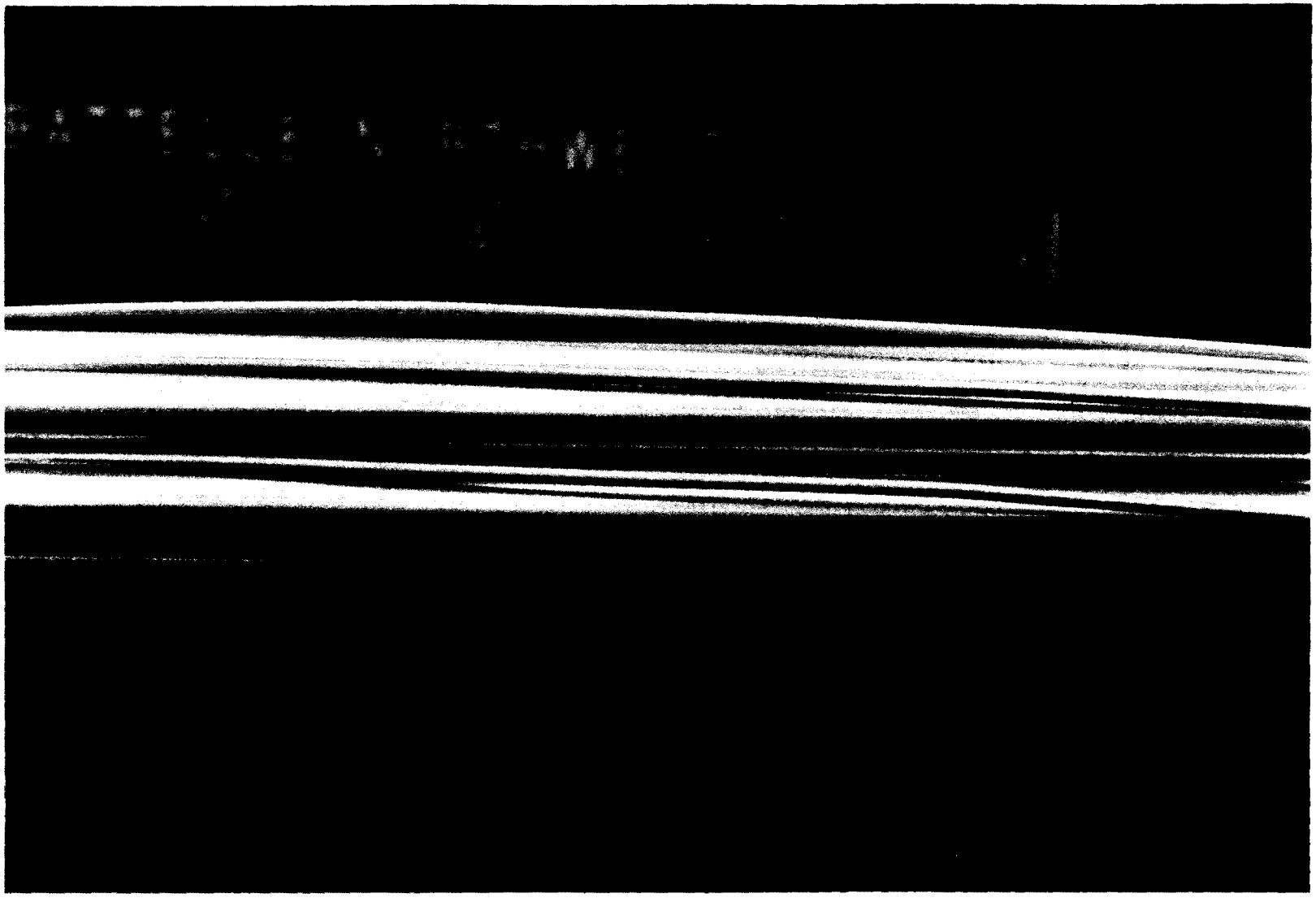

Neg 0691380

FIGURE 6. Seven Rod Cluster - Loose Wires

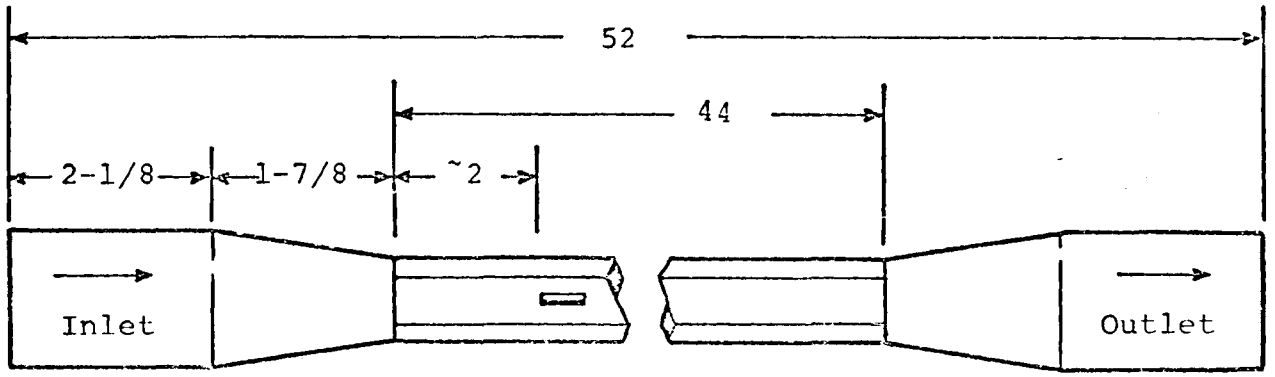

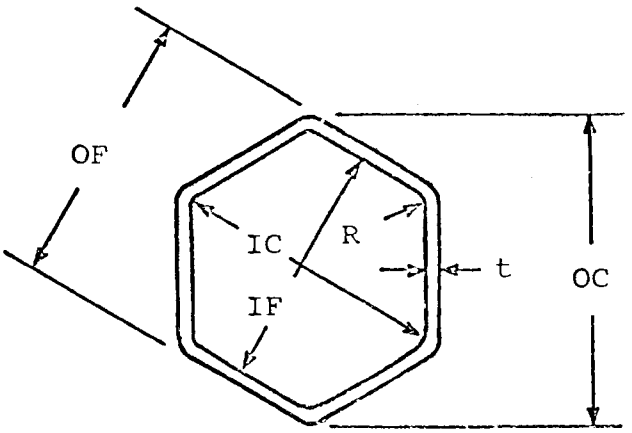

	DIMENSIONS	SPECIFICATION	MEASURED
OC	Outside Corner-to-Corner	0.964	0.918
OF	Outside Flat-to-Flat	0.833	0.832
IC	Inside Corner-to-Corner	0.808	0.782
IF	Inside Flat-to-Flat	0.703 + 0.005	0.703
t	Wall Thickness	0.065	0.062
R	Inside Corner Radius	1/32	-----

FIGURE 7
Hexagonal Duct for Seven Rod Cluster

2. Process Development and Demonstration Section

R. E. Bardsley, Manager

a. Analytical Chemistry Methods

C. A. Strand

The FFTF Analytical Chemistry Methods in Support of Driver Fuel Fabrication, BNWL-1024 (formerly identified as A-0089), was issued. Methods remaining to be completed for later incorporation into the manual include: analysis of stainless steel alloying elements and impurities, analysis of residual halogens, alpha-autoradiography to measure fuel pellets homogeneity, and fuel pellet ceramography.

b. Process Development

M. J. Barr

Fractional Factorial of Mixed Oxide Fuel Parameters

A computer analysis of green pellet data was completed. The multiple correlation factor (0.9789) indicates that 96% of the variations observed can be explained by the theoretical model. The observed green density is compared with the predicted density (from the model equation) in Figure 8. Sintering tests were begun, with about 25% of the experiment cells sintered to date.

Detailed Variables Study of Mixed Oxide Fuel Processing

1. Binder - Lubricant Evaluation

The effect of various lubricants and/or binders on sintered pellet properties is being evaluated in process experiment MJB-17. Green and sintered pellet percent of theoretical densities are presented in Table I. All test groups were prepared from the same basic powder batch (Direct denitrated PuO_2 and United Nuclear UO_2) and were sintered in the same furnace run. Test groups in Table I were arranged with respect to the green density obtained with 20,000 psi pressure.

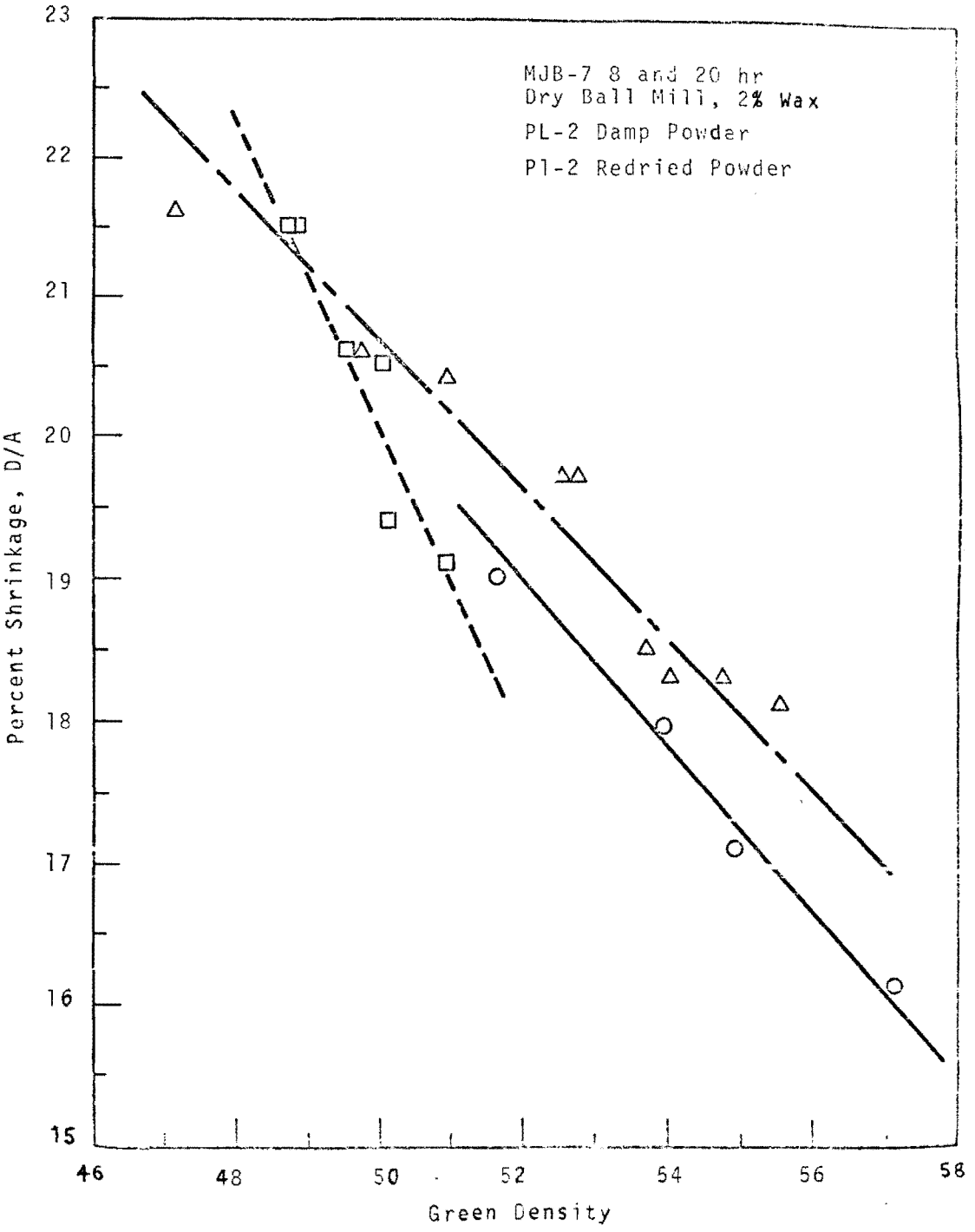

FIGURE 8. Percent Shrinkage in Diameter Versus Green Density for 25 w/o PuO_2–UO_2

TABLE I

Binder Lubricant (wt. Percent Addition)	% Theoretical Density Green	Sintered
1/2% PVA - 5% butyl-stearate	65.22	93.49
3% Carbowax	64.77	93.90
1/2% PVA - 3% butyl-stearate	64.22	93.70
5% Carbowax	64.06	93.56
1/2% PVA - 1% butyl-stearate	63.60	94.22
1% Carbowax	63.44	93.62
No Binder	62.35	93.72
1% PVA	58.74	90.67
3% PVA	57.77	85.03
5% PVA	56.73	79.83

As indicated by the increase in green density, the lubricating effect of Carbowax and butyl-stearate is readily apparent. The effect of PVA (polyvinyl alcohol) is to decrease both green and sintered densities. A significant point is that less than one percent in sintered theoretical density separates the top seven test groups. Data on pressing behavior, diameter taper, and density spread is currently being evaluated to more thoroughly understand the attributes of each system investigated. Microstructure photographs are being prepared.

2. Impurity Addition Through Milling

Wet milling is considerably more efficient than dry with respect to both size reduction and efficiency of blending per unit time. Criticality and batch size considerations have all but eliminated this technique from use in large scale production. Wet milling is still very useful for development purposes or small scale production batches. When using a wet mill, however, introduction of impurities becomes an important consideration. To determine the extent of impurity pickup from grinding media, test batches were milled with alumina (Al_2O_3) or tungsten carbide (WC) grinding media for varied times.

Table II below indicates the amount of impurity pickup with respect to milling time. Impurity levels for tungsten have been converted to W from the measured WO_3.

TABLE II

Milling Time (hours)	Impurity Pickup	
	Aluminum	Tungsten
0	20 ppm	--
1	50 ppm	Not determined
4	100 ppm	0.24% (2400 ppm)
8	200 ppm	3.6%
16	500 ppm	5.3%

The excessive tungsten pickup may be partially explained by the high ratio of grinding media to powder charge used. Conventional milling practice is to fill jars to 40-50% their volume with grinding media and add enough powder to cover the media. This "rule-of-thumb" unfortunately produces a media to powder charge weight ratio of from 5/1 to about 12/1 at the 16 hour level. (A portion of powder was taken out at various times with the media quantity remaining the same.) The media to powder charge ratios in the Al_2O_3 study were modified to produce ratios of the 1/1 to a maximum of 5/1. Additional work with WC media indicated that impurity pickup can be considerably reduced when low media to powder charge weight ratios are used and the wet slurry is relatively thick.

Analytical Working Standards, Phase II

H. T. Blair

Approximately 4,000 sintered, mixed oxide pellets were produced for analytical working standards in the Process Development and Demonstration facility following the process outlined in Figure 9. Two crossblending steps were introduced into the process following ball milling and granulation. These crossblends were included to level individual batch variations and to assure the homogeneity of the mixed oxide powder. These steps were included since

the mass safety limits in effect in the Process Demonstration Facility at the time of fabrication permitted preparation of only one third of the feed material at a time.

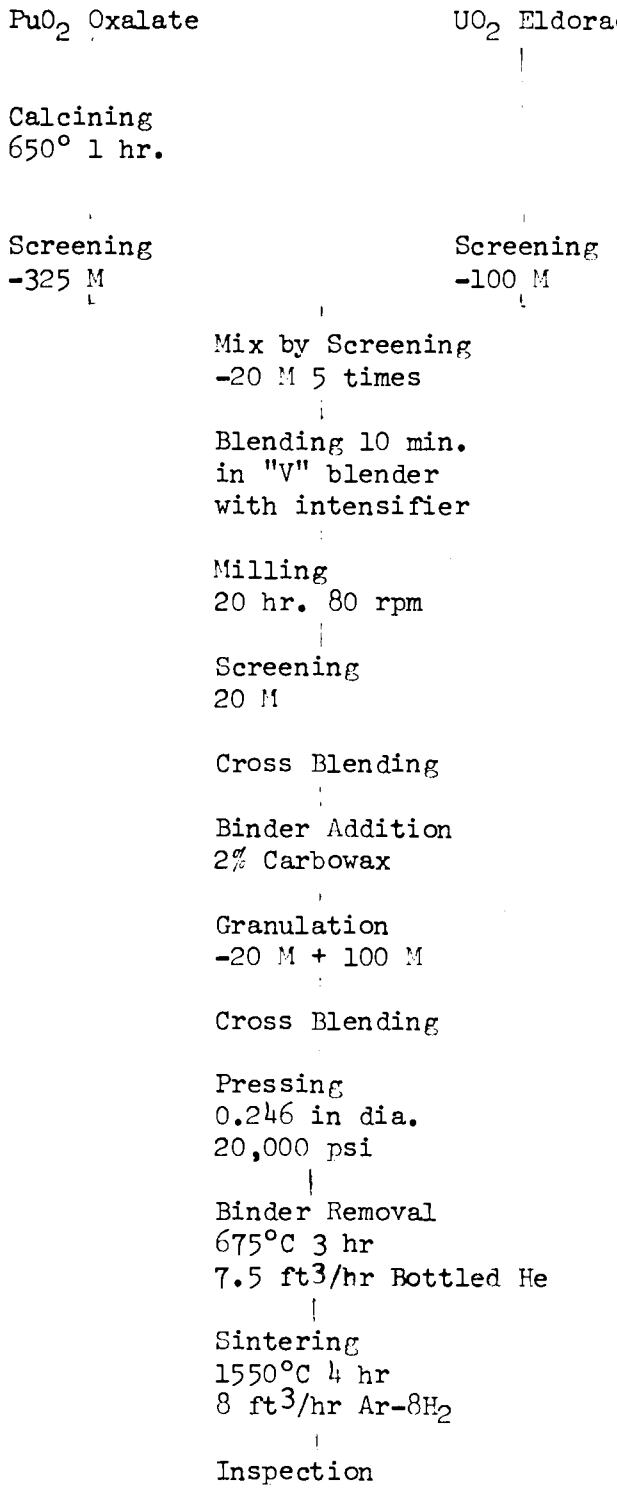

Figure 9. Flow diagram of process used to fabricate Analytical Standards Pellets, Phase II

The sampling plan followed during pellet fabrication is outlined in Table III.

TABLE III

Sampling Plan for Pellet Fabrication
Analytical Standards Program, Phase II

Process Step	Tests Performed
PuO_2 Source Lot and UO_2 Source Lot	Emission Spectrograph, Surface area, Gas Content, Water Content, F & Cl content, carbon content, % Pu or % U, History samples
Calcined PuO_2	Emission Spectrograph, Surface area, Gas content, water content, F & Cl content, carbon content, % Pu, Isotopic Analysis
1st Crossblend of mixed oxide	Emission spectrograph, Surface area, % Pu History samples
Pressed Pellets	Dimensions and Green Density
Sintered Pellets	Emission Spectrograph, Gas content, Water content, F & Cl content, carbon content, % P and U, Ceramography, alpha-autoradiography, x-ray diffraction, Oxygen-to-metal ratios, Microprobe, N_2 content, History samples

The average density of the pressed green pellets was 49.61 percent of theoretical density.

A statistical review of the dimensions and geometrically determined densities of the sintered pellets produced the following results:

Average Shrinkage: Diameter 20%
Length 19%

Average Taper: 0.0012 inch with a standard deviation of 0.0006 inch.

Average Density: 91.34% of T.D. with a standard deviation of 0.71% T.D.

There was no exhibited tendency for the pellets to assume either an hourglass or barrel shape. Both shapes were equally present with the average hourglass or bow being 0.0005 inch.

Pellet samples from the top sintering tray averaged 2.3 mills longer, 0.5 mills larger in diameter, and 0.34% T.D. lower than the overall average dimensions and density for the entire furnace load. Furnace operating characteristics are being modified to minimize this effect.

All analytical chemistry results with the exception of F and Cl content are included in Tables IV and V .

TABLE IV

IMPURITY LEVELS IN ANALYTICAL STANDARDS PELLETS, PHASE II

Impurity	Analytical Standards ppm by weight	Process Specifications (A-0097) ppm by weight
Ag	<0.1	*
Al	10	500
C	45-60	150
Ca	100	250
Cl	not received	25
Cr	25	250
Cu	1	**
F	not received	25
Fe	20	500
Mg	<5	25
Nm	1	*
Na	<2-5	500
Ni	<10	500
Pb	1	*
Sn	<5	*
V	<20	500
Zn	<50	**

* The sum of Cu, Zn, Si, and Ti - 800 ppm by weight

** The sum of Ag, Mn, Mo, Pb, and Sn - 200 ppm by weight

TABLE V

Analytical Chemistry Results on
Analytical Standards Pellets, Phase II

Analysis	Analytical Standards	Process Specifications (A-0097)
w/o Pu	22.0 - 22.2	None
w/o U	66.0 - 66.8	None
Gas Content	0.02 cc/gram	.05 cc/gram
Water Content	5 ppm by weight	30 ppm by weight

Evaluation of the homogeneity and dispersion of Pu and U in the pellets is based on ceramography, alpha-autoradiography, x-ray diffraction, and microprobe studies. The photomicrographs show an undeveloped grain structure with the largest observed grains being 4 microns across, Figure 11. Areas also exist where no grain structure is observed at 500X, Figure 12. This lack of grain growth is attributed to the low pressing pressure and low sintering temperature which were used to attain the desired density. Porosity is uniformly distributed and closed. No major pressing defects are observed. The number of phases present and state of homogeneity cannot be definitely determined from photomicrographs of such an undeveloped structure.

The oxygen-to-metal ratio of the sintered pellets was 1.99. This was the first large mass of mixed oxide pellets to be sintered in the new facility, and the relationship between O/M, load mass, and gas flow had not been well established for the new furnace. Oxygen-to-metal ratios of 1.94 had been achieved with test batches of 100 to 200 grams. Since a ratio between 1.95 and 1.97 was desired, a series of firings using Ar-8% H_2 gas was made in the demonstration facility sintering furnace to reduce the oxygen-to-metal ratio of 200 pellets, Table VI.

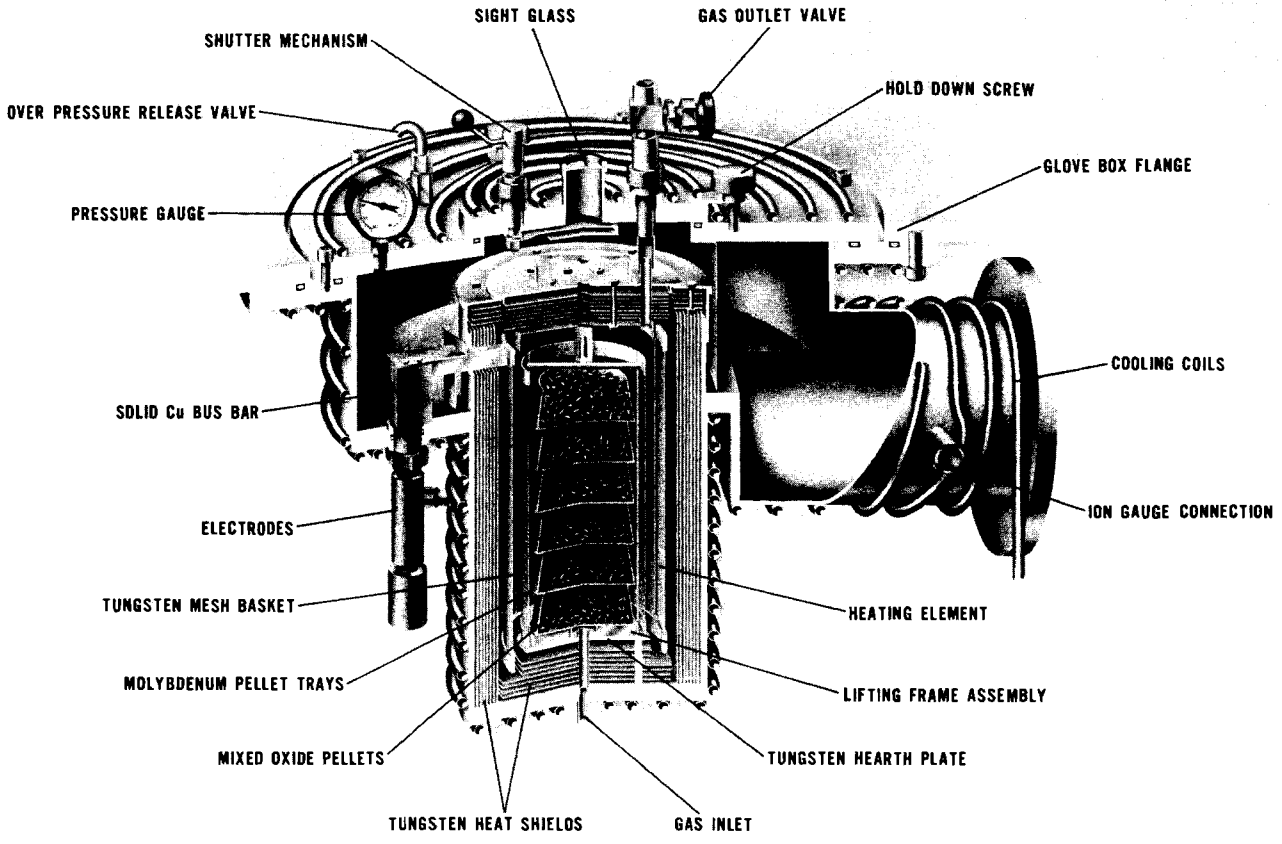

Neg 0690848

FIGURE 10. Process Development and Demonstration Facility Sintering

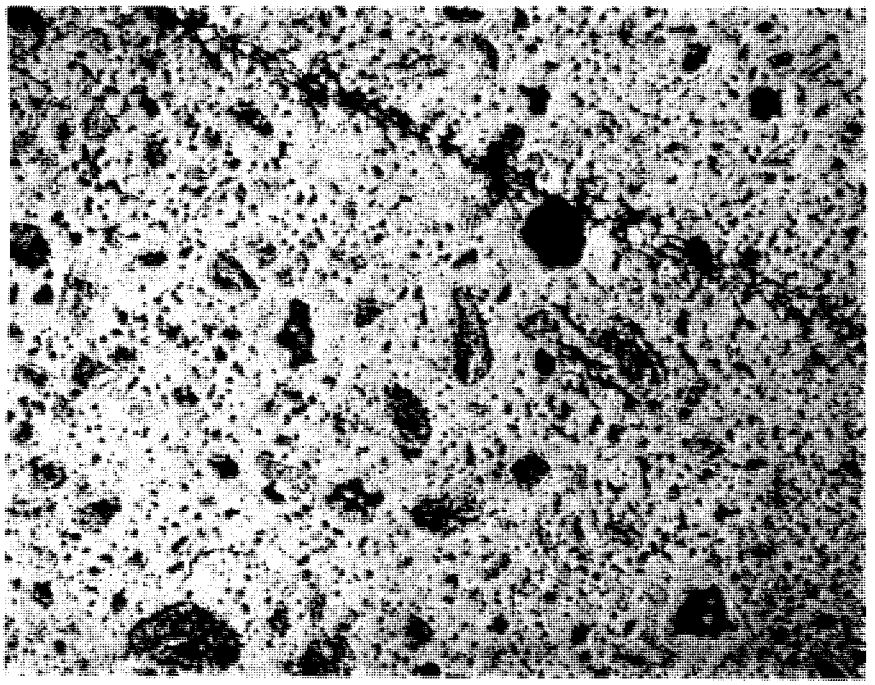

Neg 4958H 500X

FIGURE 11. Longitudinal Section of Analytical Standards Sintered Pellet

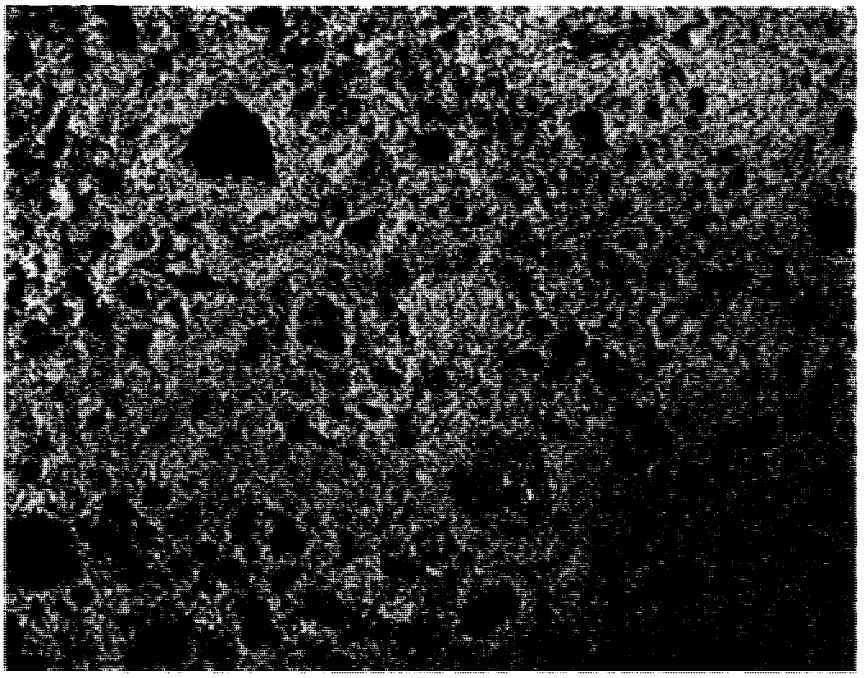

Neg 4958G 500X

FIGURE 12. Transverse Section of Analytical Standards Sintered Pellet

TABLE VI

Oxygen-to-Metal Radio Reduction of Analytical Standards Pellets, Phase II

Load Mass (g)	Gas Flow (SCFH)	Temperature (° C)	Time at Temperature (°C) hr	Average O/M
260	8	1200	3	1.989
254	8	1500	3	1.972
260	8	1650	3	1.962

The general appearance of the pellets, Figure 13, shows few cracks, pits, chips, or voids.

Centerless grinding of 100 of the sintered pellets did not alter the average density determined by geometric methods. However, the densities of the ground pellets ranged from 89.70 to 92.39% T.D. while the densities of as-sintered pellets were between 89.44 and 92.91% T.D.

3. Special Products Fabrication Section

E. T. Weber, Manager

Fabrication of Irradiation Test Fuel and Pins

R. M. Crawford, W. E. Warden, E. T. Weber

The 45% ^{235}U enriched mixed oxide pellets for EBR-II subassembly PNL-7 and the 93% ^{235}U enriched mixed oxide pellets for EBR-II subassembly PNL-8 were fabricated.

Components required to fabricate pins for EBR-II subassemblies PNL-6, 7 and 8 were procured. PNL-6,7, and 8 are EBR-II Mark F-37 assemblies, containing 37 unencapsulated fuel pins.

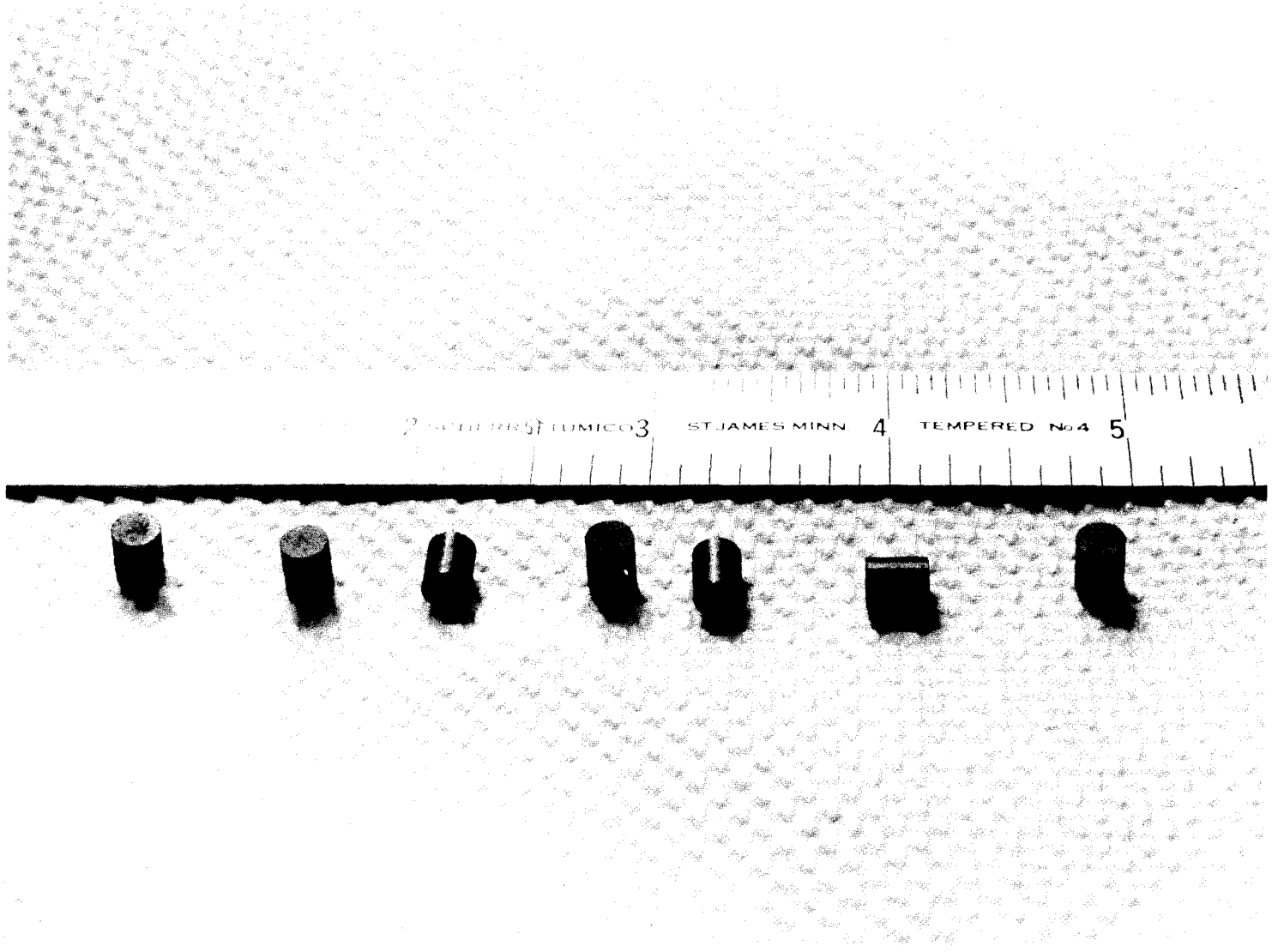

Neg 0691427

FIGURE 13. Analytical Standards Pellets, Phase II

Four pins for a xenon tagging experiment and sixteen fuel pins for two irradiation capsules calibration tests under Task FP-3 were completed. The fuel is mixed oxide. The calibration fuel required that four different diameters of sintered pellets be fabricated. The green pellet diameters were in four size ranges from 0.461 inch to 0.389 inch. The powdered oxide required preslugging to produce suitable feed material for the pressing operation. The required density (93 ± 1% T.D.) for these large pellets was obtained by sintering at 1690°C in Ar + 8% H_2 atmosphere.

Developments in Welding and Assembly of Fuel pins for Tests in EBR-II

R. M. Crawford

To aid in the rapid identification, location and removal of nonencapsulated fuel pins experiencing cladding failure during irradiation in EBR-II, ANL has developed a monitoring system requiring the addition of a small amount of an unique xenon isotopic mixture to the gas plenum of each test pin. A method of adding xenon to irradiation test pins for EBR-II during fabrication was developed and certified by ANL. A welding method for fuel pin end closures on 316 SS of 0.250 inch O.D. was developed and qualified.

An evacuate-backfill method was developed by BNW to accomplish the xenon tagging. Initially the fuel pins are evacuated to 10^{-4} Torr in the welding chamber and backfilled to atmospheric pressure with helium as is normally done prior to welding. The xenon tagging apparatus (see Figures 14 and 15) provides a means for subsequently evacuating each pin to approximately 25 microns and backfilling with the required helium-xenon mixture from a cylinder located outside the welding chamber (see Figure 16). The gas mixture in the supply cylinder is premixed and analyzed by gas mass spectrometry prior to attaching to the apparatus. Following backfill of the pin with the Xe-He mixture and removal of the vacuum seal, the end cap is quickly positioned and inserted

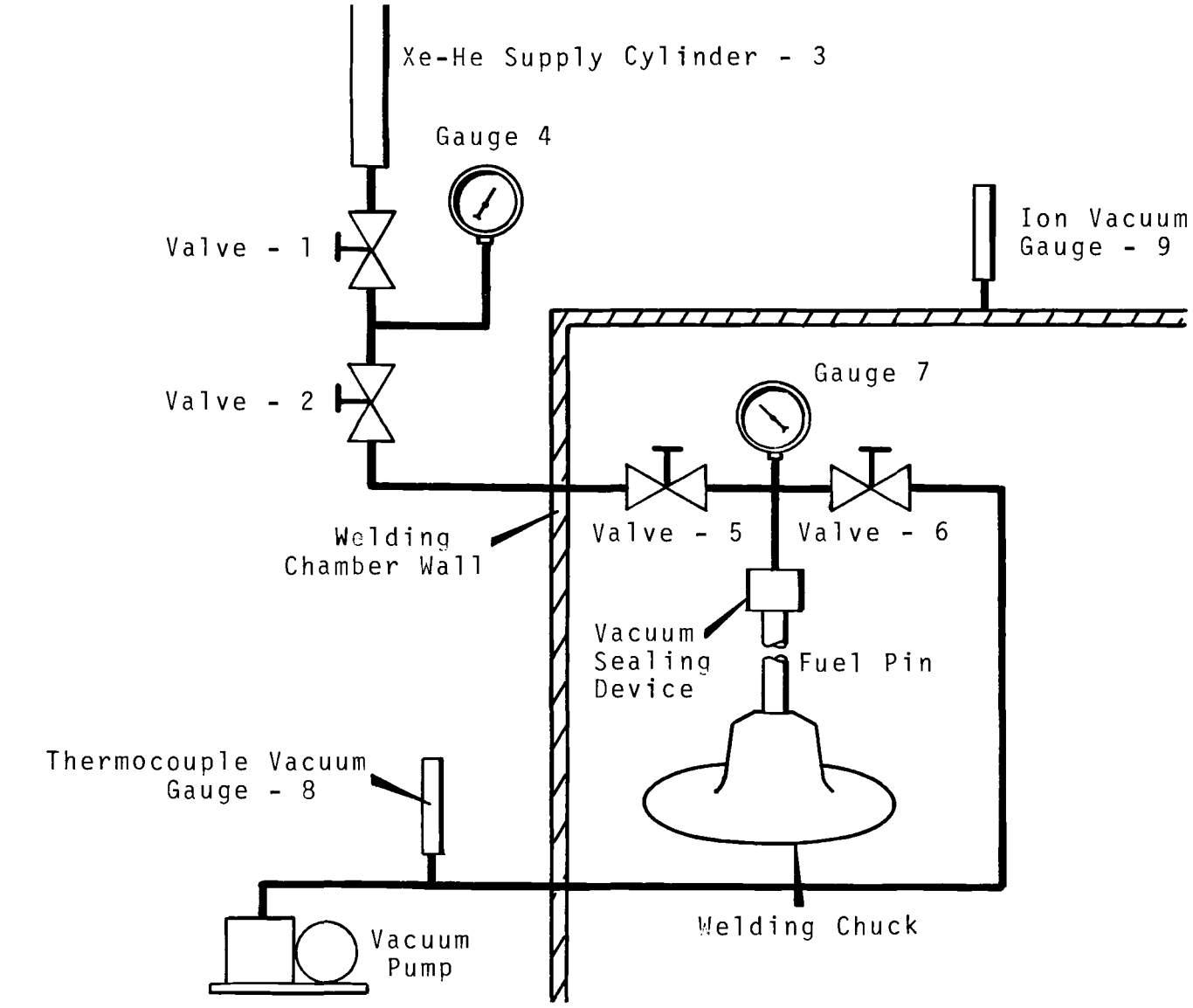

FIGURE 14. Xenon Tagging Apparatus

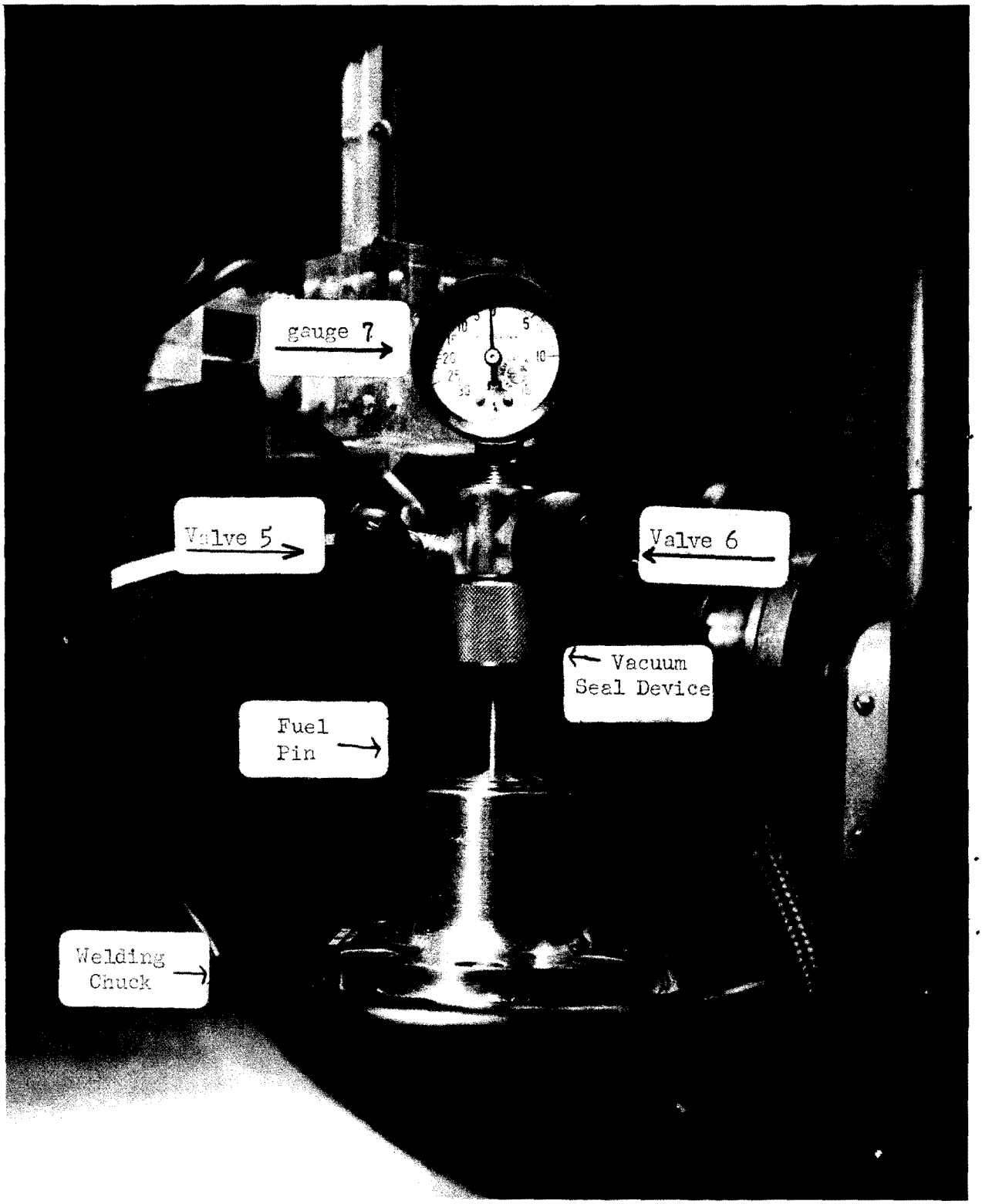

Neg 0690784-3

FIGURE 15. Xenon Tagging Apparatus Inside Welding Chamber

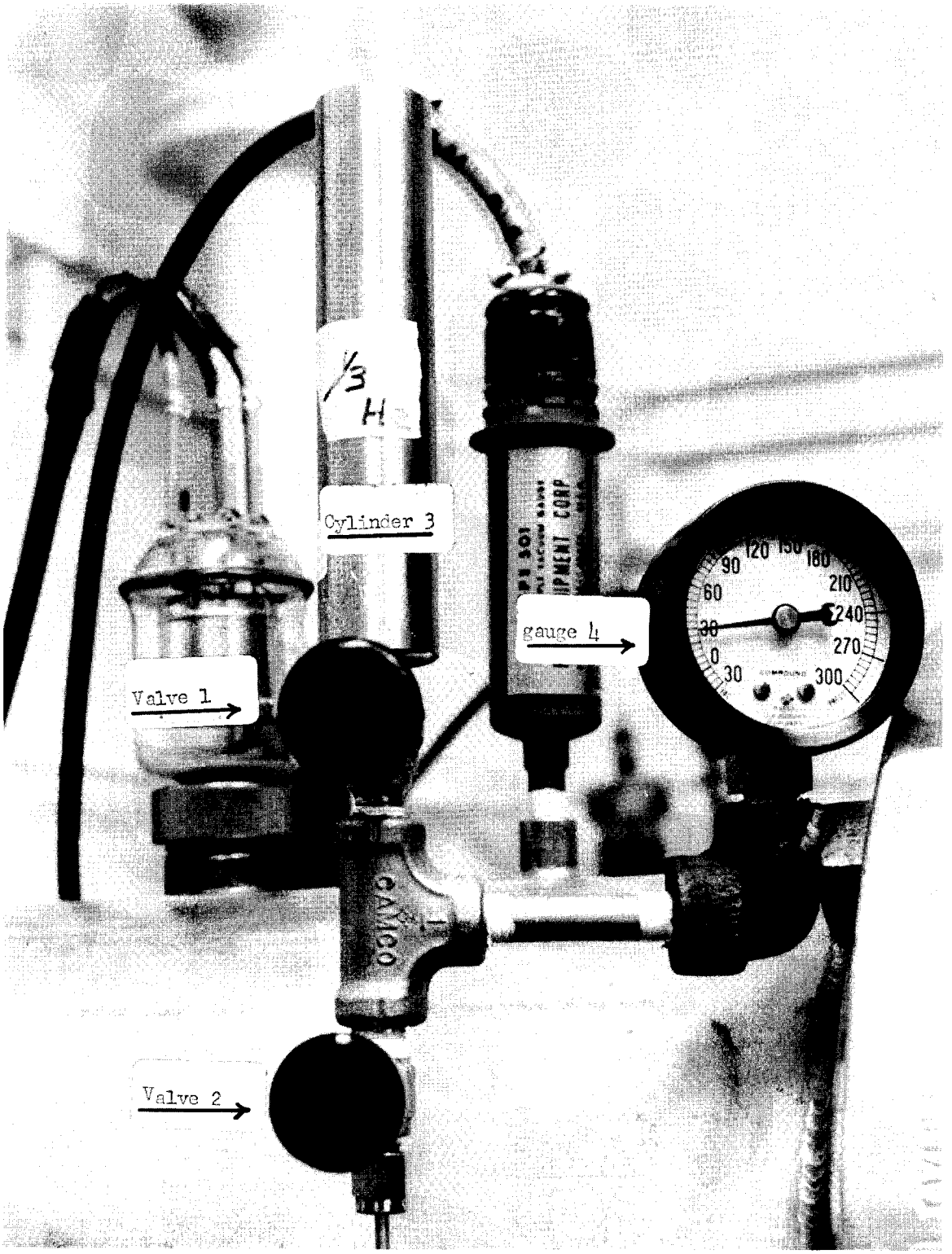

Neg 0690784-4

FIGURE 16. Xenon Tagging Gas Supply Source

(typically less than 10 seconds). The end closure is then welded in the normal manner.

Several test pins were fabricated to demonstrate the effectiveness of the procedure to representatives from ANL. The following are typical results for full length EBR-II fuel pins containing a dummy fuel column:

Mole % xenon in the supply cylinder		=	14%
Mole % of xenon in Pin	#1	=	12%
	#2	=	13%
	#3	=	13%
	#4	=	12%
*	#5	=	11%
	#6	=	12%
	#7	=	12%

* 11% was the lowest percentage on any of the pins sampled.

The BNW tagging procedure as approved by ANL will be used in tagging pins for subassemblies PNL-6, 7, 8.

A procedure for welding fuel pin end closures (316 stainless steel 0.250 inch OD cladding for PNL-6, 7, 8) was developed and qualified. This procedure requires welding with approximately 12 amps at 4 inches per minute and produces full penetration welds (see Figure 17) with 0.001 -0.0015 inch weld buildup on the diameter of the tube. A welding device rotates the electrode while the tubing remains stationary (see Figure 18).

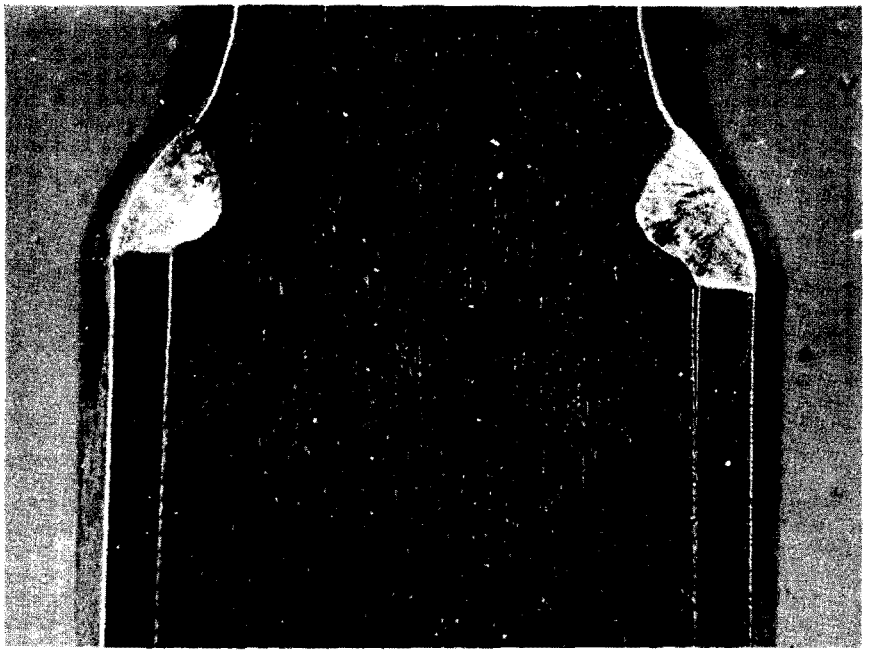

End closure
weld at 15X

Neg 469-318A

End closure
weld at 75X

Neg 496-320B

FIGURE 17. Typical Fuel Pin Closure Weld (316 SS) PNL-6,7,8

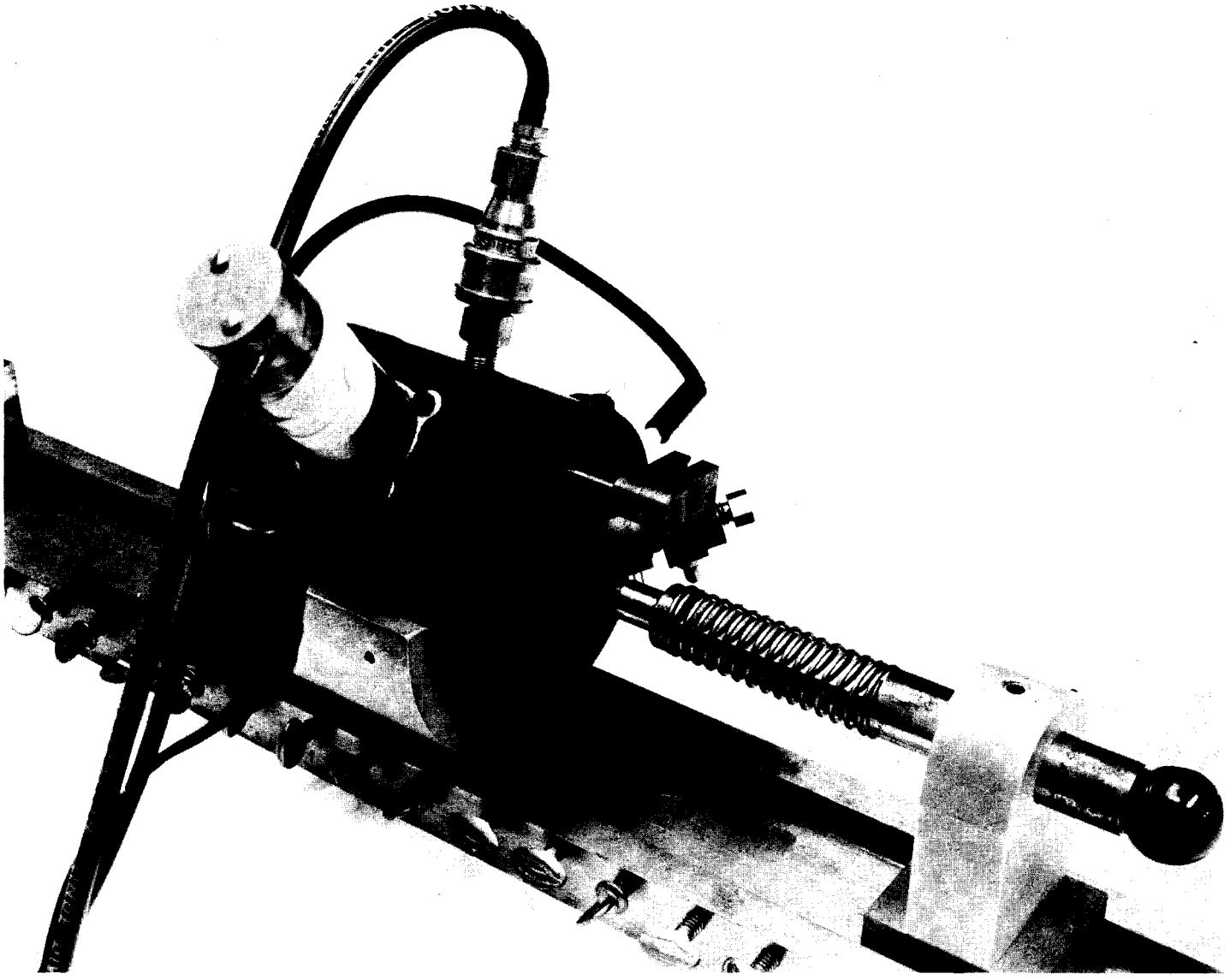

FIGURE 18. End Closure Welding Device with Rotating Electrode

Fabrication Process Development for Irradiation Test Fuels

W. E. Warden and E. T. Weber

This activity provides for development of processes to produce irradiation test fuel pellets meeting various combinations of ^{235}U enrichments, physical parameters (dimensions, density, etc.), and composition. Processing operations which conform as closely as possible to FFTF reference fuel fabrication process specifications constitute an additional requirement. The wide range of feed material characteristics resulting from blending powders to yield various ^{235}U enrichment levels continually imposes minor variations in processing. These variations are usually approached empirically based on past experience. A principal objective of this activity is to establish a stronger technical basis for controlling process conditions to yield fuel of required characteristics.

In previous fabrication of mixed oxide pellets with 93% ^{235}U enrichment (for subassembly PNL-5) difficulty was experienced in achieving bulk densities in the range 92-95% T.D. Enriched UO_2 powder is typically more difficult to sinter than the Eldorado UO_2 used when the normal enrichment (0.7% ^{235}U) is required.

During this report period, fuel pellets for EBR-II subassembly PNL-8 were fabricated. Initial fuel pellet fabrication for PNL-8 (93% enriched ^{235}U) mixed oxide resulted in bulk densities below the acceptable 93 $\pm$2% T.D. range. The sequence of unit operations is shown in Figure 19. Analysis of the sintered macrostructures, microstructures, and a review of process conditions suggested that compaction efficiency and void distribution established in the unfired compact by pressing conditions could be the controlling factor for observed variations in bulk density between 88 and 92 % T.D. The macrostructure showed a distribution of large voids throughout

Initial - Process Flow Diagram

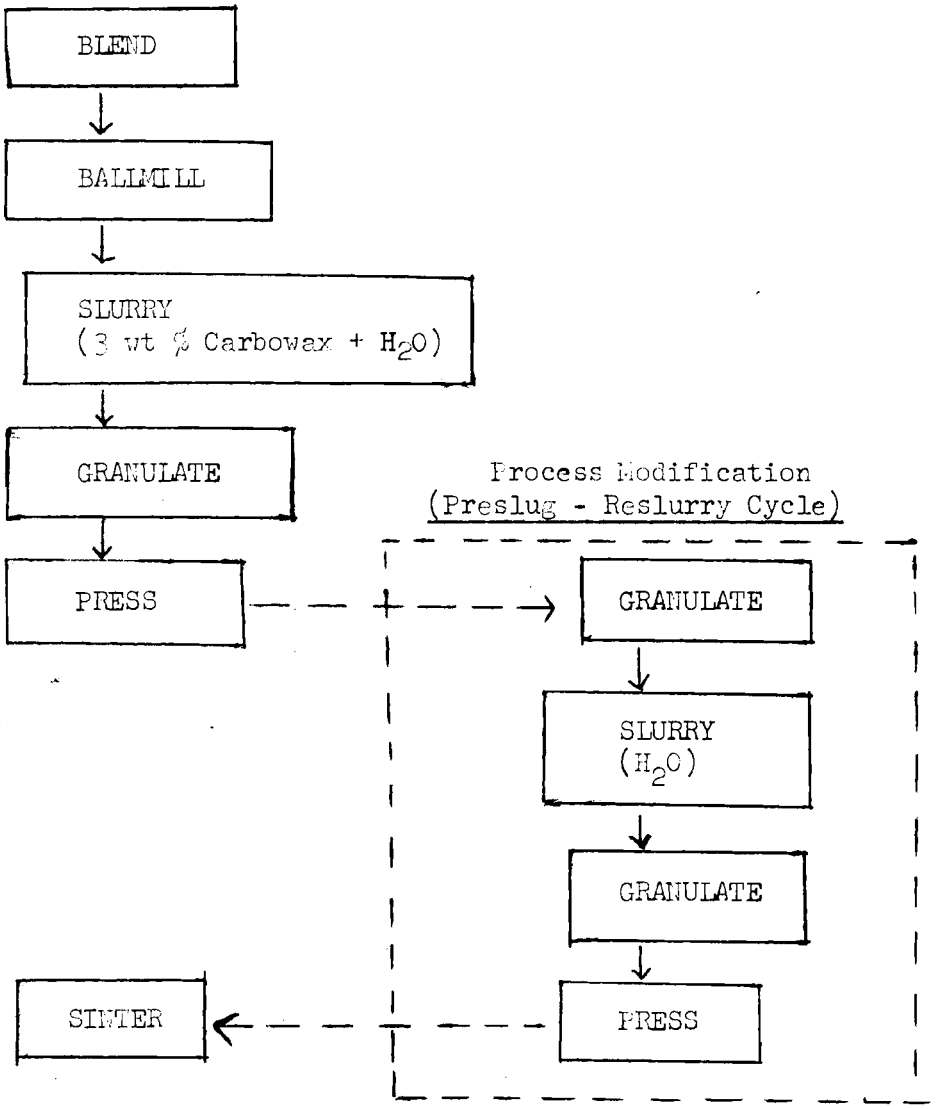

FIGURE 19

Process Flow Diagram for Mixed Oxide
Fuel Pellet Fabrication Operations Involved in the
Compaction Experiment and Fabrication of PNL-8 Test Fuel

the pellets (see Figure 20) while the microstructures showed areas of highly sintered material (sed Figure 21). The "activity" of the 93% enriched UO_2 in the mixed oxide was adequate to yield a highly densified microstructure with well developed, uniform grain structure and with small void distribution typical of "equilibrium" densification for the sintering conditions employed. An approach to increasing bulk density and obtaining a smaller density spread within batches was based on improving the compaction characteristics of the granulated powder.

Variation and control of eight process parameters were investigated: (1) preslugging and reslurrying, (2) green density, (3) feed agglomerate size, (4) moisture content, (5) improved binder homogeneity by mixing slurry during initial drying stages, (6) zinc behanate, (7) butyl stearate, and (8) additional Carbowax. All pellets in the experiment were pressed by manually filling the die cavity and pressing on automatic cycle with the Stokes press used in the production of irradiation test fuel. A single sintering run was made for all samples in the test fuel production furnace (ceramic muffle) with Ar-8% H_2 atmosphere, at 1690°C with a six hour soak.

All pellets made with preslugged-reslurried material achieved densities between 93 and 94% T.D., while pellets made from non-preslugged material reached densities between 89 and 92% TD. All the other parameter variations gave only minor density variations relative to the effect of the preslug-reslurry operation. Macro- and microstructures from samples representative of the two conditions with the greatest density difference are shown in Figures 22 and 23. The pellets in Figure 22 processed from non-preslugged material show considerably more of the larger "macro-voids" which are thought to arise from compaction conditions.

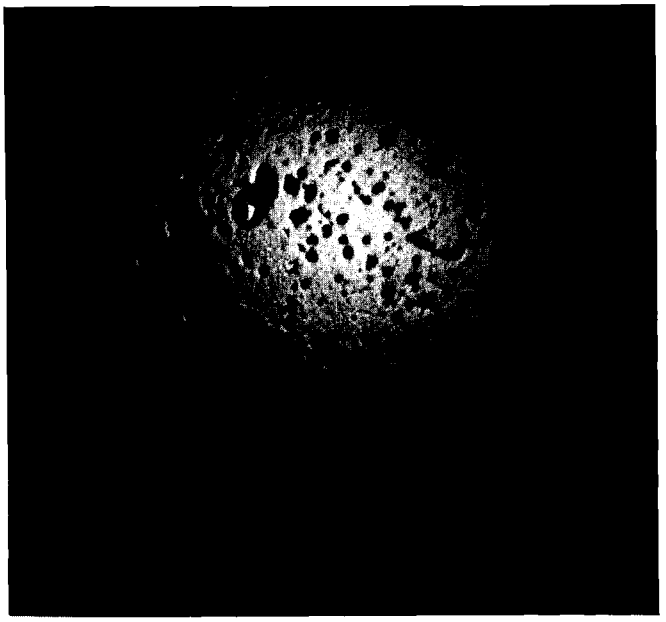

10X

FIGURE 20. Photomacrograph of Typical PNL-8 Fuel Pellet (91.7% T.D. Average for Batch) Resulting from Initial Processing Conditions

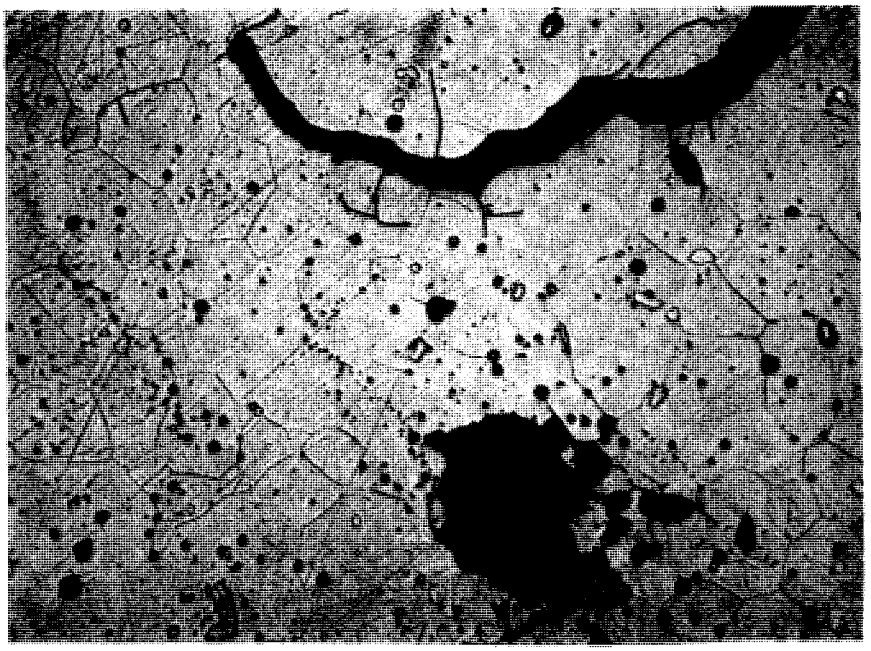

500X

FIGURE 21. Photomicrograph of Typical well Sintered Portion of Microstructure in Fuel Pellet (91.7% T.D. average for batch) Resulting from Initial Processing Conditions

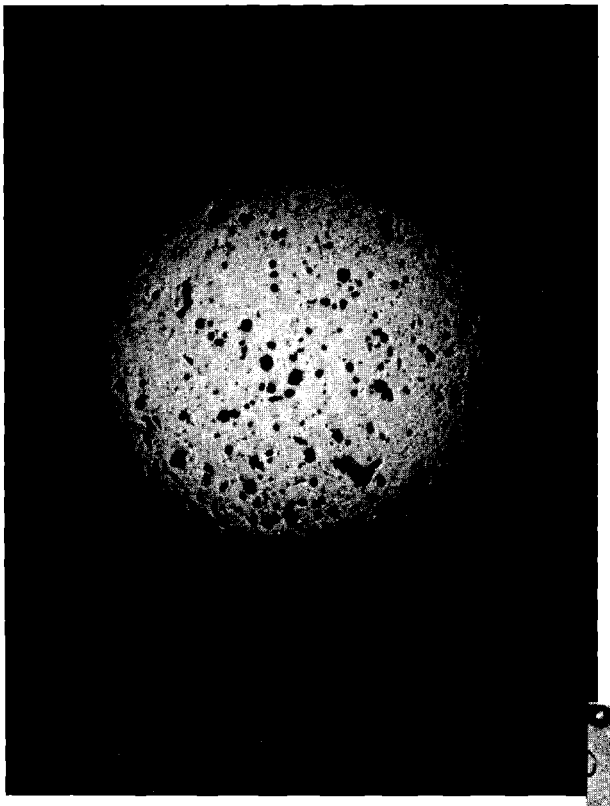

Neg MEE 392-2A
10X

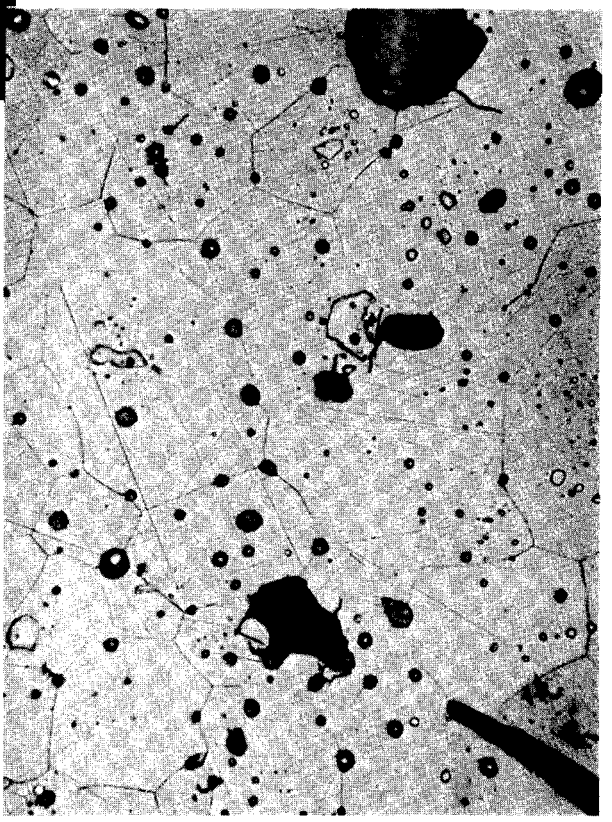

MEE 892-2A

FIGURE 22. Macro and Microstructure of Sintered Pellet (90.7% TD Average for 10 Pellet Group) Fabricated from Nonpreslugged Feed Material During Compaction Experiment

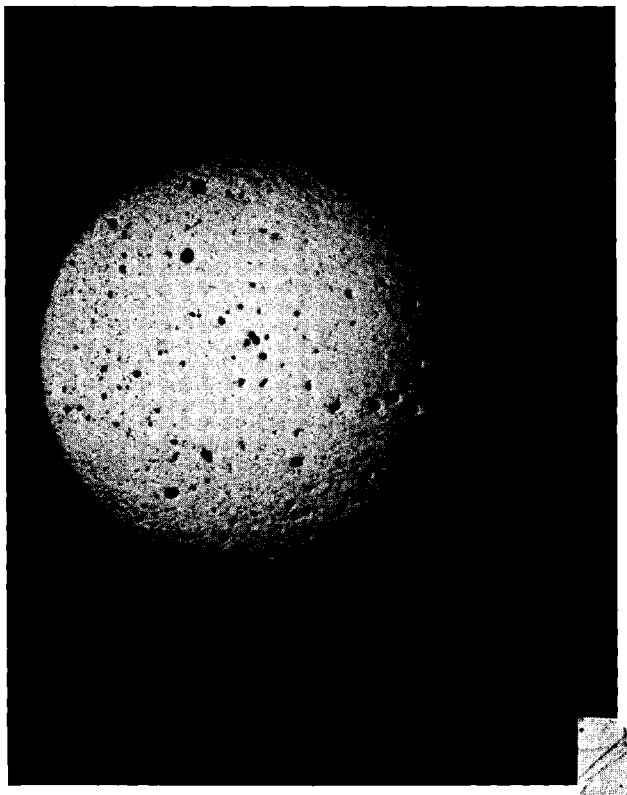

10X

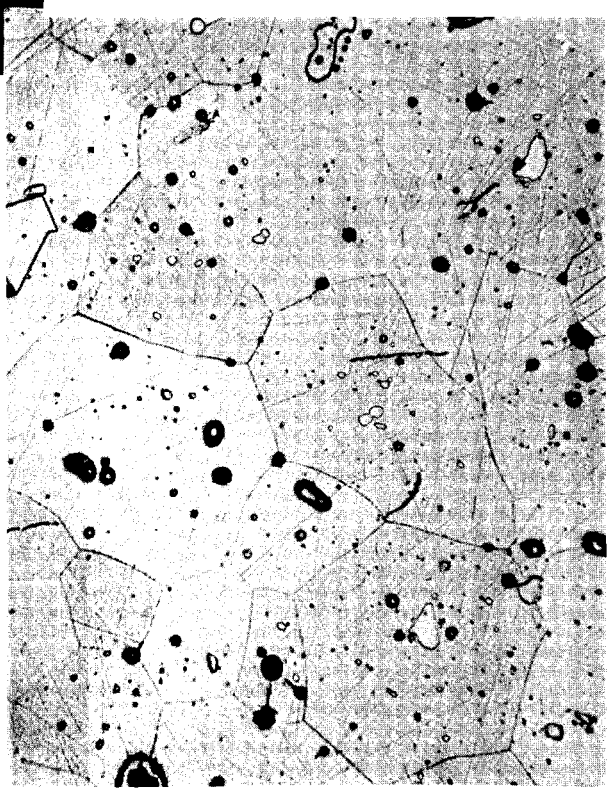

500X

FIGURE 23. Macro and Microstructure of Sintered Pellet (93.4% TD Average for Pellet Group) with Preslugged-Reslurried Feed Material During Compaction Experiment

Density differences between the two samples are qualitatively related to this macro-void fraction, since the microstructures from the two cases have essentially equivalent grain structure and micro-void distribution. Further evaluation of the binder distribution or particle morphology effects involved in the improved compaction behavior will be conducted using scanning electron microscopy.

The beneficial preslugging-reslurrying operations were employed for PNL-8 fuel as shown in the inset in Figure 1. The PNL-8 fuel produced with the modified process sequence consisted of sintered pellets in the density range 93.5 ±1%, based on 80 samples from a 600 pellet batch. In general, the pellets from the preslugged-reslurried material also had a much smaller density range than earlier batches of 93% enriched mixed oxides.

4. FFTF Data Acquisition System

A. W. DeMerschman

The SEL810B data acquisition equipment was installed and manufacturers acceptance testing completed. Equipment modifications necessary to meet FFTF specification requirements will be made by Systems Electronic Laboratory before final acceptance is given.

Programming efforts and software installation are being implemented by the Control and Instrumentation Department. Initial program installation on inventory and criticality control will be completed during this fiscal year.

B. CLADDING DEVELOPMENT T. T. Claudson

1. Cladding Development and Process Section - J. C.Tverberg

a. Procurement Activities

Plenum Springs - R. J. Lobsinger

Procurement was initiated for Inconel X-750 fuel pin plenum springs for use in fuel vendor prequalification contracts and PNL subassemblies 9, 10, and 11. The original specification was revised to accommodate vendor exceptions to design tolerances and halogen contamination limits. The vendor responsible for the fabrication encountered difficulties on this order. During heat treatment the springs warped and suffered extensive relaxation resulting in rejection of all springs. Discussion with the vendor revealed no obvious reasons for this problem. However, discussions with the International Nickel Company, Huntington Alloys Division, indicated that such extensive dimensional change could only occur if the springs were subjected to extreme temperatures far in excess of that required for precipitation hardening. Very little, if any dimensional change should occur at the aging temperature of 1350°F (730°C). To circumvent this difficulty, negotiations were conducted with the second lowest bidder to procure these springs from an alternate source.

Fuel Pin Reflectors - R. J. Lobsinger

Approximately 500 feet of 0.200 inch diameter nickel rod was purchased and received for use as reflector material in fuel vendor prequalification contracts. This material meets all requirements of HWS-1001, however, the material is being re-examined by the vendor to verify that the halogen contamination limits of 0.0005 mg/in^2 were not exceeded.

A quantity of Inconel-600 reflectors was fabricated from characterized 5/8 inch diameter rod by swaging, annealing, and centerless grinding operations. Details of the reduction process were retained for possible further evaluation. These reflectors will be used for bare-pin subassemblies PNL-9, 10, 11, 14, 15 and 16.

Fuel Pin End Caps - R. J. Lobsinger

Material from a special melt of double vacuum melted,controlled chemistry 316 stainless steel, meeting prototypic FFTF pin chemistry requirements, was converted into 0.250 and 0.230-in. diameter rods for end cap stock by Crucible Steel Company. The 0.250-in. diameter material is being supplied both straight and coiled. The former condition is required for end cap fabrication by fuel vendors during prequalification and the latter is necessary for re-drawing operations to produce wire for fuel pin fabrication. The 0.230-in. diameter material will be used to produce end caps for fuel pin fabrication. Bright annealing of the 0.250-in. straight rod was required to be done by the vendor to satisfy requirements of the specification.

Plenum Tubes - R. J. Lobsinger

Approximately 1860 feet of 0.187-in. O.D. by 0.014-in. wall 316 stainless steel tubing was shipped from Carpenter Technology Corporation for use as plenum tubes during fabrication of the prequalification fuel pins. All material meets requirements of the revised prototypic development specification HWS-1001, Appendix D.

Fuel Pin Cladding - R. J. Lobsinger

An order has been placed for 30,000 feet of prototypic FFTF Cladding 0.230 ±.001-in. O.D. x 0.200 ± .001-in. I.D. x 10 feet long. This material is of vacuum-melted 316 stainless steel and will conform to

specifications B-58991 and B-58992. Preproduction quantities (~200 feet) of material with 0, 5, 10, and 20% cold work were received. A supplemental 4300 foot quantity is also onsite, fabricated to the preproduction requirements, but applying to the main order. Extensive evaluation of the material is in progress, however preliminary data generated by ultrasonic and eddy-current testing show impressed metal particles on both exterior and interior surfaces as illustrated in Figure 24 . These particles are generally stainless steel, however iron particles have been found. Defect depth ranges from less than a mil to several mils deep. Results of the testing indicate the eddy-current test is more sensitive than the ultrasonic test to finding this condition due to the apparent magnetic aspect of the cold worked impressed particle. Testing has also begun on the supplemental 4300 feet of 20% cold worked preproduction tubing. Defects similar to those described have been found. Discussions with the vendor indicates that contamination of the tubes with metal particles from deburring operations may be at fault. Approximately 1/3 of the tubing has defects of rejectable depth of 1 mil or greater. The tubing is also contaminated with a chlorinated rubber drawing sub-coat discussed elsewhere in this report. Evaluation efforts will result in a modified process that will eliminate these problems.

Pre Qualification Fuel Pin Cladding - R. C.Aungst

An order was processed for 10,000 feet of 0.250-in. O.D. by .218-in. I.D. fuel clad tubing in 7 foot lengths. An urgent need existed to meet commitments under task 12153/PD-B for the fabrication of prototype prequalification fuel pins both at PNL and offsite. To meet the deadline,material was diverted from an existing order with the same fabricator for prototypic FFTF cladding and the tubing

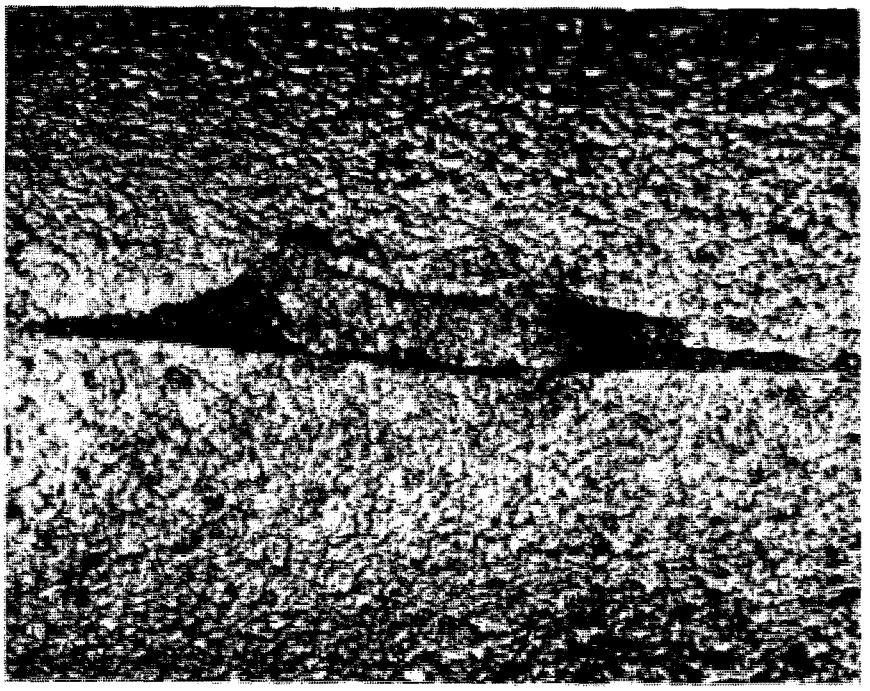

100 X ID Inclusion Neg. 469-656A

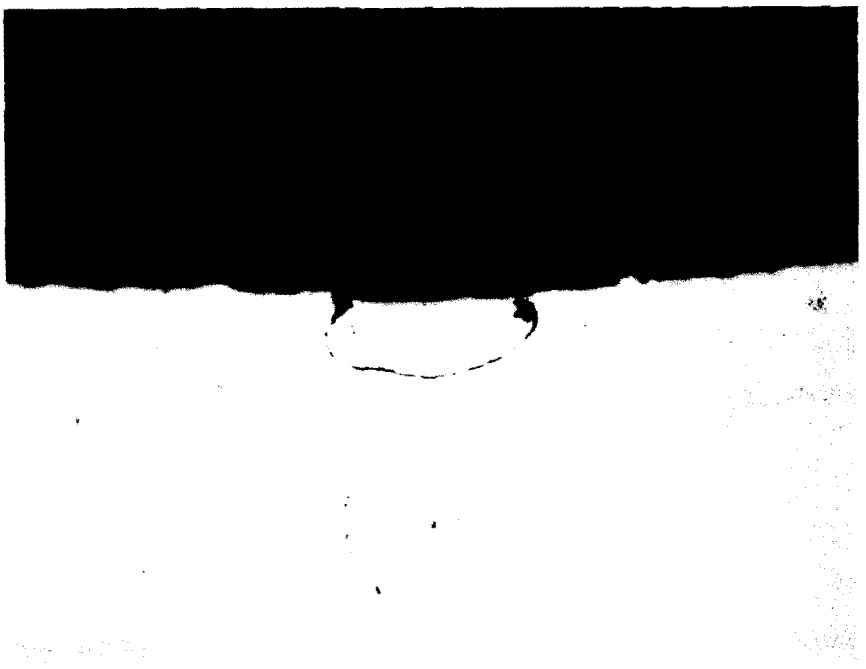

250 X Transverse Section Neg. 469-656C

FIGURE 24. Impressed Metal Particle Found in Preproduction Tubing

was fabricated to the less stringent specification, ASTM-A213.

The tubing was received in mid-March. About 700 feet was purchased by ORNL for use in their irradiation program and 400 feet reserved for evaluation at PNL. The remainder is to be used for onsite and offsite prequalification fuel manufacturing.

Tube Cleaning - R. R. Studer, R. C. Aungst, J. C. Tverberg

Two types of blemishes were found on fuel tubing, each one being peculiar to tubing received from a particular vendor.

The first type is a brown or multi-colored spot about .010- in. diameter on the outer surface of the tubes. The brown spots are obviously rust resulting from a superficial contamination by carbon steel. This type of blemish appears to be due to three basic causes. The first cause, illustrated in Figure 25 is due to flakes of either stainless steel or carbon steel being welded into the surface of the cladding by the belt polishing operation. The second cause is believed to be due to residues of alkaline cleaning compounds surrounding minor surface irregularities in which no correlation with microstructural or compositional variables could be made. The third cause was believed due to rust forming around a surface mar caused by contact with a carbon steel body in which the steel smeared on to the stainless steel cladding surface. During elevated temperature burst testing these blemishes were visually accentuated, however, there was no apparent adverse effect on the burst strength properties.

The second type of blemish was determined to be a residue of drawing lubricant not removed from the tubing inner surface during the vendor's cleaning operations. The residues are sometimes associated with pits on the order of 1/2 mil deep as illustrated in Figure 26.

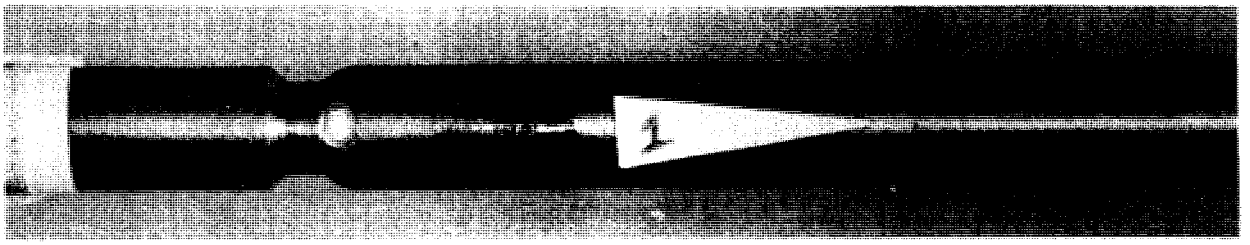

(a) Location of Rust Blemish Near End Cap of Belt Polished Fuel Tube 2 1/2X

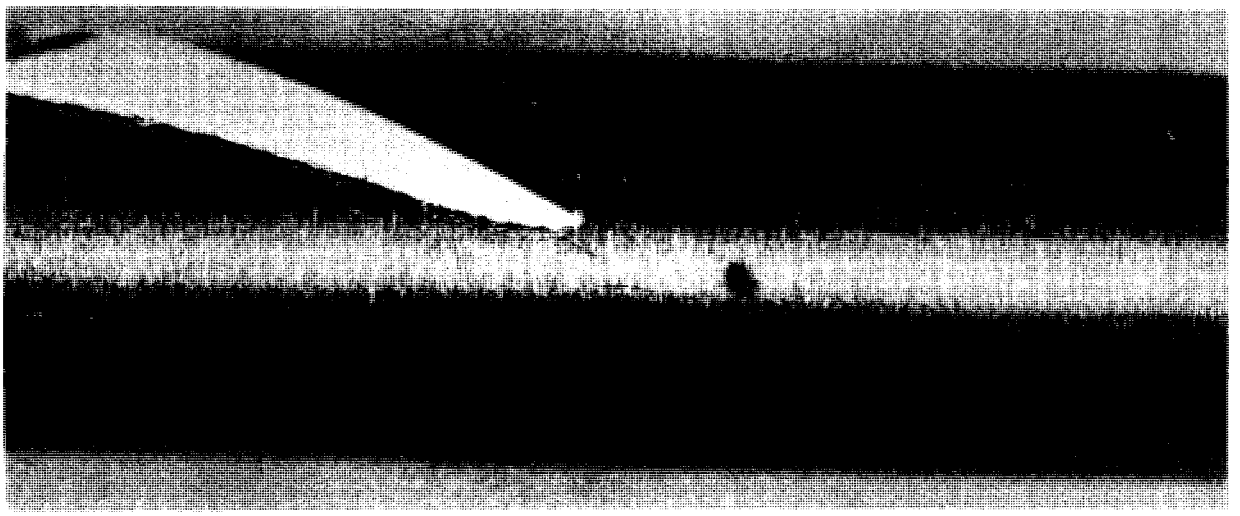

(b) Same Blemish Except at Higher Magnification 9X

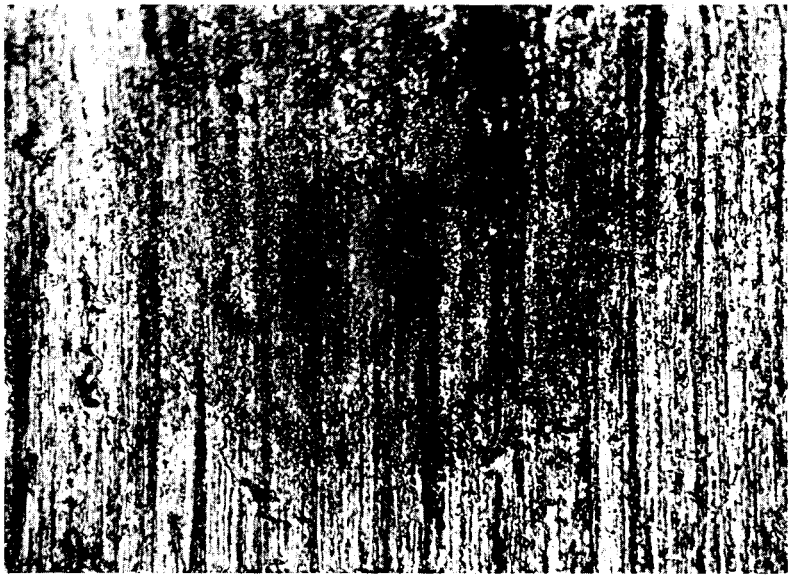

(c) Highly magnified View of Blemish Showing Belt Sanding Scratches, Stain Halo and Cold Welded Metal Flakes, Probably Carbon Steel on Surface 500X

FIGURE 25. Surface Stains on Belt Polished 316 SS Tubes

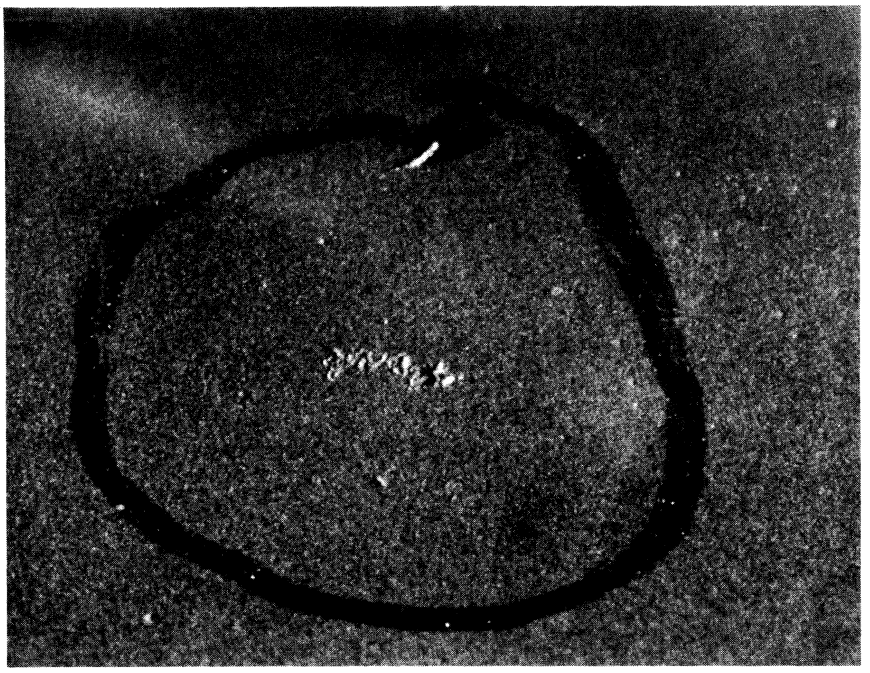

20X

(a) Area of pitting observed under a spot of organic residue on the inner surface of a fuel cladding tube.

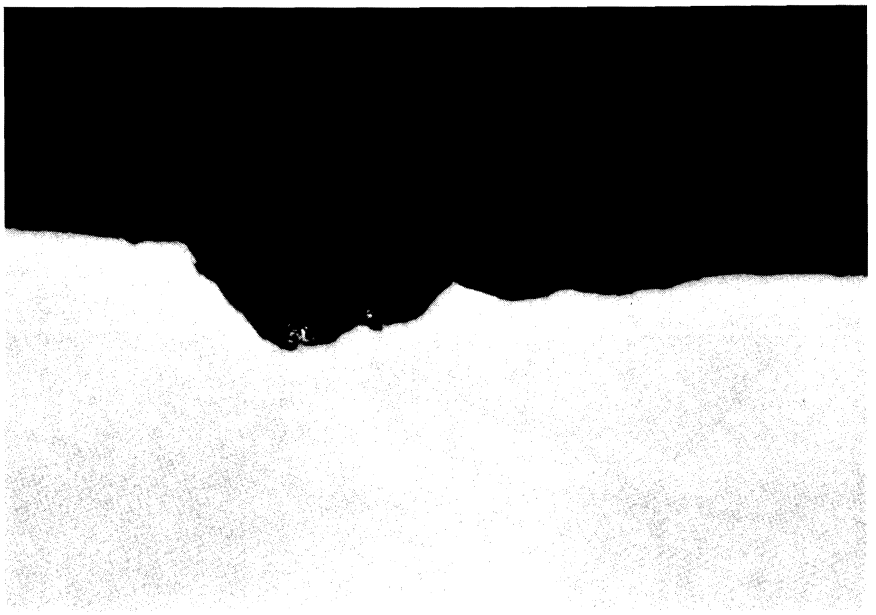

(b) Section through pit 500X

FIGURE 26. Area of Pitting Under a Spot of Organic Residue on the Inner Surface of a Fuel Cladding Tube

Again, no coincident changes in tubing microstructure or composition were found.

Cleaning procedures to remove each type of soil were developed and appropriate tank and handling equipment is either in place or being installed. The specific cleaning process for removing the brown stain on the fuel cladding tubes involves the following:

1. Degrease in a caustic cleaner at 90 °C.
2. Rinse in flowing process water.
3. Passivate 2 minutes in 60 °C, 10% nitric acid.
4. Rinse in flowing process water.
5. Rinse in 60 °C deionized water.
6. Air dry.

This treatment effectively removes included ferritic particles and reduces the surface halides to within the specified limits. Removal of residual organic contaminants on the tubing was accomplished by the following procedure:

1. Soak the tubes for 30 minutes in room temperature toluene or amyl acetate to loosen the residual organic.
2. Blow a stiff bristle brush through each tube to move the residue.
3. Follow with the above cleaning treatment to remove other surface contaminants.

No evidence of intergranular attacks by the use of hot nitric acid at this stage of cleaning was found as evidenced by the photomicrographs of Figure 27.

Fabrication Demonstration Line Fuel Clad Tubing - R. C. Aungst

A purchase requisition, product description and work statement were prepared for the procurement of 25,000 feet of fuel clad tubing, to be used in the fuel fabrication line in the 308 building to demonstrate the fuel subassembly process. These subassemblies will be fully

Neg 469-707 500X

(a) Outer surface of as received tube

Neg 469-653B 500X

(b) Outer surface of same tube following the hot nitric acid passivation treatment. Note absence of intergranular attack.

FIGURE 27. Comparison of Tubing Surfaced Before and After a 10 min 55 °C (130 °F) 10% HNO_3 Passivation Treatment. No intergranular attack was observed.

characterized and tested so it is essential that the cladding be of the best obtainable quality. In assessing the effects of cladding parameters on the performance of the subassemblies it is required that the fabrication history of the cladding be known in detail. To provide this detailed knowledge the product description and statement of work for this order were adapted from the documents drafted for use with the vendor development contracts now being processed. Whereas vendor development contracts are designed primarily to develop the vendors capabilities, this purchase order is to provide cladding for a specific purpose in a minimum time. BNW will supply the material for this order in the form of special chemistry, highly characterized 1-3/16 in. diameter solid bar.

Cladding Receiving, Inspection and Storage Facility - R. C. Aungst

With deliveries of tubing soon to grow to substantial volume, a facility will be needed to receive, inspect, and store this material. This facility will provide for a high degree of accuracy in measuring the dimensions and properties of the tubing and will allow handling and storage to preserve the quality built into the components at considerable cost. Room 162 in 306 building is proposed for this facility. A layout of equipment and facilities for the 40 foot by 60 foot area was prepared as illustrated in Figure 28 and appropriation requests initiated for air-conditioning and furnishings. Plans are well advanced for the relocation of present occupants of the area. It is intended that a brightly lighted,"clean room" environment be established that will expedite the functional aspects of the facility for the FFTF project and its relationship to the LMFBR program.

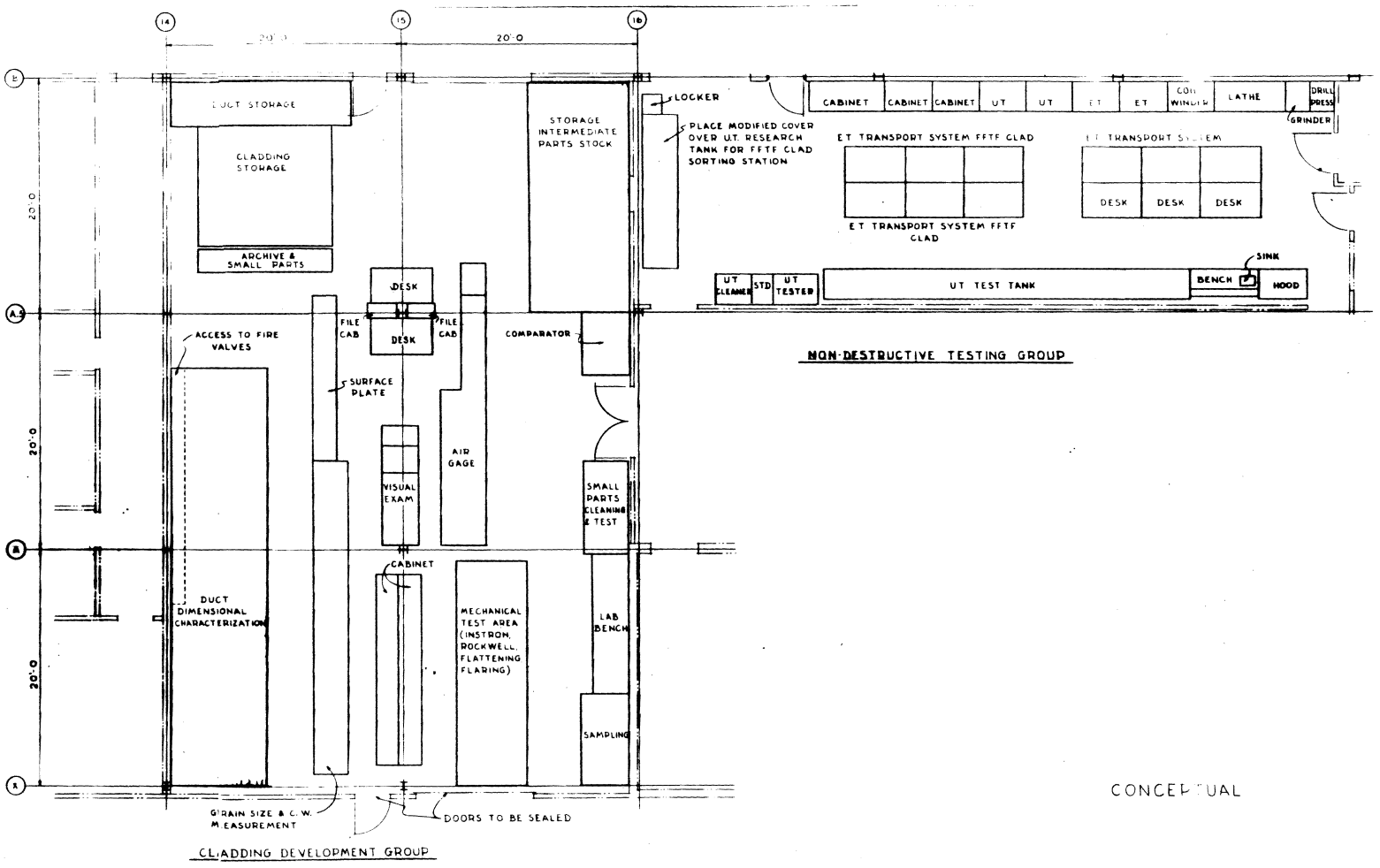

FIGURE 28. Conceptual Layout of Cladding Receiving, Inspection and Storage Facility

b. Fuel Cladding Vendor Development Program - J. C.Tverberg

A fuel cladding vendor development program was established with the objectives of developing specifications for the FFTF driver fuel cladding that will guarantee the quality needed for reliable FTR operation, and of developing processes in the plants of commercial vendors that will be in accordance with these specifications. Precise controls within the vendors plants are required at all stages of the fabrication process, including a high level of precision for nondestructive testing, a close tolerance for cold work level, and overall process reproducibility. Other areas of difficulty include steel chemistry control with regard to:boron, nitrogen and inclusions within the steel; cleaning and surface preparation; and meeting stringent mechanical property requirements.

Bid packages were sent to 18 different vendors who expressed interest in participating in the vendor development program. Five of those submitting proposals were selected for award of vendor development contracts. These five vendors utilize fabrication processes that cover essentially all of the tube fabrication procedures in industrial use today. Figure 29 illustrates the fabrication procedures that will be investigated during this development phase.

Contract negotiations with the five vendors were completed and the product descriptions and work statements revised and submitted for final approval by both the vendor and the AEC. Some of the earlier contracts are scheduled for completion by July 1969 while the later negotiated contracts will not be completed until March 1970. Approximately 45,000 feet of fuel clad tubing will be produced in this program to exacting specifications with quality control never before used in

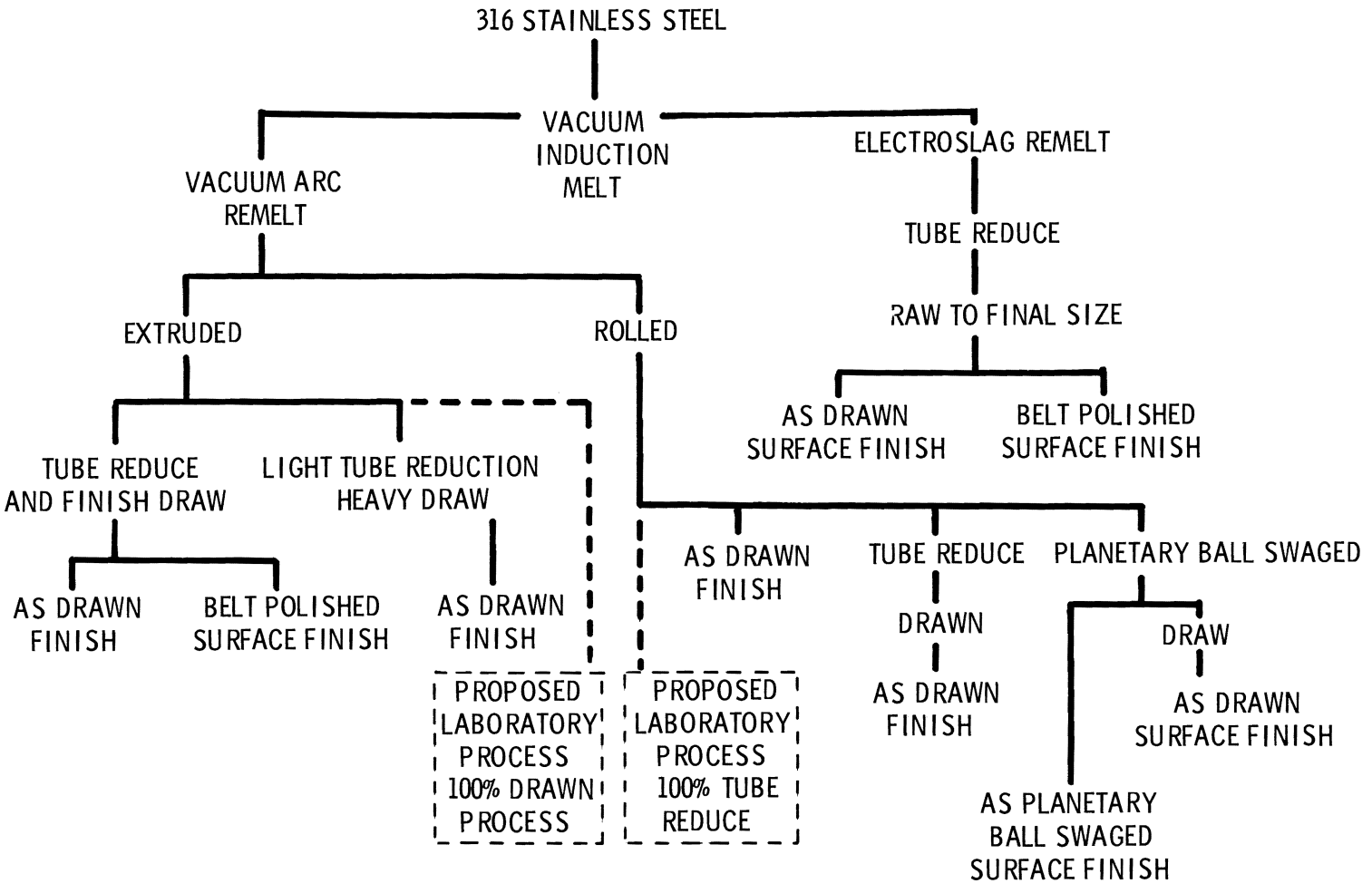

FIGURE 29. Fabrication Processes to be Used in Vendor Development of FFTF Cladding

industry, exceeding even the requirements for aircraft or space applications.

c. Parameter Studies

Variable Ingot Chemistry Study - R. C. Aungst

The Nuclear System Programs Department of the General Electric Company is producing 13 heats of modified Type 316 stainless steel to study the effects of several compositional and melting parameters. The heats will be based upon the following composition:

	Percent
Carbon	0.04 - 0.06
Managanese	1.00 - 2.00
Phosphorous, Max.	0.03
Sulphur, Max.	0.03
Silicon, Max.	0.75
Nickel	12.0 - 14.0
Chromium	16.0 - 18.0
Molybdenum	2.0 - 3.0
Copper, max.	0.20
Cobalt, Max.	0.10
Boron, max.	0.001
Nitrogen	0.02 - 0.03
Iron	Balance

Three series of heats will be made from virgin materials by vacuum induction melting with the average composition as indicated above except for the deviations specified for individual elements in each heat.

The first series will investigate effects of variations in molybdenum content, as follows:

Heat No.	Molybdenum, %
1.	0.9 - 1.1
2.	1.9 - 2.1
3.	2.9 - 3.1
4.	3.9 - 4.1

The second series will investigate the effects of ferrite formation on weldability and on the presence of sigma phase. The balance between austenitizers and ferritizers has been chosen according to the

Schaeffler equation:

$$Ni + 1/2Mn + 30\,(C + N) = \frac{(Cr + 1.8MO + 2.5Si + 2Cb - 16)}{12} - 12$$

(Austenitizers) (Ferritizers)

This series of heat will be constituted as follows:

Heat No.	C	N	Ni	CR	Austenitizer	Ferritizer
5	0.02	0.01	12.0	18.0	13.7	17.9
6	0.05	0.03	13.0	17.0	16.2	16.5
7	0.08	0.07	14.0	16.0	19.3	15.5

The third series will examine the effects of different deoxidation practices and will be made up as follows:

Heat No.	Deoxidizer	Residual Deox. (max. %)
8	None	----------
9	Yttrium	0.01
10	Rare Earths (misch metal)	0.002 (each element)
11	Silicon	0.75
12	Aluminum	0.1
13	Hydrogen	----------

The fourth series is a single heat to serve as a control made by a single vacuum induction remelt of billets provided by BNW. This material was double vacuum melted by Crucible Steel Co. to the composition specified above. Treatment will be as follows:

Heat No.	Treatment
14	Remelt BNW material, cast in ingot

All heats will be cast in 5-in. ingots and homogenized 72 hours minimum at 2200° - 2250°F. All ingots will be clearly marked with an identifying heat number and a certified analysis will be provided for each ingot.

This stockpile of material will be used to determine the effects of compositional variables on the fabricability and performance of FFTF fuel cladding. It is anticipated that these ingots will be reduced into tubing by a standardized reduction process and that the resulting tubing will be evaluated by both ex-reactor and in-reactor tests. The outcome of these tests will provide the basis for the steel composition specification for later procurement of FFTF fuel cladding.

In the preparation of the 13 experimental compositions a series of master heats will be used as the primary feed material in the making of the thirteen individual 100 lb. ingots. In the case of these ingots, following remelting of the primary feed material, additions will be made of other elements as required to achieve the desired composition. Careful analysis of the master heats prior to remelting should more certain achievement of desired compositions.

At the present time three of the 400 lb. master heats have been vacuum induction melted and cast into ingots of about 115 pounds each. One ingot of each master heat was cut and sampled at top and bottom for chemical analysis. The analyses that have been completed on the first and second master heats show good homogeneity of ingot and excellent retention of the elements added to the melt.

The raw materials used for these master heats are described in Table VII. The practice is to compact the iron and chromium into eight inch diameter billets,making loading of the charge in the crucible easier and preventing bridging of the charged material during melting. The nickel plates and extra chromium briquettes are placed around

TABLE VII

RAW MATERIALS USED IN MASTER HEATS

Element	Type	Purity	Typical Impurities
Iron	Electrolytic Chip (Glidden)	99.9+	.007C, 93 ppm O
Nickel	Electrolytic Squares	99.95	.004Cu, .04Co, .007Fe, .0016S, 62 ppm O
Chromium	Electrolytic Brickettes	99.5	.30Fe, .03C, .03Si, .012S, 150 ppm N_2, 400 ppm O
Molybdenum	Type Mo-G-10+60 mesh	99.9	.014Fe, .06W, 170 ppm O
Manganese	Electrolytic Powder Remelted into Ingot	99.95	Analysis in Progress
Silicon	Lump	99.5	.10Al, .10Fe
Carbon	Reactor Grade Rod	99+	Not Analyzed
Nitrogen as CrN	NSP Ingot	99.9	4.2% N_2 in Cr

the pressed billets in the crucible. The additions of molybdenum, silicon, chromium nitride and carbon are made after the iron-nickel-chromium charge is molten.

An alumina crucible is used for these master heats. Since the total charge of 400 lbs. cannot be added initially the practice is to melt about 270 lbs. under vacuum (<5 micron) and cool in the crucible; break vacuum, add the balance of the charge to the crucible, outgas the furnace and complete the melt including the small addition elements. To suppress vaporization of the addition elements, the furnace pressure is increased to one third atmosphere by back filling with argon gas. The ingots are cast under one third atmosphere of argon.

Master heats are cast into three graphite molds of the same size used for the 100 lb. heats. The use of a hot top and tundish on each mold was found to be desirable to obtain sound castings.

A retort is being fabricated from Inconel sheet in preparation for homogenization heat treatment of the 100 lb. ingots. This retort will contain three ingots and will be equipped with gas lines to maintain an argon protective atmosphere over the ingots during homogenization at 2200°F for 72 hours.

The program schedule indicates that the last heat should be completed about June 12. Homogenization, X-ray inspection and chemical analyses should be completed to permit shipment of the ingots by June 30.

Cladding Fabrication Program - R. R. Studer

Oak Ridge National Laboratory is providing assistance in the study of fabrication variables and their effects on the performance of fuel clad tubing. Special vacuum induction melted Type 316 stainless steel produced by Crucible Steel company has been shipped to ORNL to serve as

the base material for this study. Part of this material will be remelted using the consumable-electrode vacuum arc process to adjust the carbon and nitrogen contents as follows:

Heat No.	Carbon Wt. %	Nitrogen Wt. %
1	0.02	0.07
2	0.08	0.07
3	0.02	0.01
4	0.08	0.01
Basic material	0.04	0.02

This material will be fabricated into tube hollows by hot extrusion, then surface conditioned to obtain the necessary dimensional control. Compositional variables will be correlated with tube reducing parameters to determine their effects on tooling pressures, permissible reduction per pass and between anneals, and power requirements. In the same manner compositional variables will be related to drawing parameters.

In addition some semi-finished tubing will be selected from one of the compositional variations and given the final 20% cold work by planetary ball swaging over a mandrel. The normal bench drawn material will have the finishing schedule varied to produce tubing with 0, 5, 10, 20 and 40% cold work after the final bright anneal. All the material will be characterized for metallurgical structure, surface finish, short-term mechanical properties at room temperature and 1000°F, and for structural soundness.

2. Cladding Evaluation - J. J. Holmes

a. Acceptance Testing and Clad Characterization - M. M. Paxton

The objective of this program is to assure that acceptable cladding material is obtained and utilized throughout the FFTF fuel development and irradiation testing program. Under this program, lot to lot variations in selected mechanical properties of AISI 304 and 316 stainless steel tubing are being determined and evaluated.

A check chemical analysis has been completed on five tube lengths from G lot tubing, Table VIII. The check analysis agrees reasonably well with the analysis supplied by the vendor except for phosphorous. The values supplied by the vendor are lower by a factor of two than the values received on the check analysis.

Metallography on five G lot tube lengths has been completed. Figures 30-33 are typical transverse and longitudinal photomicrographs from 100 X to 1000 X. The grain size as determined from the five samples varies between ASTM size 7 to 8.

Burst tests on tubing lots E, F, G, and H have been completed. The results are tabulated in Table IX and shown graphically in Figures 34-37. in terms of internal gas pressure required to burst the tube related to the reciprocal of absolute temperature. The lines drawn through the data are for a least squares fit to the equation.

$$y = B_0 + B_1(1/x) + B_2(1/x)^2$$

where y = pressure, psi

x = temperature (°K)

B_0, B_1, and B_2 are the regression coefficients

Burst pressure may be calculated at any temperature in the range 1000 to 1800°F using the above equation and the appropriate values for B_0, B_1, and B_2 given in Table X.

TABLE VIII

CHEMICAL ANALYSIS "G" LOT TUBING 316 STAINLESS STEEL

Vendor Analysis:

Percent

Heat No.	C	Mn	P	S	Si	Ni	Cr	Mo	B	N_2	Cu	Fe
	.05	1.60	.010	.012	.49	13.32	17.63	2.41	.0007	.047	.11	Bal
	.05	1.56	.012	.016	.56	13.29	17.70	2.42	.0013	.052	.10	"
	.05	1.56	.011	.015	.53	13.29	17.63	2.41	.0009	.054	.11	"
	.05	1.53	.010	.015	.58	13.34	17.63	2.45	.0012	.050	.15	"
	.06	1.58	.010	.012	.56	13.31	17.33	2.50	.0010	.049	.11	"

Check Analysis by Lukens Steel

Identification	C	Mn	P	S	Si	Ni	Cr	Mo	Cu	B	N
G-081	.049	1.55	.026	.015	.52	13.42	17.62	2.37	.13	.0008	.043
G-163	.047	1.55	.025	.014	.53	13.42	17.65	2.37	.13	.0010	.044
G-238	.048	1.55	.026	.013	.52	13.42	17.60	2.37	.13	.0008	.035
G-257	.048	1.55	.026	.014	.52	13.42	17.60	2.39	.13	.0010	.042
G-320	.050	1.55	.024	.014	.52	13.42	17.55	2.40	.13	.0010	.040

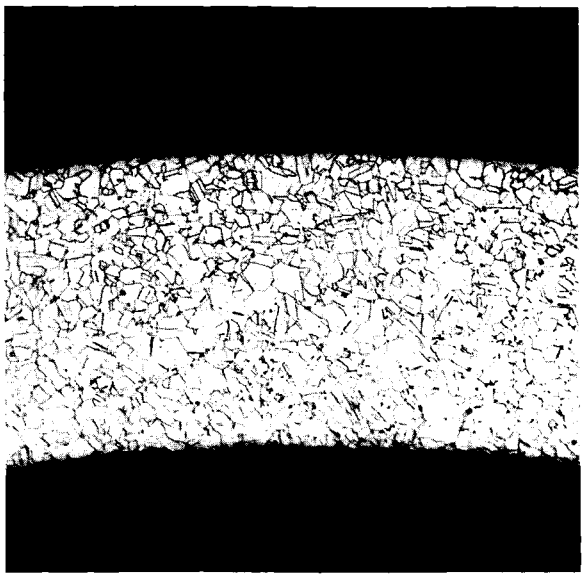

Neg 46972A 100X

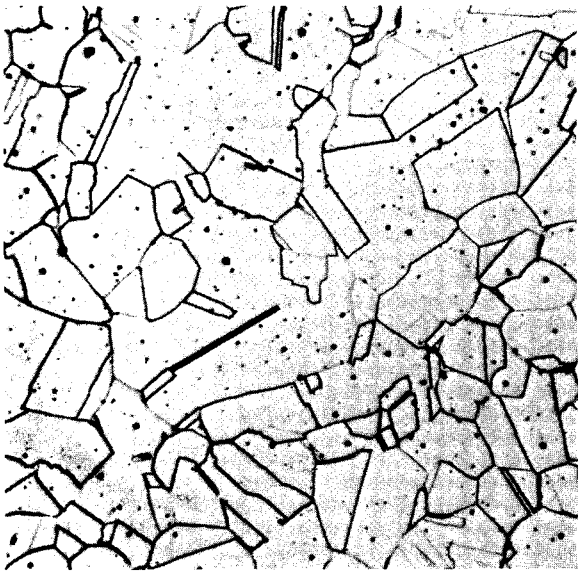

Neg 469-72 250X

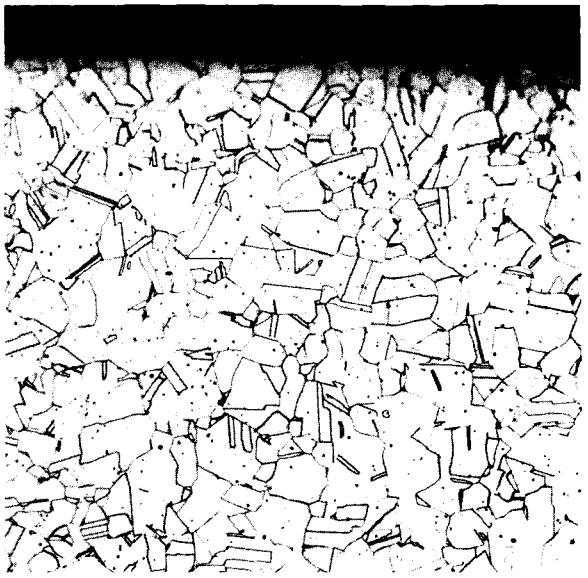

Neg 46972B 500X

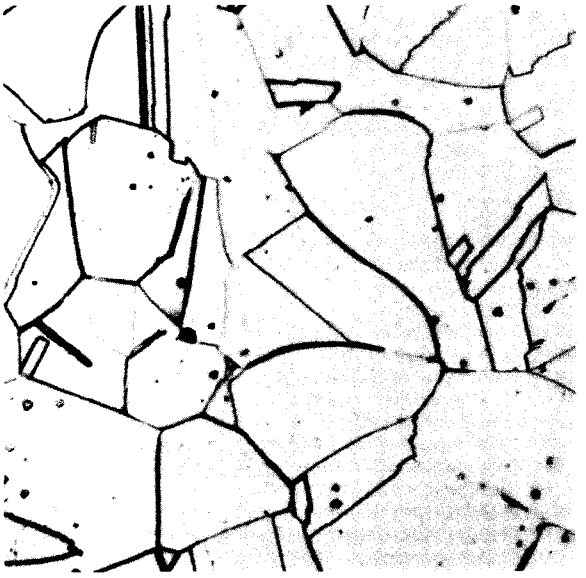

Neg 46972C 250X

FIGURE 30. Tubing G Mill Annealed 316 Stainless Transverse Etch 25% Alcohol 75% HCl (elec.)

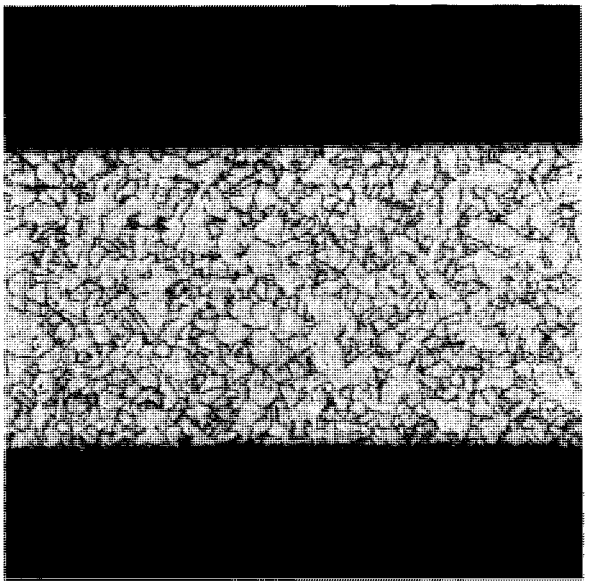

Neg 46977A 100X

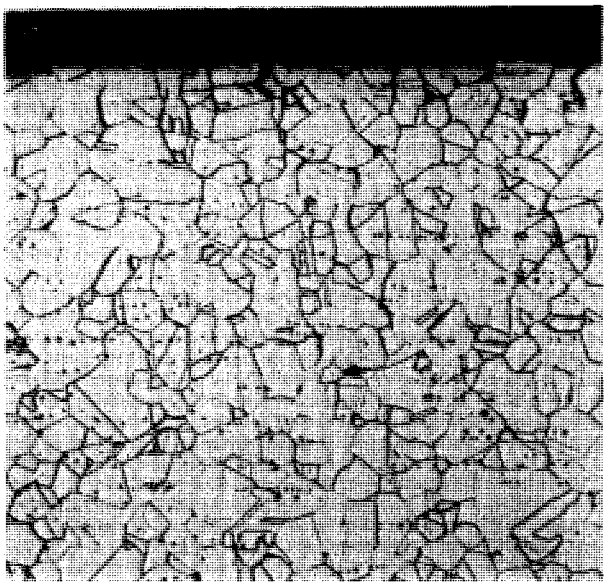

Neg 469-27 250X

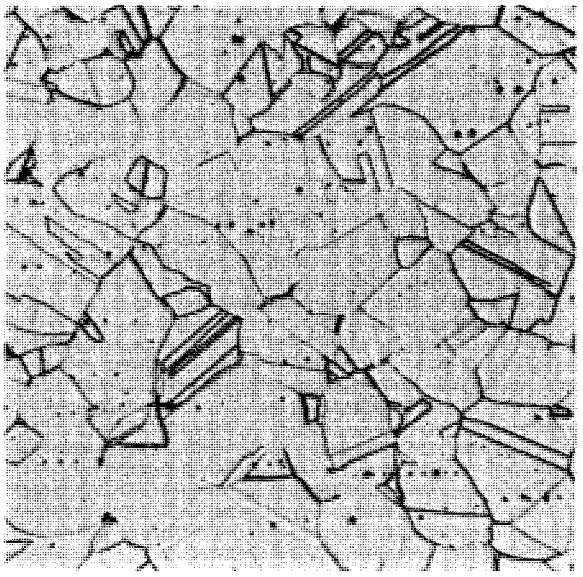

Neg 46977B 500X

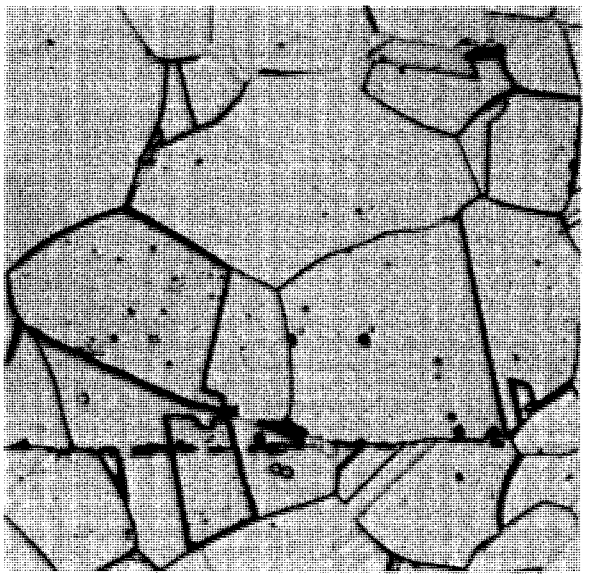

Neg 46977C 100X

FIGURE 31. Tubing G Mill Annealed 316 Stainless Transverse Etch 25% Alcohol 75% HCl (elec.)

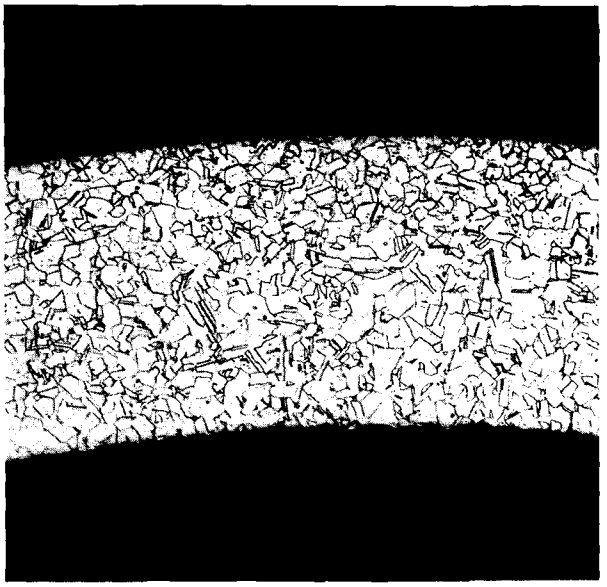

Neg 46976A 100X

Neg 469-76 250X

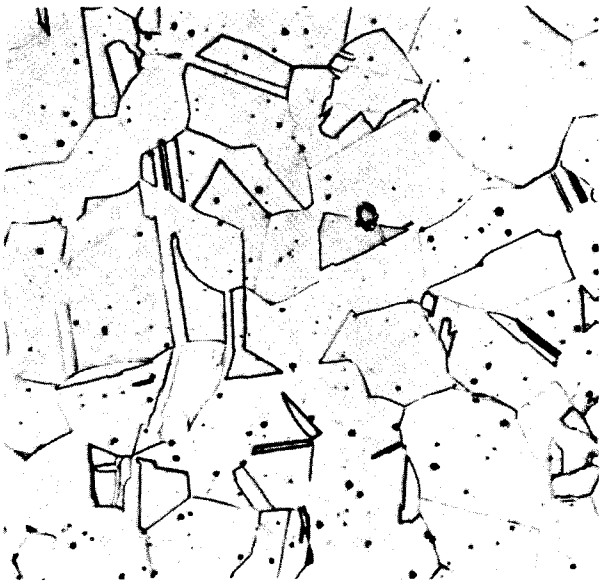

Neg 46976B 500X

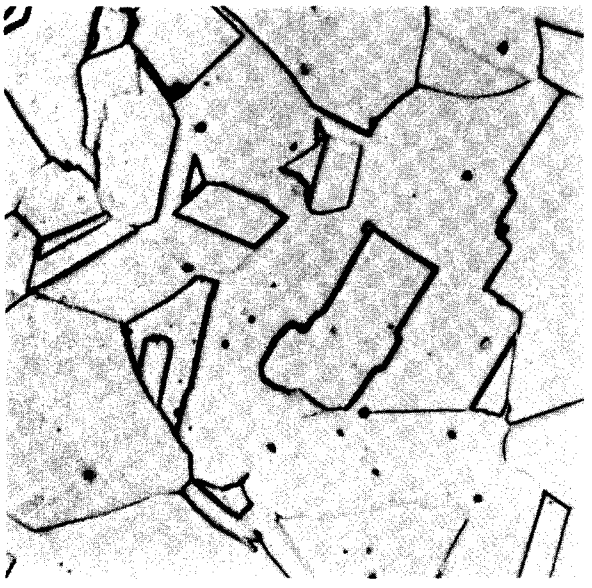

Neg 46976C 1000X

FIGURE 32. Tubing G Mill Annealed 316 Stainless Transverse Etch 25% Alcohol 75% HCl (elec.)

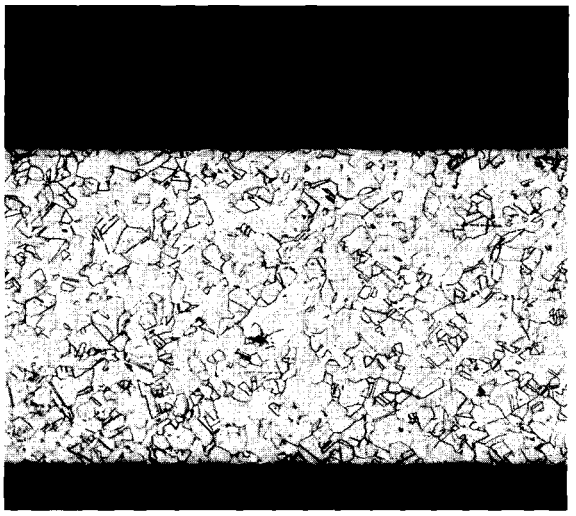

Neg 46973A 100X

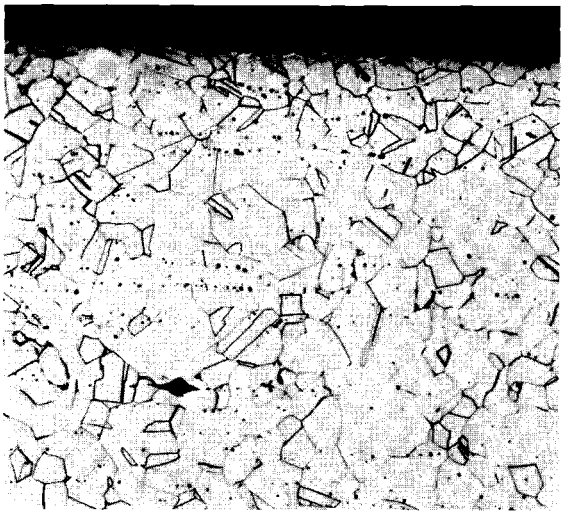

250X

Neg 46973B 500X

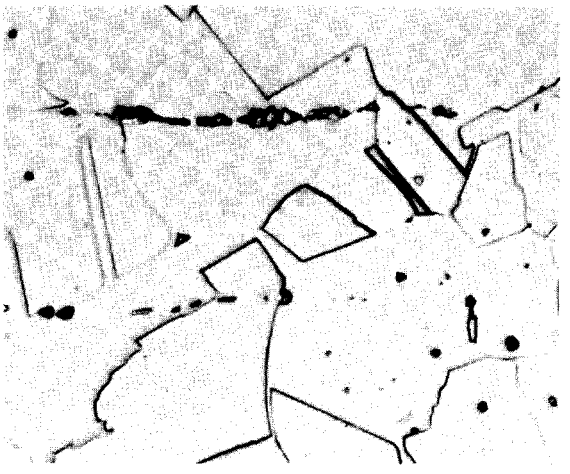

Neg 46973C 1000X

FIGURE 33. Tubing G Mill Annealed 316 Stainless Transverse Etch 25% Alcohol 75% HCl (elec.)

TABLE IX

BURST DATA

Temp.	Burst-Pressure, psi	Hoop Stress, psi	Load Time	Δ D/D, %
E Lot Tubing Mill Annealed 304 Stainless Steel				
1000°F	7,390	50,325	10 min.	18.7
	7,430	50,600	8 min.	16.5
	7,410	50,460	12 min.	18.9
1200°F	6,260	42,630	<6 min.	17.3
	6,280	42,770	<6 min.	18.1
	6,230	42,430	<6 min.	16.9
1400°F	5,000	34,050	<6 min.	16.9
	5,060	34,460	<6 min.	16.1
	5,020	34,190	<6 min.	15.3
1600°F	3,530	24,040	<6 min.	17.3
	3,550	24,180	<6 min.	14.5
	3,510	23,900	<6 min.	18.5
1800°F	2,600	17,710	<6 min.	13.3
	2,460	16,750	<6 min.	21.3
	2,340	15,940	<6 min.	20.7
RT	10,700	72,870	1.0-1.25 min.	20.0
	10,700	72,870	1.0-1.25 min.	22.0
	10,700	72,870	1.0-1.25 min.	19.0
	10,800	73,550	1.0-1.25 min.	22.0
	10,800	73,550	1.0-1.25 min.	22.0
F Lot Tubing Mill Annealed 304 Stainless Steel				
1000°F	7,075	48,180	8 min.	16.1
	7,070	48,150	6 min.	17.3
	7,020	47,810	7 min.	17.7
1200°F	5,790	39,430	<6 min.	20.1
	5,830	39,700	<6 min.	18.1
	5,820	29,630	<6 min.	18.1
1400°F	4,400	29,960	<6 min.	20.1
	4,450	30,300	<6 min.	24.1
	4,460	30,370	<6 min.	20.9
1600°F	3,090	21,040	<6 min	20.1
	3,200	21,790	<6 min.	21.7
	3,170	21,590	<6 min.	20.1

TABLE IX (Continued)

Temp.	Burst-Pressure, psi	Hoop Stress, psi	Load Time	ΔD/D %
1800°F	2,100	14,300	6 min.	26.7
	2,000	13,620	6 min.	22.9
	2,040	13,890	6 min.	22.1
RT	9,950	67,760	1.0-1.25 min.	21.0
	9,950	67,760	1.0-1.25 min.	21.0
	9,900	67,420	1.0-1.25 min.	20.0
	9,950	67,760	1.0-1.25 min.	21.0
	9,950	67,760	1.0-1.25 min.	24.0
G Lot Tubing Mill Annealed 316 Stainless Steel				
1000°F	8,110	55,230	17 min.	16.9
	8,300	56,520	17 min.	16.1
	8,150	55,500	16 min.	16.5
1200°F	6,960	47,400	6 min.	18.1
	7,220	49,170	6 min.	17.3
	7,210	49,100	6 min.	18.7
	6,950	47,330	5.75 min.	22.5
1400°F	5,610	38,200	1 min.	20.1
	5,620	38,270	1 min.	19.7
	5,640	38,410	1 min.	22.5
	5,500	37,460	.75	21.3
1600°F	3,950	26,900	.67	22.5
	4,050	27,580	.67	18.7
	4,160	28,330	.60	21.7
	4,050	27,650	.50	21.3
1800°F	2,780	18,930	.30	24.1
	2,740	18,660	.30	27.3
	2,980	20,290	.60	8.1
	2,580	17,570	.33	20.9
RT	10,950	74,570	1.0-1.25 min.	21.0
	11,100	75,590	1.0-1.25 min.	21.0
	10,700	72,870	1.0-1.25 min.	21.0
	10,750	74,230	1.0-1.25 min.	21.0
H Lot Tubing Mill Annealed 316 Stainless Steel				
1000°F	8,380	57,070	10.75	18.9
	8,260	56,250	9.0	16.9
1200°F	6,940	47,260	1.0	15.3
	7,120	48,490	.75	22.1
	7,140	48,620	.80	19.3
1400°F	5,450	37,110	.67	20.9
	5,440	37,050	.67	17.7
	5,340	36,980	.50	22.1

TABLE IX (Continued)

Temp.	Burst-Pressure, psi	Hoop Stress, psi	Load Time	ΔD/D %
1600°F	3,880	26,420	.50	14.5
	3,820	26,010	.50	23.7
	3,950	26,900	.70	23.4
1800°F	2,580	17,570	.50	20.7
	2,640	17,980	.50	14.5
	2,630	17,910	.40	18.9
RT	10,750	73,210	1.0-1.25 min.	20.0
	9,750	66,400	1.0-1.25 min.	16.0
	10,650	72,530	1.0-1.25 min.	19.0
	11,000	74,910	1.0-1.25 min.	20.0
	10,900	74,230	1.0-1.25 min.	19.0

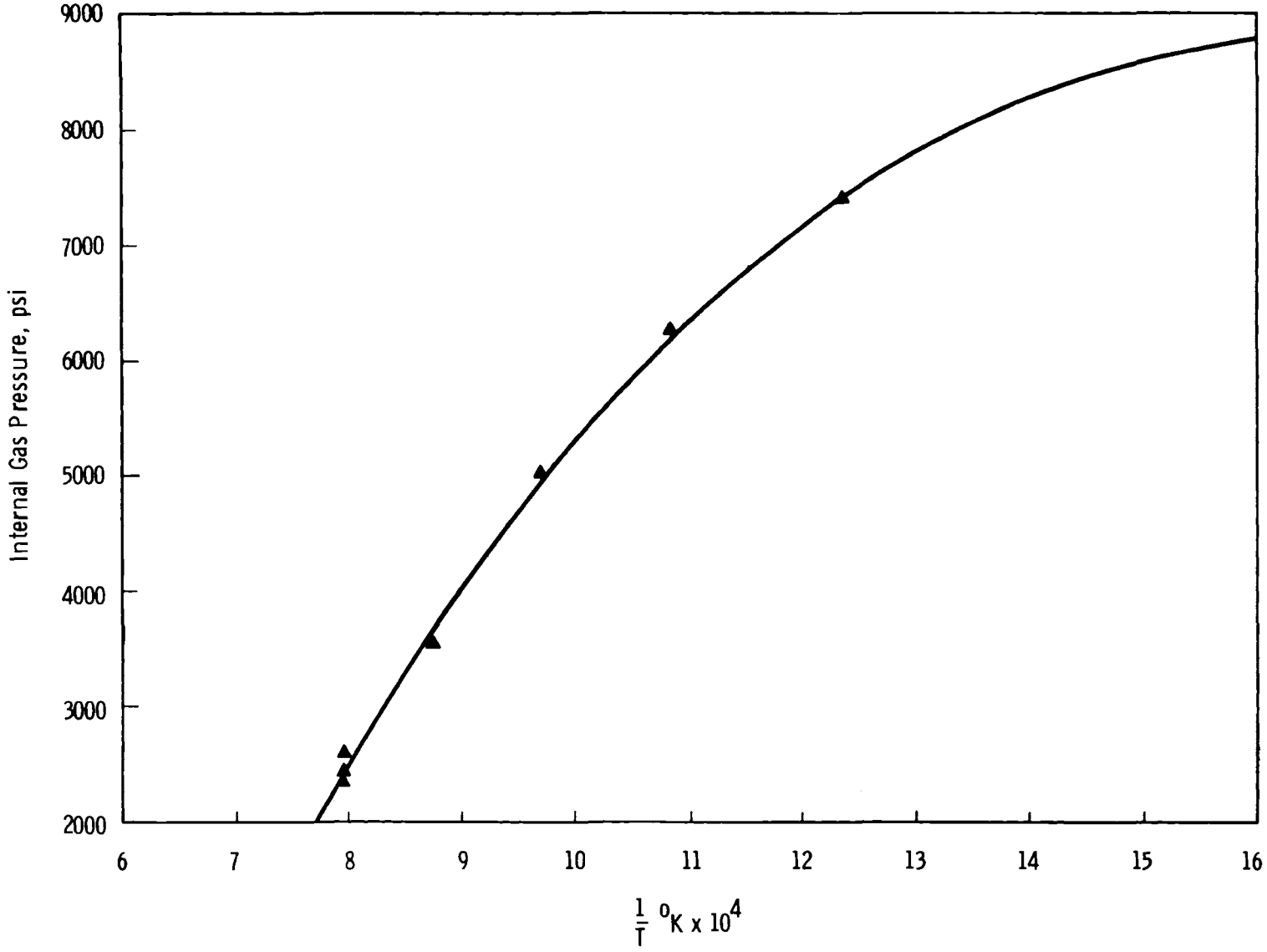

Neg 0691325-2

FIGURE 34. E Lot Burst Data 1000-1800 °F Mill Annealed 304 Stainless Steel

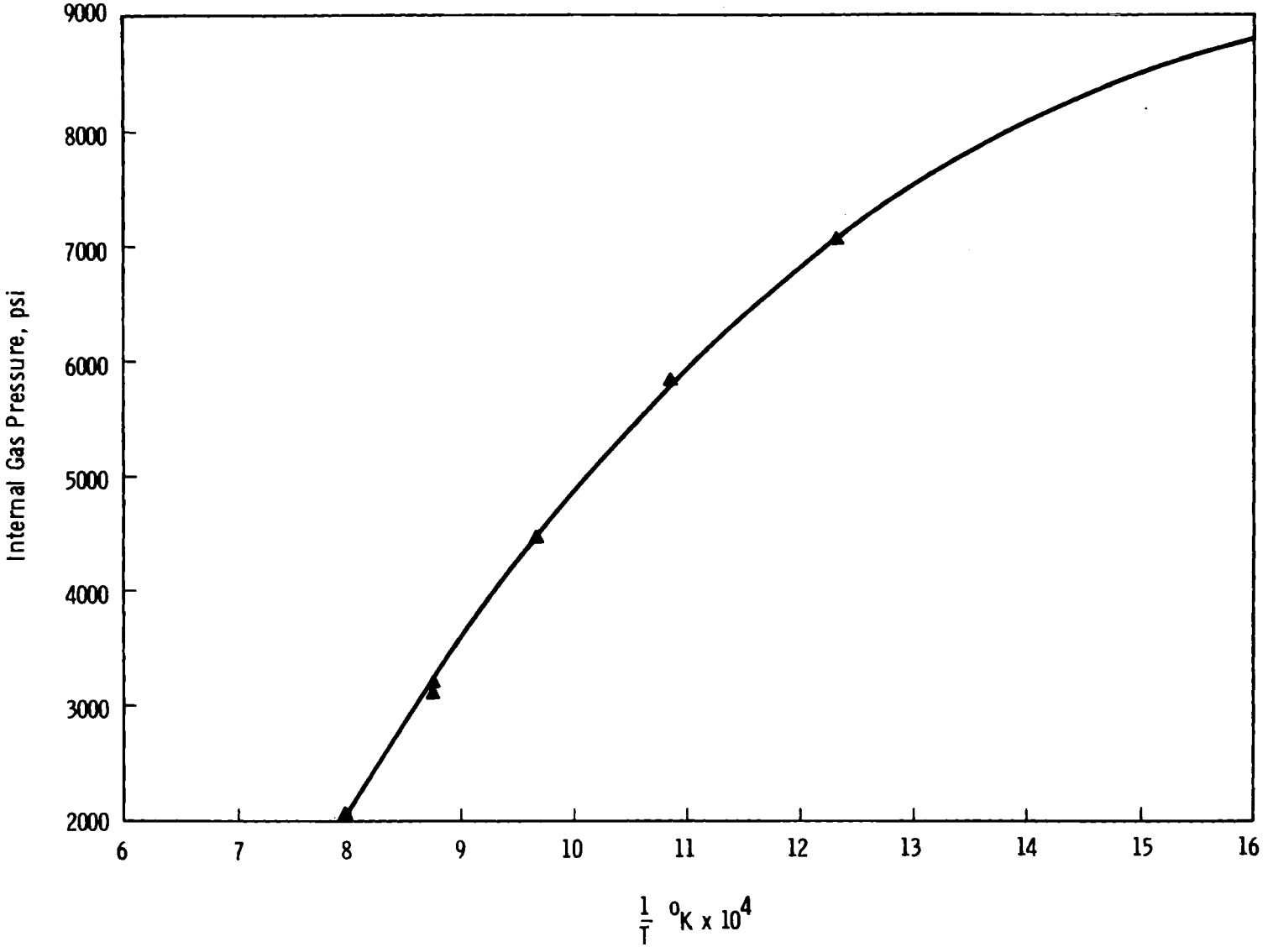

Neg 0691325-2

FIGURE 35. F Lot Burst Data 1000-1800 °F Mill Annealed 304 Stainless Steel

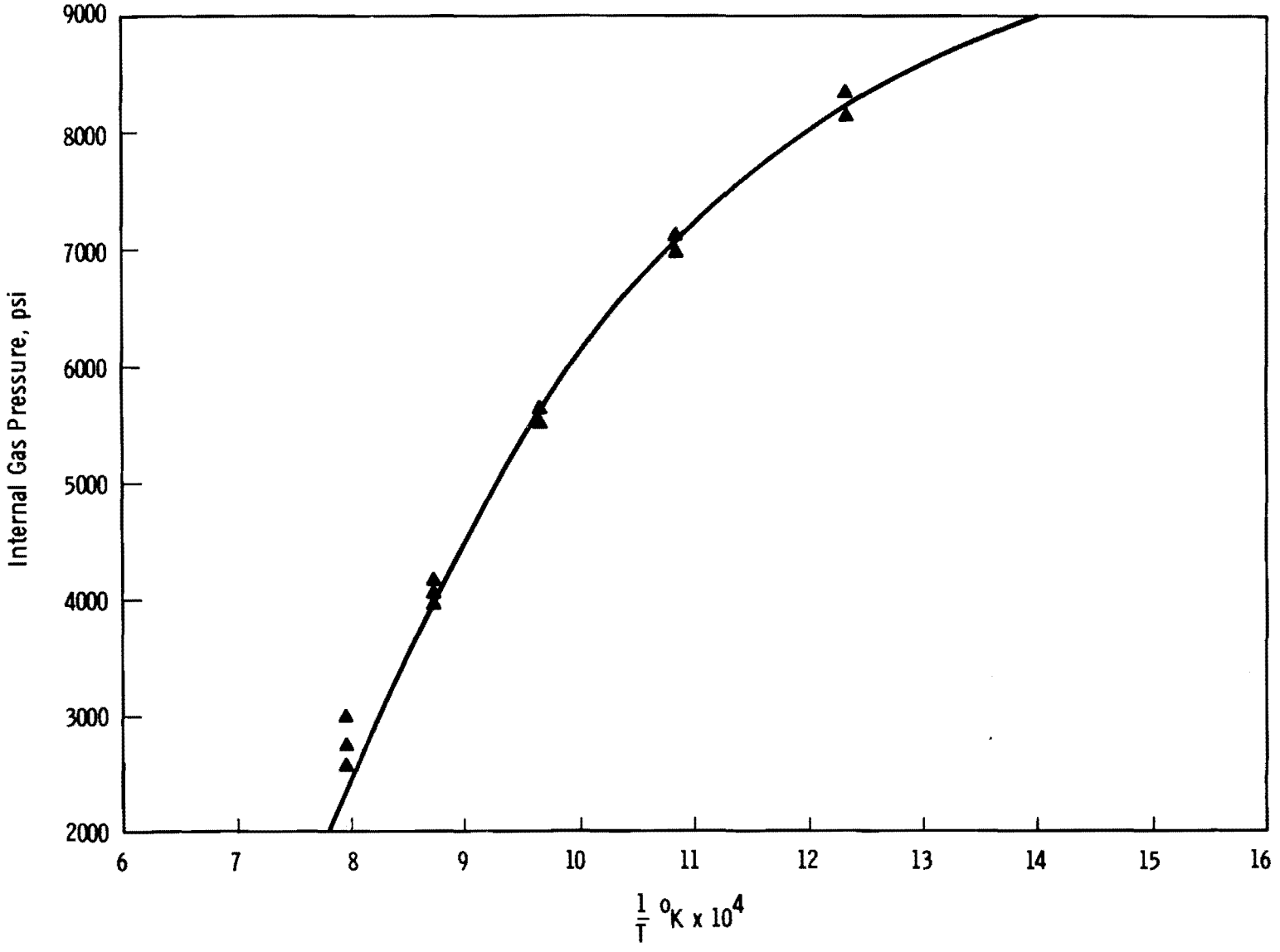

Neg 0691325-3

FIGURE 36. G Lot Burst Data 1000-1800 °F Mill Annealed 316 Stainless Steel

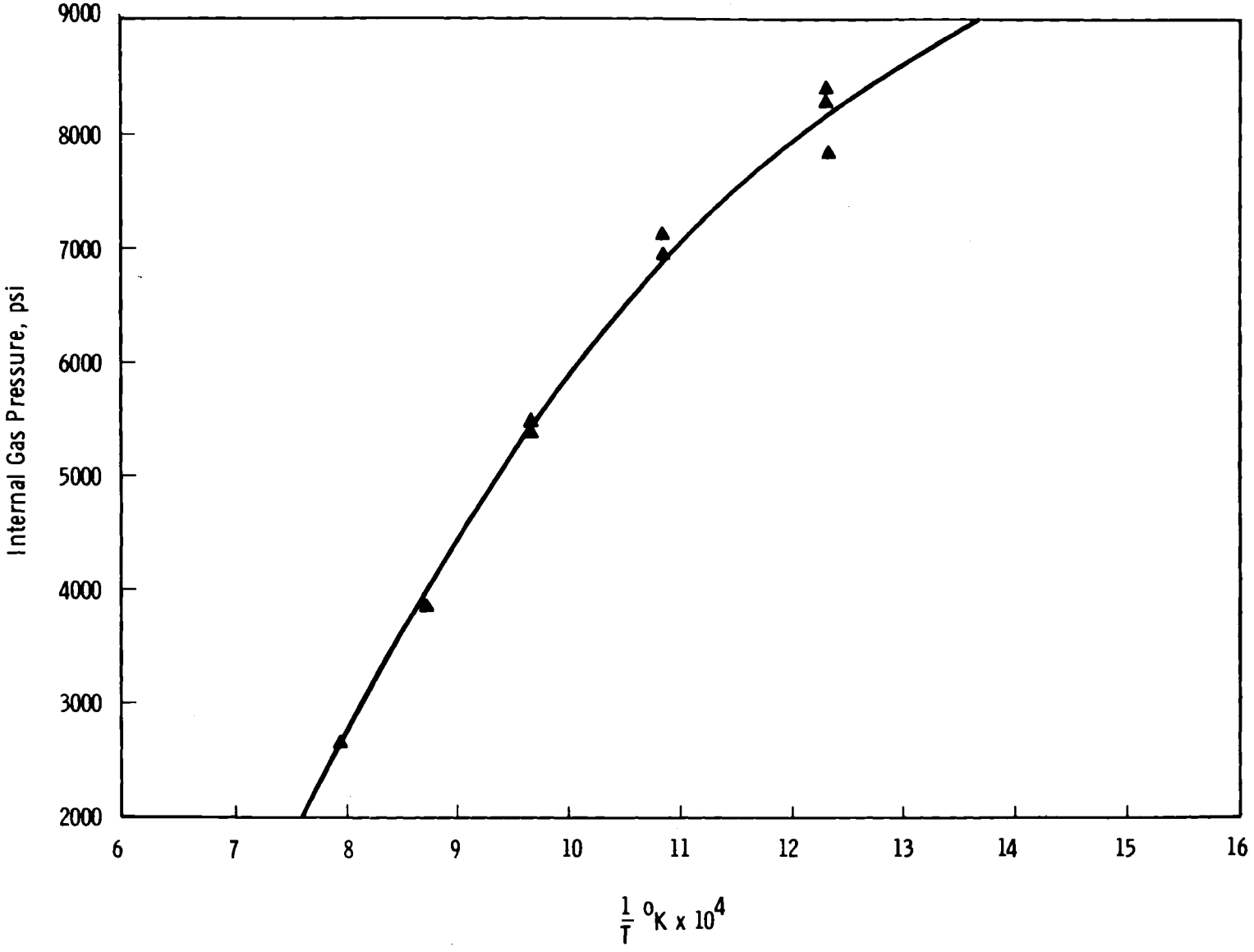

Neg 691325-4

FIGURE 37. H Lot Burst Data 1000-1800 °F Mill Annealed 316 Stainless Steel

TABLE X

REGRESSION COEFFICIENTS FOR BURST DATA

Tubing Lot	B_0	B_1	B_2
E	-1.9714×10^4	3.71978×10^7	-1.26778×10^{10}
F	-1.68999×10^4	3.16296×10^7	-9.88663×10^9
G	-2.94949×10^4	5.70268×10^7	-2.14467×10^{10}
H	-2.24968×10^4	4.3455×10^7	-1.50741×10^{10}

Burst results depend on the rate of loading and are, therefore, not unique unless the rate of loading is specified and controlled. The rate of loading effect is clearly evident in tests performed on E lot reported previously,[1] which burst at 1400 psi in 10-14 minutes and at 2500 psi in 1-3 minutes. In order to eliminate loading time as a variable, a series of short term, 0.01 to 1 hour, stress rupture tests were performed on G and H lot tubing. The results are tabulated in Table XI and shown graphically in Figures 38-39. If the results of the burst tests are treated as very short term stress rupture tests, Figures 40-41 the two tests give comparable results except at 1800°F. In treating a burst test as a stress rupture test the stress at rupture is taken as the stress to cause rupture and the time to rupture is the load time for the burst test.

Stress rupture tests on tubing lots E, F, G, and H have been completed at 1200°F for rupture times less than 1400 hours. The tests completed to date are tabulated in Table XII and shown graphically in Figures 42-46. The ductilities, shown as $\Delta\Gamma/\Gamma$ were taken well away from the failed region, since most specimens failed in an explosive manner.

The difference between the creep rupture properties of lot E and lot F is being investigated. Lot E was found to be considerably stronger than lot F in creep rupture. The main difference between these two is a larger grain size in E than in F and a lower interstitial concentration in F than in E. Literature data[2-4] have shown that creep rates are related to total interstitial concentration. In order to more fully understand how these differences affect rupture life, a series of biaxial creep tests was conducted. The biaxial creep curves were determined by periodically interrupting the test and measuring diametral strain every 1/4 inch along the specimen. The secondary creep rates for these tests are given in

TABLE XI

SHORT TERM STRESS RUPTURE DATA

Temp.	Gas Pressure psi	Hoop Stress psi	Rupture Time Hours	ΔD/D%
G Lot Mill Annealed 316 Stainless Steel				
1800°F	1,620	11,080	0.026	17.3
	1,320	8,990	0.189	20.1
	1,170	7,970	0.251	18.7
	1,030	7,010	0.449	20.5
	940	6,400	0.755	24.1
1600°F	3,810	25,950	0.008	20.1
	2,960	20,160	0.045	28.9
	2,640	17,980	0.100	25.3
	2,350	16,000	0.178	22.9
	2,130	14,500	0.394	20.5
	1,910	13,010	0.852	24.1
1400°F	5,210	35,480	0.018	22.8
	5,000	34,050	0.028	24.9
	4,670	31,800	0.067	26.1
	4,130	28,130	0.175	27.7
	3,860	26,290	0.371	31.7
	3,660	24,920	0.636	27.3
1200°F	6,800	46,310	0.034	21.6
	6,600	44,950	0.072	20.8
	6,320	43,040	0.450	21.3
	6,170	42,020	0.562	19.3
	6,020	41,000	0.818	23.3
H Lot Mill Annealed 316 Stainless Steel				
1800°F	1,610	10,960	0.044	20.1
	1,320	8,990	0.117	18.1
	1,170	7,970	0.233	20.9
	1,030	7,010	0.716	25.7
	940	6,400	1.00	22.1
1600°F	2,930	19,950	0.048	22.1
	2,640	17,980	0.110	23.7
	2,350	16,000	0.195	23.7
	2,130	14,500	0.446	23.3
	1,910	13,010	1.00	18.9
1400°F	4,700	32,010	0.044	21.3
	4,130	28,130	0.194	22.9
	3,860	26,290	0.346	22.5
	3,660	24,920	0.789	24.1
	3,550	24,180	1.00	23.3
1200°F	6,800	46,310	0.036	21.7
	6,600	44,950	0.133	22.0
	6,320	43,040	0.340	20.3
	6,170	42,020	0.413	18.1
	6,020	41,000	0.672	17.3

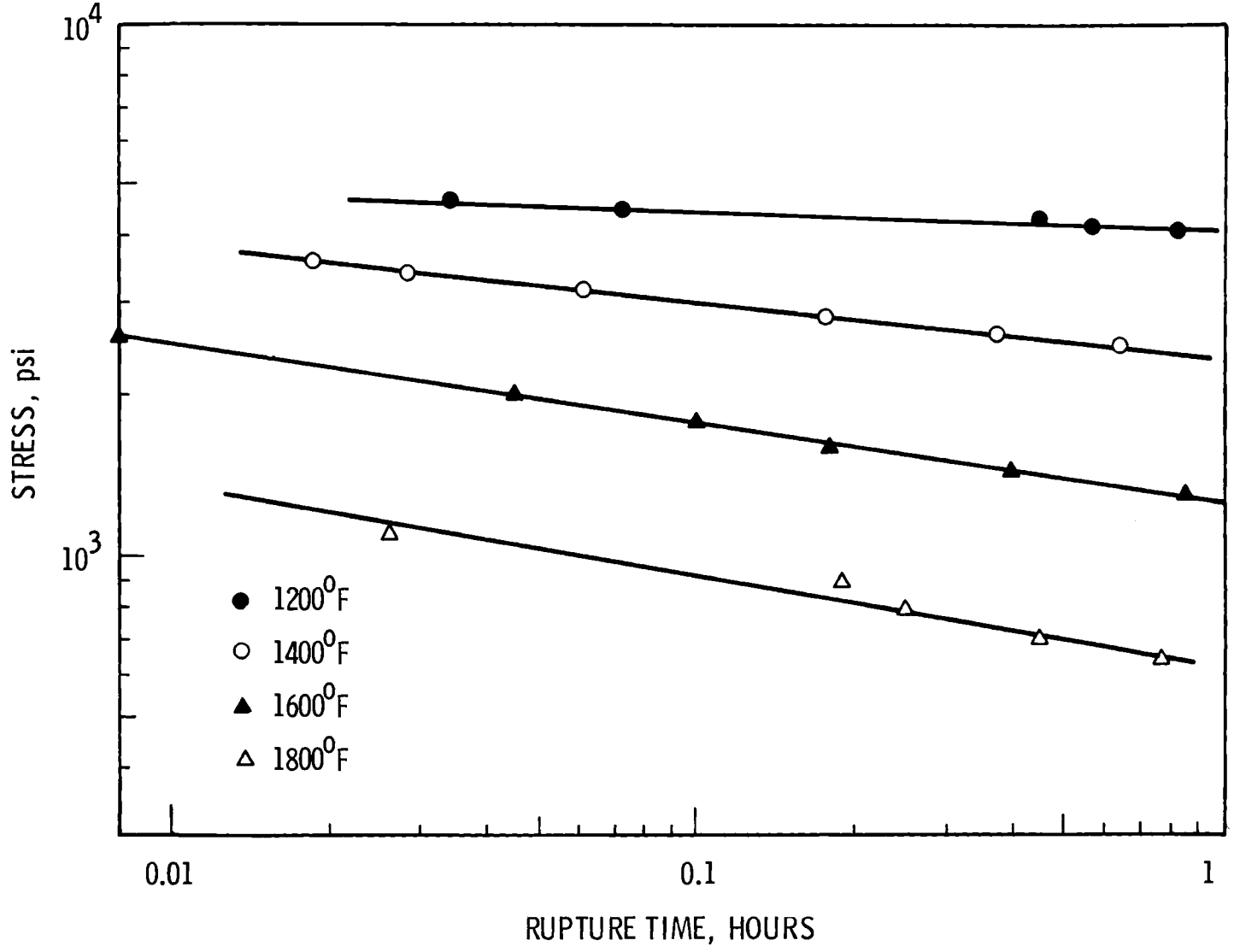

Neg 0691325-9

FIGURE 38. Short Term Stress Rupture G Lot Tubing - Mill Annealed 316 Stainless Steel

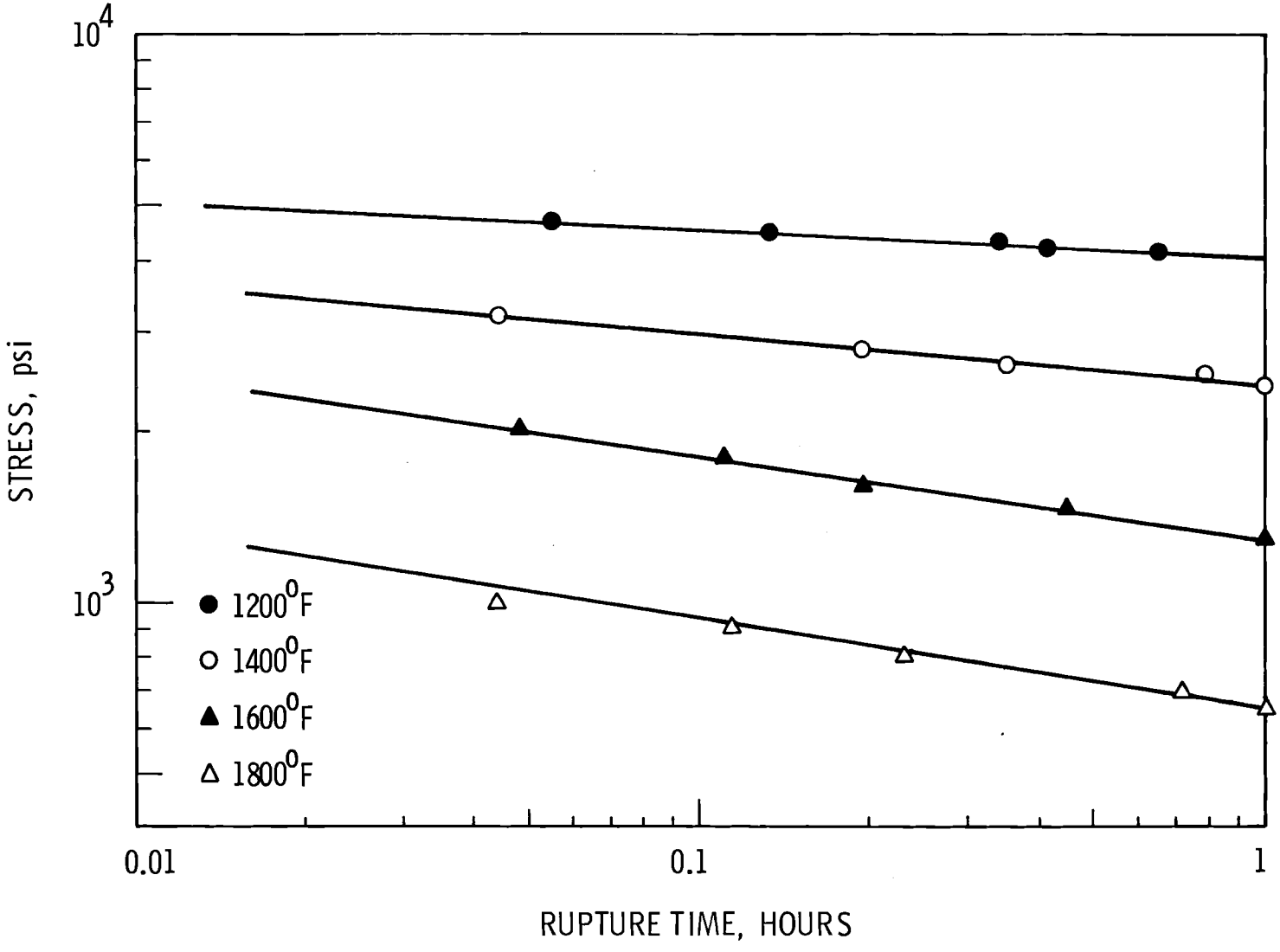

Neg 0691713-1

FIGURE 39. Short Term Stress Rupture H Lot Tubing - Mill Annealed 316 Stainless Steel

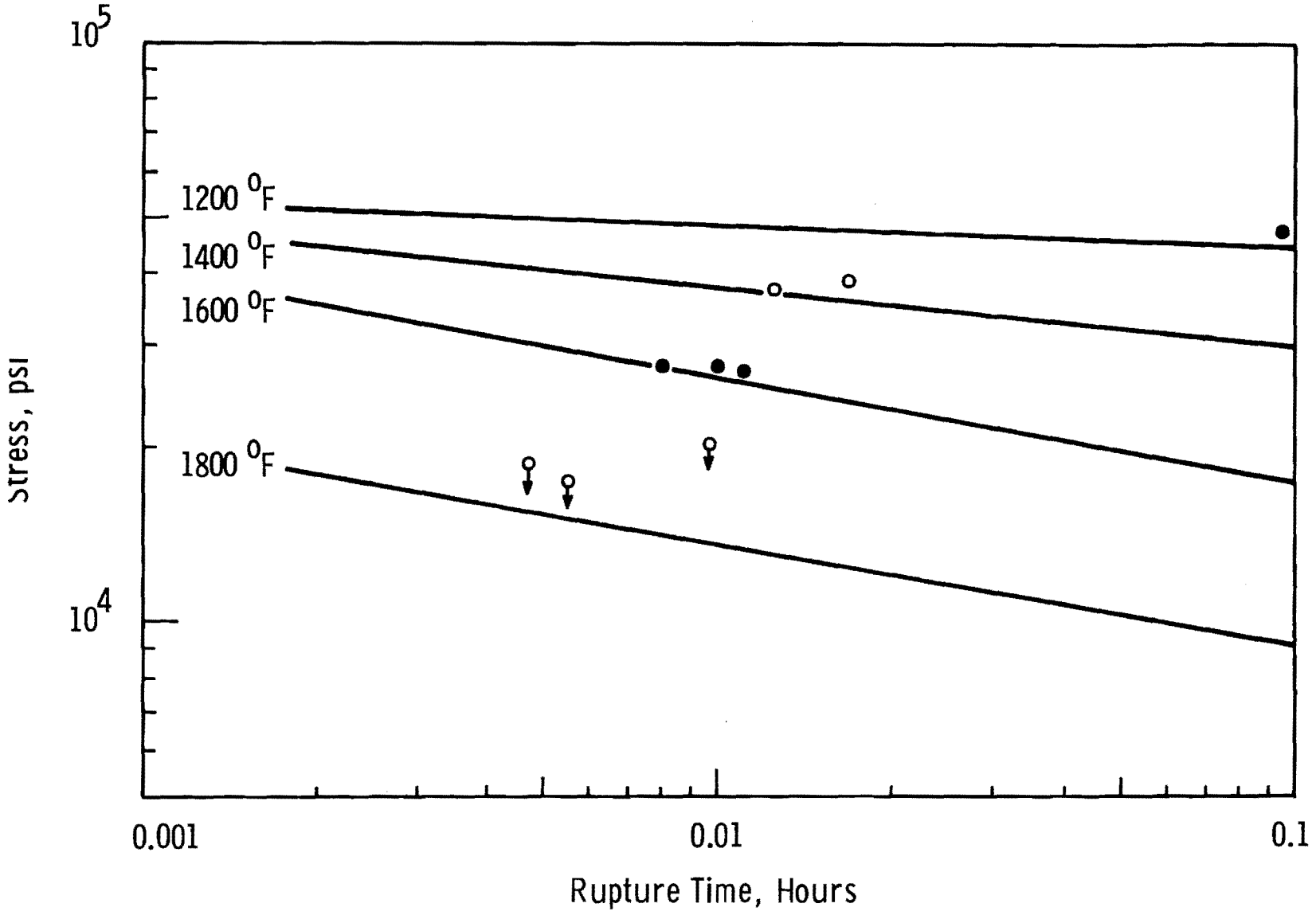

FIGURE 40. Comparison of Burst and Short Term Stress Rupture Data for G Lot Tubing - Mill Annealed 316 Stainless Steel

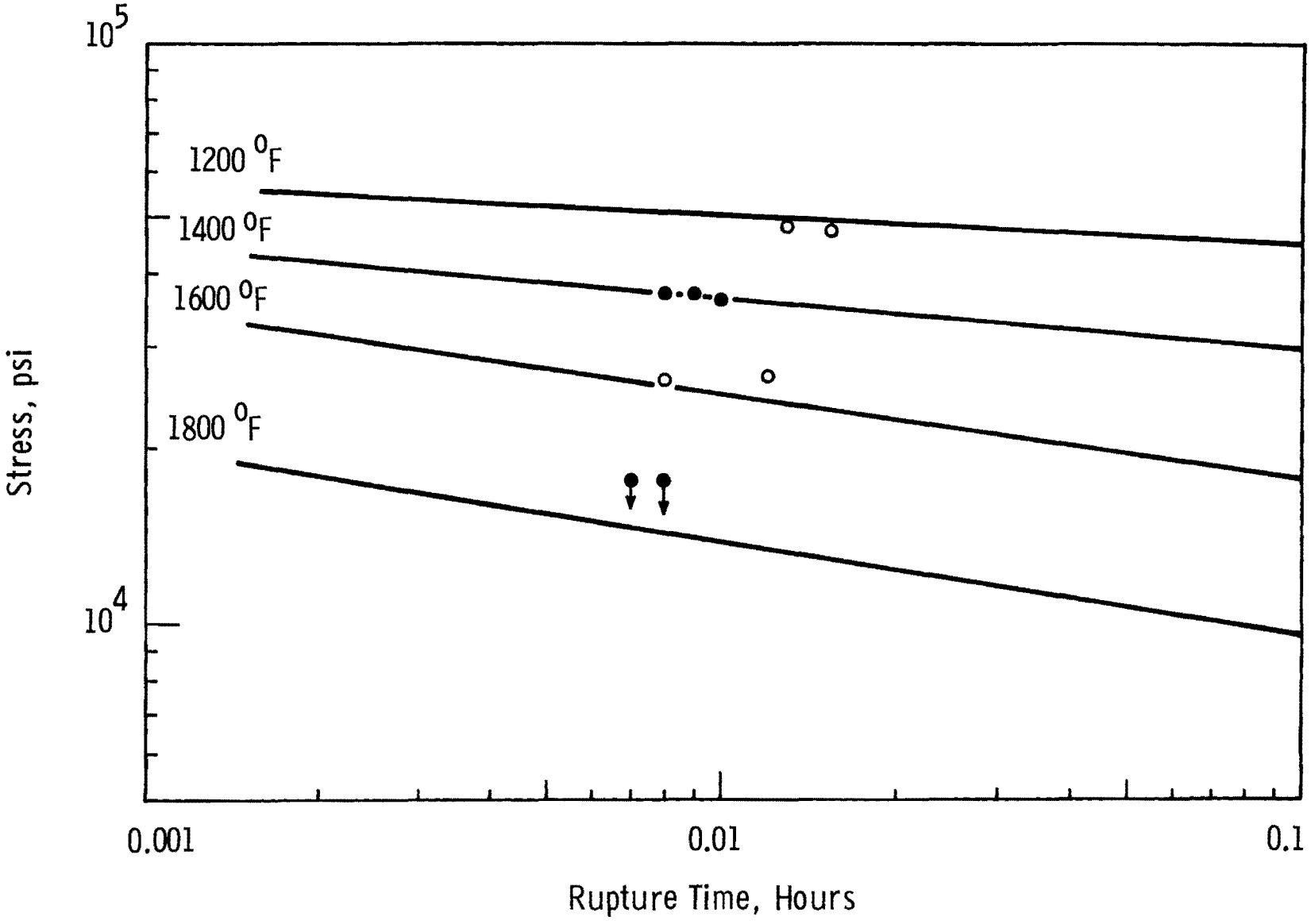

Neg 0691983-6

FIGURE 41. Comparison of Burst and Short Term Stress Rupture Data for H Lot Tubing - Mill Annealed 316 Stainless Steel

TABLE XII

LONG TERM STRESS RUPTURE DATA

Temp.	Gas Pressure, psi	Hoop Stress, psi	Rupture Time Hours	ΔD/D%
E Lot Mill Annealed 304 Stainless Steel				
1200°F	4,810	32,760	9.8	10.1
	4,260	29,010	44.5	12.8
	3,700	25,200	125.0	6.5
	3,310	22,540	268.2	4.4
	3,820	26,010	80.0	---
	3,010	20,500	816.0	6.0
	3,010	20,500	853.0	7.0
F Lot Mill Annealed 304 Stainless Steel				
1200°F	4,260	29,010	5.8	10.1
	3,790	25,800	17.8	10.9
	2,950	20,090	281.9	13.3
	2,580	17,570	1388.9	7.7
	3,670	24,990	41.8	---
	3,310	22,540	112.6	---
G Lot Mill Annealed 316 Stainless Steel				
1200°F	5,150	35,070	8.3	15.7
	4,730	32,210	20.9	22.5
	4,400	29,960	42.4	20.9
	4,110	27,990	84.2	20.5
	4,130	28,130	94.9	18.9
	3,840	26,150	172.1	14.5
	3,670	25,000	327.8	11.3
	3,250	22,130	818.4	9.3
H Lot Mill Annealed 316 Stainless Steel				
1200°F	5,580	38,000	1.5	26.1
	5,150	35,070	3.6	13.0
	4,730	32,210	10.5	13.5
	4,110	27,990	60.5	11.0
	3,670	24,990	222.9	6.9

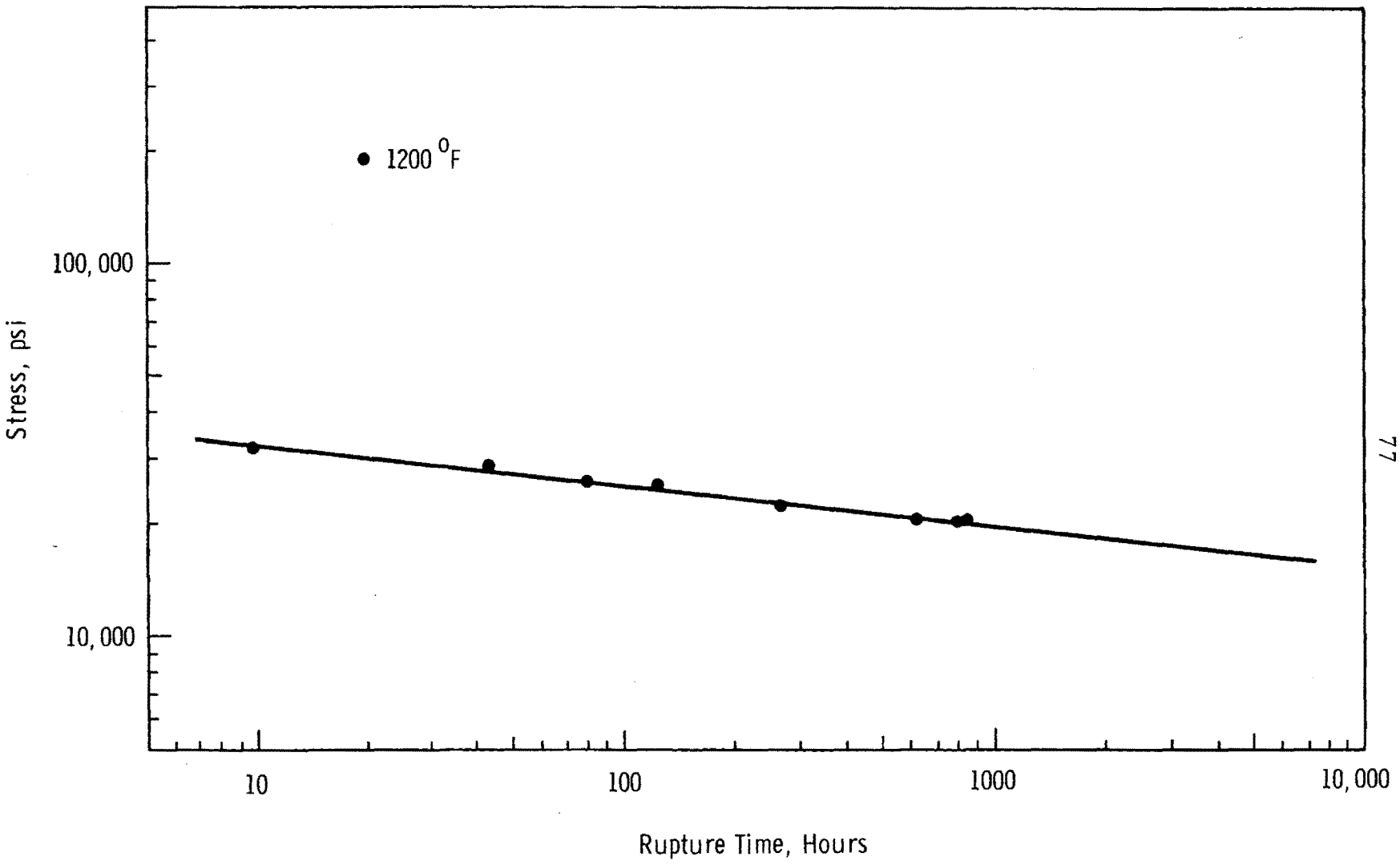

Neg 0684519-2

FIGURE 42. Stress Rupture 1200 °F E Lot Tubing - Mill Annealed 304 Stainless Steel

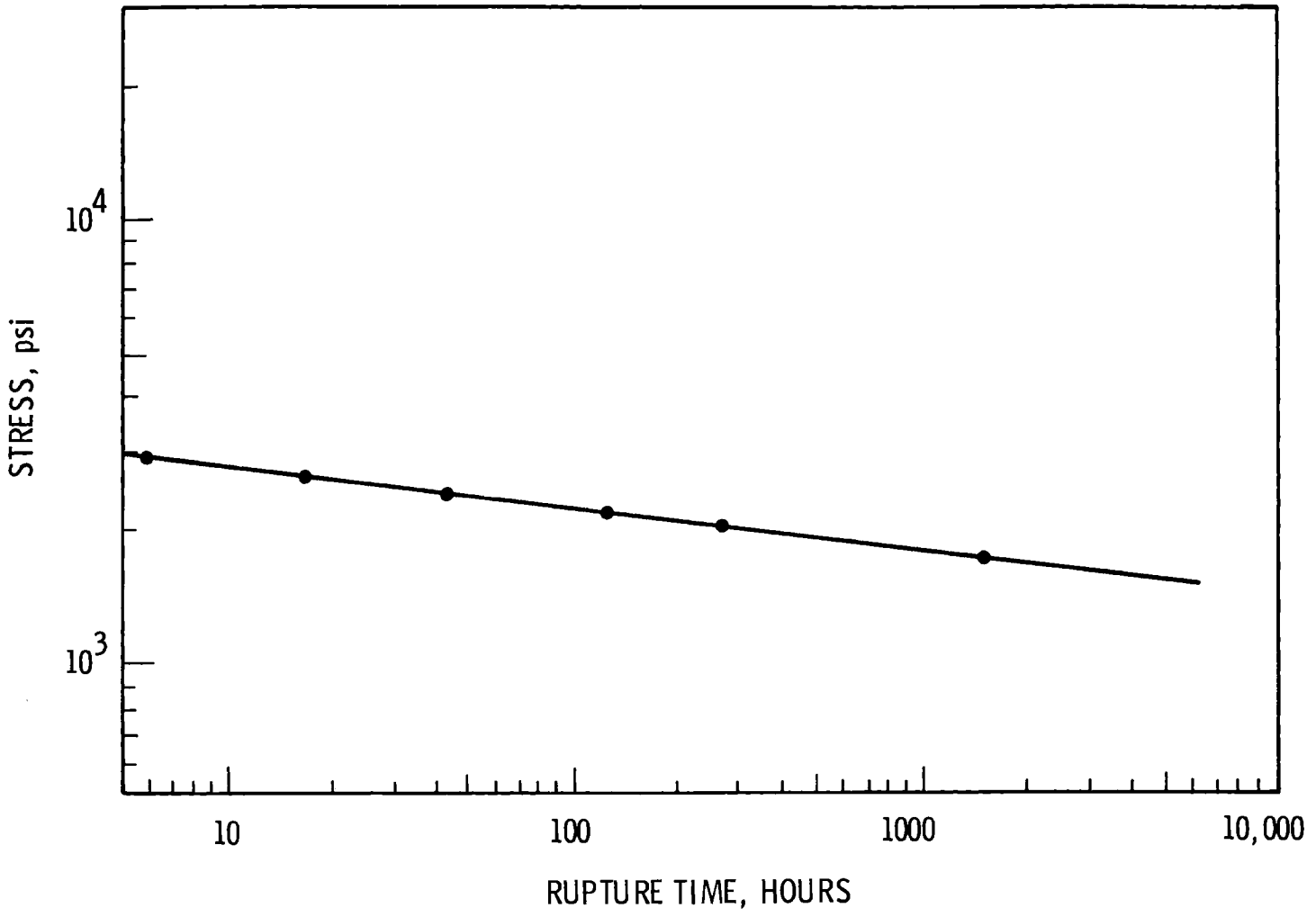

Neg 0691325-10

FIGURE 43. Stress Rupture 1200 °F F Lot Tubing - Mill Annealed 304 Stainless Steel

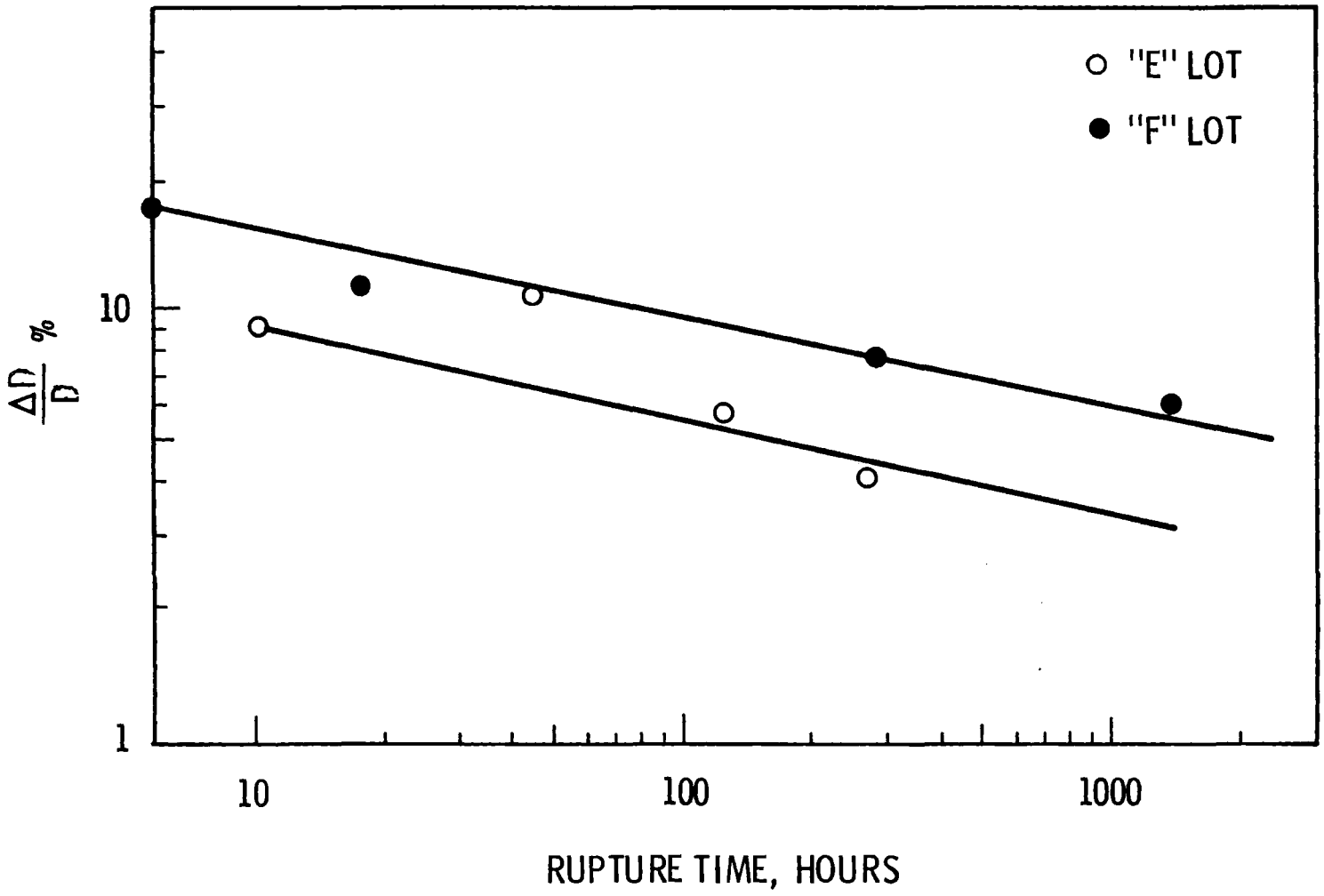

Neg 0691325-1

FIGURE 44. E and F Lot Tubing 1200 °F - Mill Annealed 304 Stainless Steel

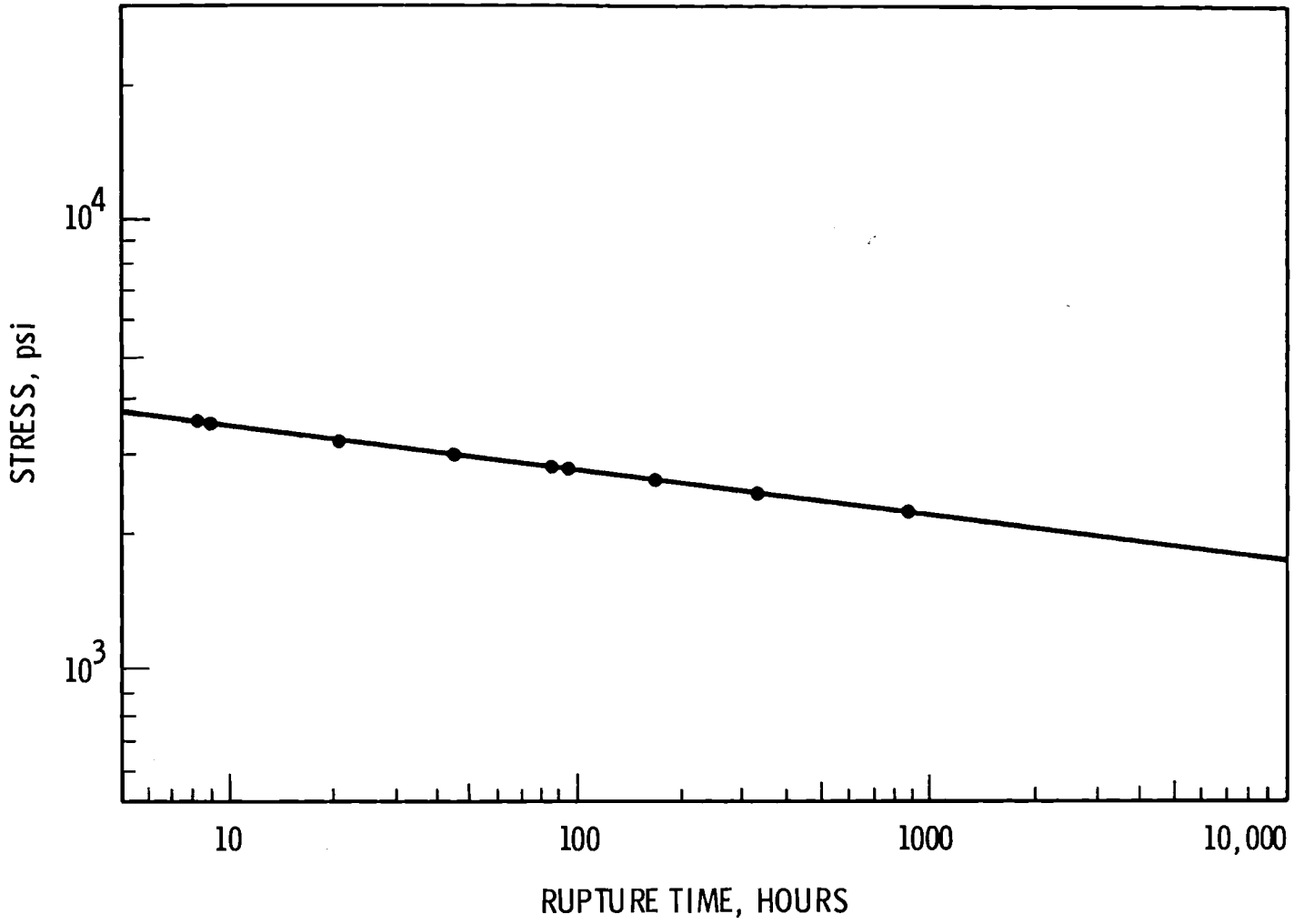

Neg 0691325-7

FIGURE 45. Stress Rupture 1200 °F G Lot Tubing - Annealed 316 Stainless Steel

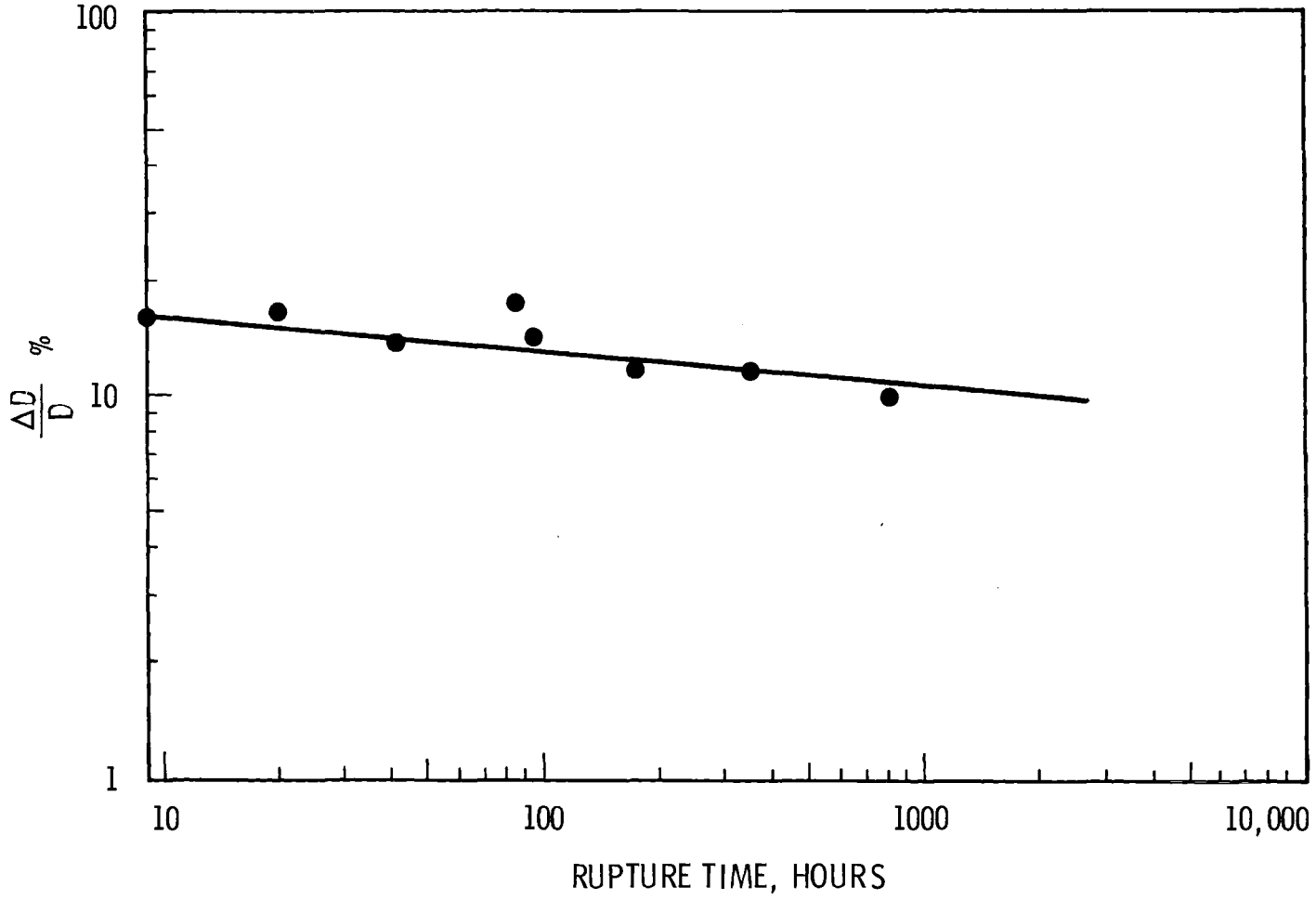

Neg 0691325-8

FIGURE 46. ΔD/D % Versus Rupture Time for G Lot Tubing 1200 °F - Mill Annealed 316 Stainless Steel

Table XIII and the creep curves are presented in Figures 47-50. The effects of grain size and composition cannot be unambiguously accounted for in these tests, however, if one assumes the relationship between interstitial content and creep rate given by Stone[2] holds and the rupture life is assumed to be inversely proportional to secondary creep rate, then the rupture life of the two lot F tests would increase from 24 to 30 hours and 84 to 105 hours at an interstitial concentration equivalent to E lot. The remaining differences in rupture life should be attributed to grain size differences in the absence of side effects such as heat treatment of fabrication variables.

The estimated grain size effect can be applied to the Garofalo equation[5] to calculate the grain size giving minimum creep rates for 304 stainless steel. The above data indicates a grain size of ASTM 7 is optimum for creep resistance.

The biaxial creep curves on F lot specimens, Figures 49-50, are shown as two curves. In both tests the upper curve, dashed line, represents the creep of a localized bulge that appeared near the top of each specimen. Specimen F-1, Figure 50, failed in the bulged area, whereas specimen F-2, Figure 49, did not fail in the bulge. On close examination of the diametrical measurement throughout the test shows that the failed region of F-2 to be slightly constricted, approximately 0.0005 inches. Such a constricted area did not appear on the F-1 specimen. Optical metallography of the two F specimens is in progress to explain the anomalous behavior.

Test E-2 was terminated before failure. Inspection of the specimen after 122 hours at test conditions revealed a crack, Figure 51, which will result in failure if the test is continued.

TABLE XIII

BIAXIAL CREEP RATES AT 1200°F AND σmax = 26,850 psi

Specimen	Measured Hr^{-1}	Corrected Hr^{-1}
E-1	2.78×10^{-4}	---
E-2	2.45×10^{-4}	---
F-1	2.40×10^{-3}	6.9×10^{-4}
F-2	2.79×10^{-3}	8.0×10^{-4}

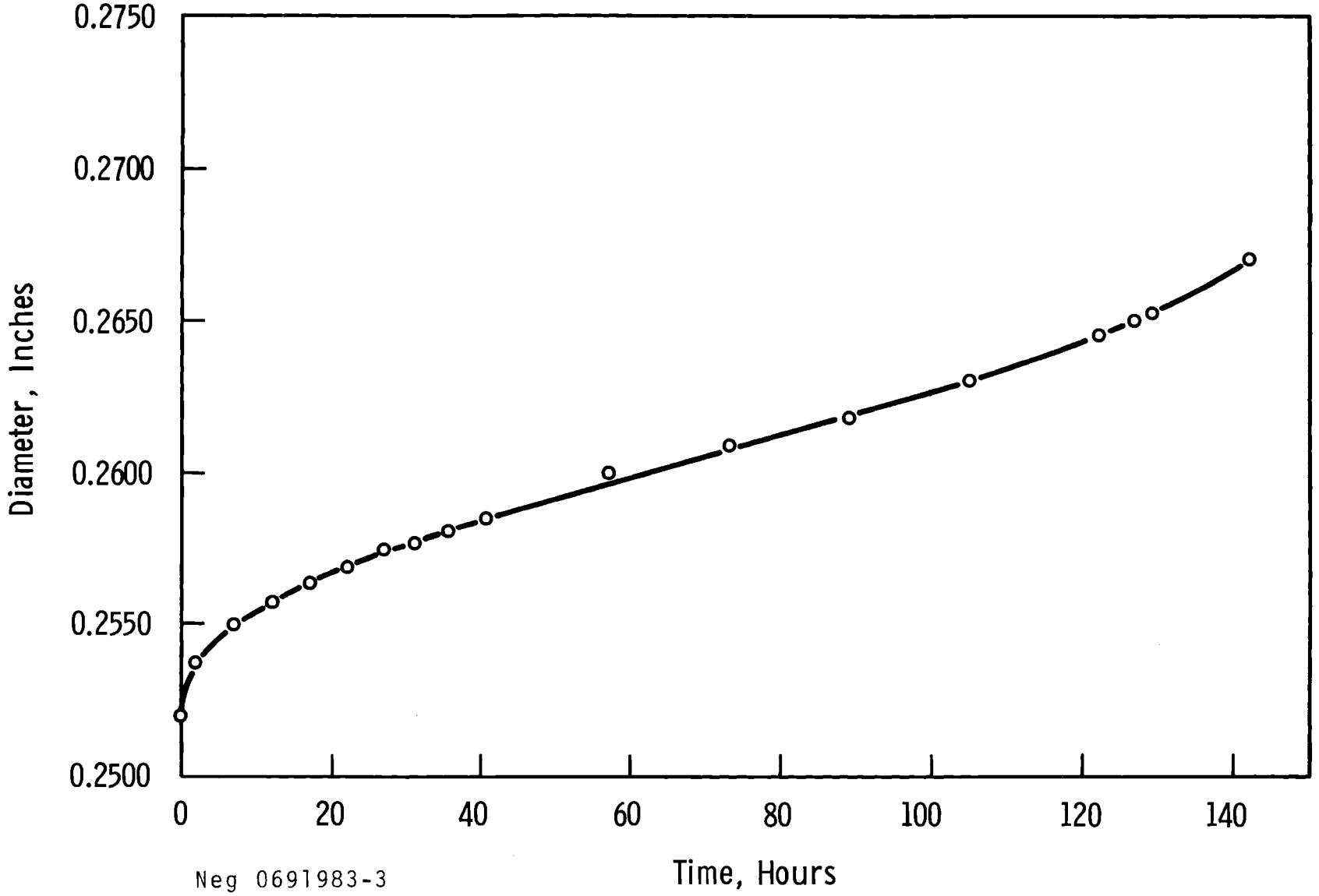

Neg 0691983-3

FIGURE 47. Biaxial Creep - Specimen E-1 1200 °F σ_{max} = 26,850 psi, Tubing Lot E, Mill Annealed 304 Stainless Steel

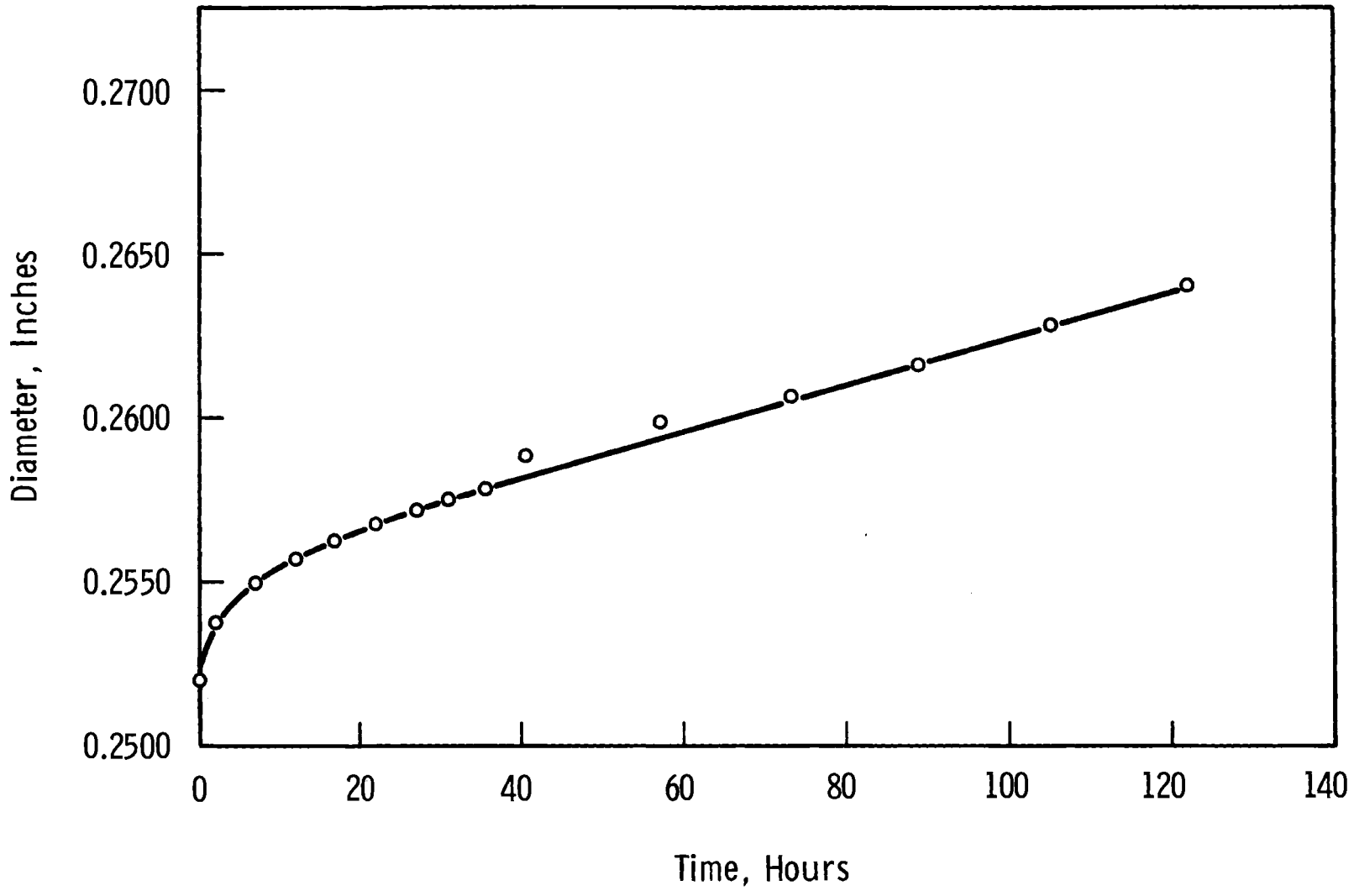

Neg 0691983-2

FIGURE 48. Biaxial Creep - Specimen E-2 1200 °F σ_{max} = 26,850 psi, Tubing Lot E, Mill Annealed 304 Stainless Steel

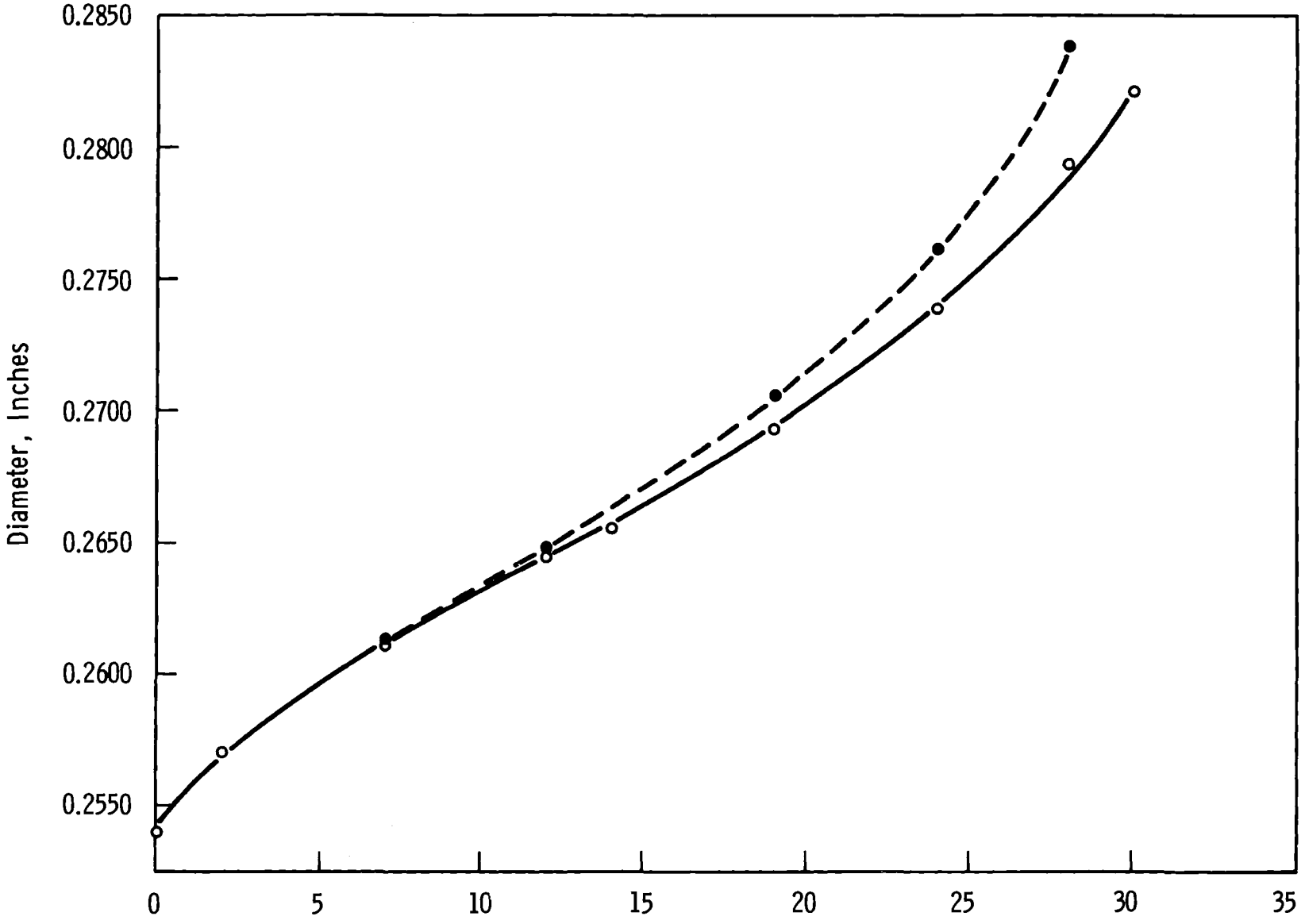

Neg 0691983-1

FIGURE 49. Biaxial Creep - Specimen F-2 1200 °F σ_{max} = 26,850 psi, Tubing Lot F, Mill Annealed 304 Stainless Steel

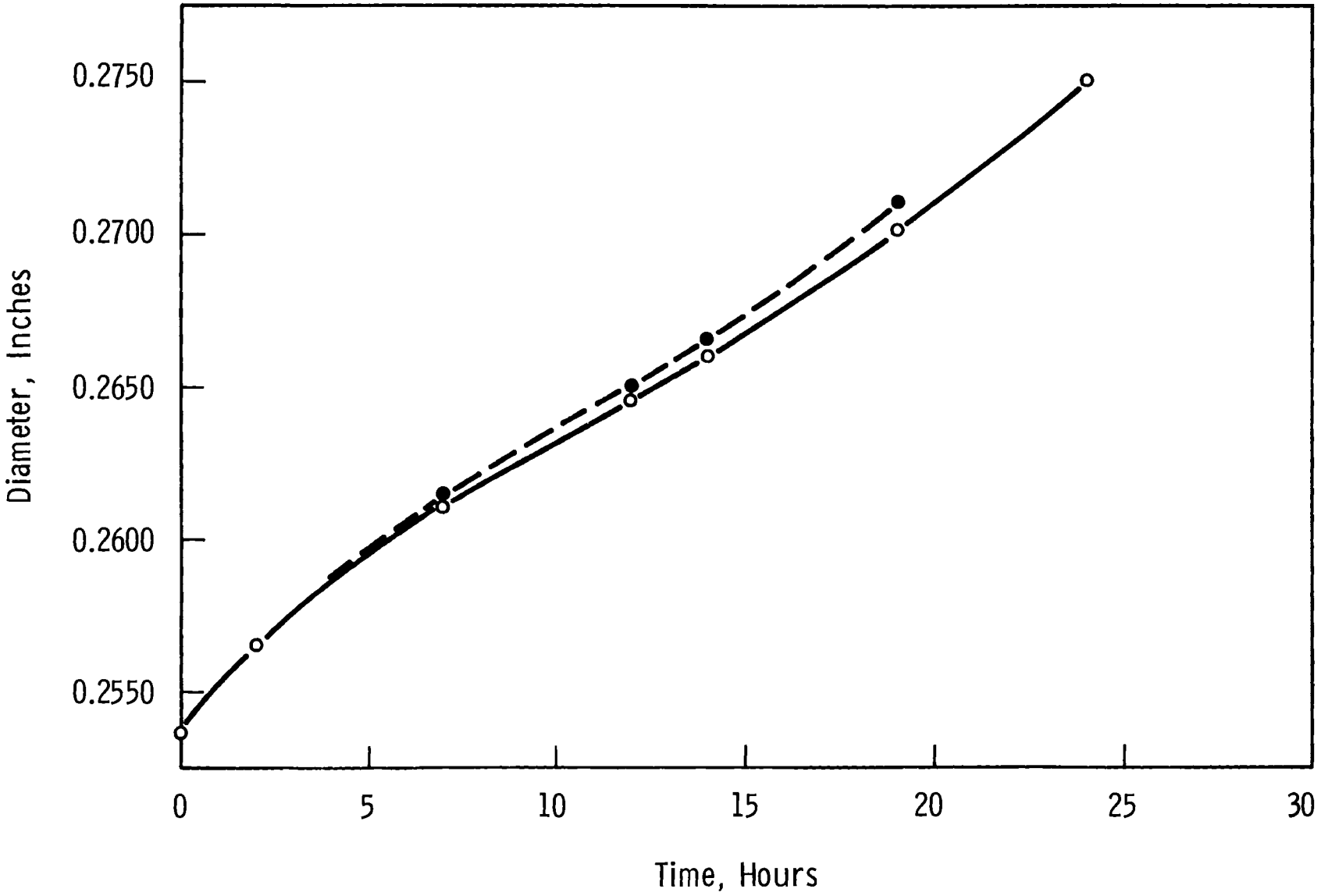

FIGURE 50. Biaxial Creep - Specimen F-2 1200 °F σ_{max} = 26,850 psi, Tubing Lot F, Mill Annealed 304 Stainless Steel

Neg 469635 25X

FIGURE 51. Macrograph of Crack in Biaxial Creep - Specimen E-2
1200 °F σ_{max} = 26,850 for 122 hr

b. EBR-II Irradiations - P. K. McDaniel

The EBR-II irradiations program is to provide coordination and direction for the timely accomplishment of fast reactor irradiations on structural materials. Structural materials irradiation experiments are in various stages of development; some in design, some under construction and others under irradiation in the EBR-II. The status of these experiments is as follows.

A number of subassemblies, X-009, X-101, X-014, X-018, X-021 (including X-021A), X-022, and X-030 containing BNL structural material experiments have been discharged from EBR-II. The suffix "A" designates pin interchange. A summary of these irradiation experiments is given in Table XIV . All flux monitors from these experiments, with the exception of X-010 and X-018 have been counted. Mechanical properties tests of specimens irradiated in X-009 and X-014 have been completed. Uniaxial and biaxial tests on specimens irradiated in X-022 are in progress.

Experiments presently in EBR-II include subassemblies X-019, X-020, X-027, X-067 and full subassemblies X-021, (now X-021B) X-041, and X-057. The details of these subassemblies are given in Table XV.

Subassembly X-067 consists of four pins from Battelle-Northwest, two from Argonne National Laboratory, one from General Electric. The four Battelle-Northwest pins contain specimens for a study of the effect of fast reactor irradiation on 304 and 316 stainless steel weldments in support of the FFTF pressure vessel and fuel ducts. The goal exposure is 1×10^{22} n/cm^2 (E> 0.1 MeV).

This report section will provide for the periodic updating of the status of irradiation experiments in the EBR-II.

TABLE XIV SUMMARY OF EXPERIMENT DISCHARGED FROM EBR-II

Subassembly Designation	Reactor Position	Date Charged	Date Discharged	Type of Specimen	Material	Accumulated Exposure n/cm^2 (4)
X009(1)	4A2	3-24-66	11-15-66	18 Tensile 10 Uniaxial Creep	304 SS	2.0×10^{22}
X010(1)	7F3	3-24-66	4-24-69	18 Tensile 10 Uniaxial Creep	304 SS	6.6×10^{22}
X014(1)	2D1	7-17-66	12-31-66	50 Tensile	304 SS	1.7×10^{22}
X018	2B1	12-6-66	2-25-69	198 Tensile or Uniaxial Creep	304 SS, 316 SS, 348 SS, 321 SS	4.4×10^{22}
X021(2)	2D1	2-27-67	9-16-68	127 Tensile or Uniaxial Creep	304 SS, 316 SS,(3) Ni Base Alloys	3.2×10^{22}
X021A(2)	2D1	9-27-68	11-16-68	86 Density 16 Biaxial Creep 14 Tensile 10 Uniaxial Creep	316 SS(3) Ni Base Alloys	5.0×10^{21}
X022	7C4	2-27-67	6-15-68	595 Tensile or Uniaxial Creep 65 Biaxial Creep	304 SS, 316 SS, 348 SS, 321 SS	1.1×10^{22}
X030(1)	6E1	10-10-67	3-6-68	5 Tensile 3 Uniaxial Creep	304 SS	5.2×10^{21}

) Mark A pins irradiated on space available basis, all others pins are B-7 type.

) Single pin interchange.

) Variety of other alloys also included.

) E>0.1 MeV

TABLE XV SUMMARY OF EXPERIMENT IN EBR-II

Subassembly Designation	Reactor Position	Date Charged	Estimated Discharge Date	Type of Specimens	Material Contained	Accumulated Exposure n/cm^2 (2)	Goal Exposure n/cm^2
X-019	6D2	1-13-67	July 69	64 Tensile 24 Uniaxial Creep	304 SS 316 SS	2.5×10^{22}	1.9×10^{22}
X-020	6B5	1-13-67	July 69	28 Tensile 8 Uniaxial Creep	304 SS 316 SS	2.7×10^{22}	1.9×10^{22}
X-021 (1)	2D1	2-27-67	Aug. 70	501 Tensile or Uniaxial Creep 65 Biaxial Creep	304 SS, 316 SS, 348 SS, 321 SS Ni Base Alloys (3)	4.1×10^{22}	8.8×10^{22}
X-027	4B3	11-21-67	Aug. 70	5 Tensile 3 Uniaxial Creep	304 SS	2.7×10^{22}	5×10^{22}
X-041	7C4	7-24-68	May 70	713 Tensile or Uniaxial Creep 74 Biaxial Creep	304 SS, 316 SS, 321 SS, 348 SS	1.0×10^{22}	3×10^{22}
X-057	2B1	2-24-69	March 71	577 Tensile or Uniaxial Creep 164 Biaxial Creep 58 Density	304 SS, 316 SS, (3) 321 SS, 348 SS, Ni Base Alloys	4.8×10^{21}	6.0×10^{22}
X-067	4FZ	1-5-69	Sept. 69	204 Tensile or Uniaxial Creep 20 Fatigue	304 SS, 316 SS, Weldment	None	1×10^{22}

1) Original space available with two single pin interchanges.

2) Accumulative to end of run 33, (E>0.1 MeV)

3) Variety of other alloys.

c. Biaxial Stress-Rupture Studies - R. W. Barker

The objective of this program is to determine the combined effects of environment and fast reactor irradiation on the biaxial stress-to-rupture properties of candidate fast reactor cladding alloys. The current program is specifically directed at providing a description of material change during fast reactor service.

Biaxial stress-rupture tests have been initiated on AISI Type 304 stainless steel irradiated to $\sim 0.8 \times 10^{22}$ n/cm^2 (E >0.1 MeV) in EBR-II. The specimens being tested are composed of segments of irradiated cladding (0.208-in. diameter x 0.008-in. wall) to which unirradiated fittings have been welded.[6,7]

Four tests on the irradiated cladding have been completed. The test temperature was 1200°F and the environment and pressurizing gases were argon. Specimens were stressed sufficiently to cause rupture in 0.1 to 1,000 hours in unirradiated material. The test results are summarized in Table XVI. Hoop stresses are determined using the hoop stress formula for thin walled tubes:

$$\sigma = \frac{PD}{2t}$$

where P = internal gas pressure

D = inside diameter

t = minimum wall thickness

Irradiated test numbers 4 and 5 failed by the gas pressure leaking through a pin hole or fissure in the cladding. Test number 7 failed in an explosive manner, tearing the specimen in three separate pieces. The fourth test, number 11, lost pressure slowly at failure, the rupture being a very small fissure or pin hole. The small localized rupture is not characteristic

TABLE XVI

Biaxial Stress-Rupture Tests on AISI Type 304 Stainless Steel Irradiated To ∿ 0.8×10^{22} n/cm^2 (E >0.1 MeV) in EBR-II. Test Temperature was 1200°F. The Irradiation Temperature was 1000°F ± 100.

UNIRRADIATED SPECIMENS*				IRRADIATED SPECIMENS		
Hoop Stress (psi)	Rupture Time (hrs)	Rupture Strain (%)	Irradiated Test No.	Hoop Stress (psi)	Rupture Time (hrs)	Rupture Strain (%)
34,000	0.1	16.5	11**	34,000	0.06	2.4
29,000	1.0	14.5	7	29,000	1.55	14.8
19,000	100	11.8	5	19,000	30.4	0.96
15,800	1000	10.5	4	15,800	110	2.66

*Stress and strain values were taken from unirradiated specimen test curves at rupture times shown.

**Test specimen appeared to have failed prematurely.

of other tests at the pressures required for short rupture times. Normally, the energy of the compressed gas serves to explode the test piece in a violent manner, once the fissure has developed. Rupture strain appears less than that which might be expected at rapid creep rates. As a result of the peculiar behavior this test is weighted very low in comparison with the other tests in analyzing the data.

Based on these initial tests, the data shown in Figure 52, suggest some increase in rupture strength for short rupture times, and loss in rupture strength for longer rupture times, for irradiated AISI type 304 stainless steel cladding. Thus the line describing the irradiated data crosses the unirradiated control curve at about 3 to 5 hours. The data further suggest an increasing loss in rupture life with increasing rupture times.

A great deal of scatter is observed in the rupture strain, shown in Figure 53. However, it can be observed that rupture strain of irradiated cladding will be markedly less than of unirradiated cladding for the longer rupture times.

Biaxial stress-rupture tests on AISI type 316 stainless steel irradiated in EBR-II to $\sim 0.8 \times 10^{22}$ n/cm^2 (E >0.18 MeV) were begun. Tests for short rupture times at 1200 °F have been completed. The data obtained from these tests is given in Table XVII.

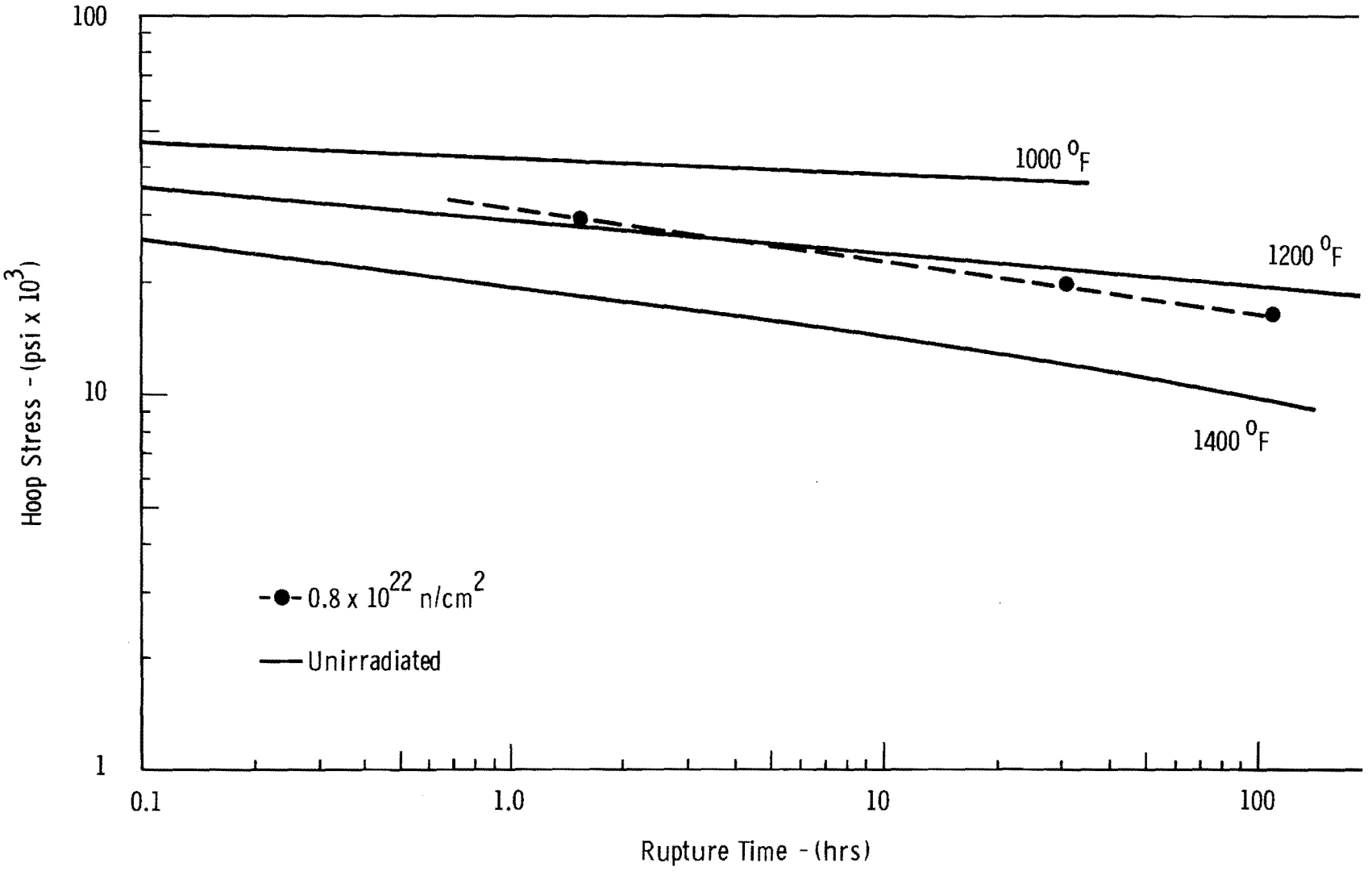

Neg 0691998-1

FIGURE 52. The Effect of Biaxial Stress on the Rupture Life of AISI Type 304 Stainless Steel Irradiated to ~0.8 × 10^{22} n/cm^2 (E > 0.1 MeV) at Approximately 1000 °F

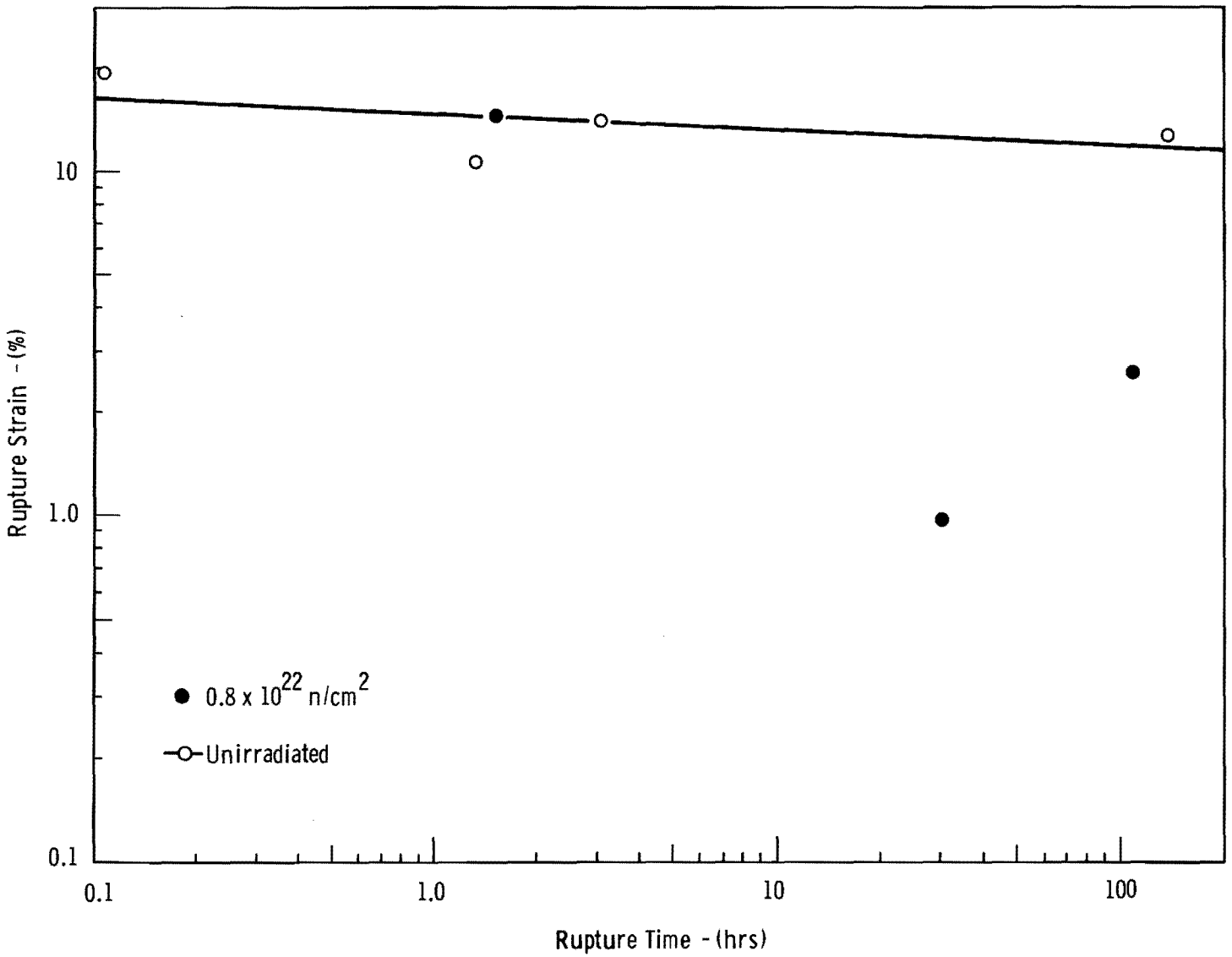

Neg 0691998-2

FIGURE 53. The Effect of Biaxial Stress on the Rupture Strain of AISI Type 304 Stainless Steel Irradiated to ~0.8 × 10^{22} n/cm^2 (E > 0.1 MeV) at Approximately 1000 °F

TABLE XVII

BIAXIAL STRESS-RUPTURE TESTS ON AISI TYPE 316 STAINLESS STEEL IRRADIATED TO $\sim 0.8 \times 10^{22}$ n/cm^2 (E >0.1 MeV) IN EBR-II TEST TEMPERATURE WAS 1200°F. THE IRRADIATION TEMPERATURE WAS 1000°F ± 100.

UNIRRADIATED SPECIMENS*				IRRADIATED SPECIMENS		
Hoop Stress (psi)	Rupture Time (hrs)	Rupture Strain (%)	Irradiated Test Number	Hoop Stress (psi)	Rupture Time (hrs)	Rupture Strain (%)
42,000	0.1	+	-			
36,000	1.0	10	12	36,000	2.1	1.9
30,000	10.0	7	13	30,000	32	+
24,500	100.0	5	-			

*Stress and strain values were taken from unirradiated test curves at rupture times shown.

+ To be measured

d. Damage Anlaysis - J. L. Straalsund and H. R. Brager

The objectives of this effort are to determine the radiation induced swelling characteristics of FFTF alloys, to relate fast reactor induced substructural changes in microstructure to corresponding changes in mechanical properties,and to provide a basis for extrapolation and interpolation of data using both microscopic modeling and empirical approaches.

Recent experiments concerning the effects of fast reactor irradiation on stainless steels have demonstrated that a considerable volume change occurs during neutron bombardment.[8] Unlike volume changes in fuel materials, swelling in structural alloys and pure metals is due to the condensation of irradiation-produced excess vacancies in the form of cavities. United Kingdom investigators have found as much as 6.8% volume change in 316 stainless steel irradiated to 7.8×10^{22} n/cm^2 total fluence. Volume changes of this magnitude, if not taken into account, are sufficient to cause distortion in reactor components.

Maximum target fluences for FFTF are as high as 10^{24} n/cm^2. Since such a high fluence cannot be attained in a reasonable time using currently available reactors, design data for high exposures will be based on extrapolation using physically realistic swelling models, the approach taken in this study. study

Equations describing the effect of fluence and temperature on swelling in solution treated 304 and 316 stainless steel and in 20% cold worked 316 stainless steel have been refined and the results agreed upon by Westinghouse and PNL. The agreed upon equations have the general form:

$$\frac{\Delta V}{V} = A(\phi t)^n [e^{-Q1/RT} - \alpha\, e^{-Q2/RT}]$$

Specifically, the equations are as follows:

Solution Treated 304 and 316:

$$\frac{\Delta V}{V} = 5.0 \times 10^{-36} (\phi t)^{1.66} \left[e^{-\frac{6800}{RT}} - (1.87 \times 10^4)\, e^{-\frac{27{,}000}{RT}} \right] \text{- - - - (1)}$$

20% Cold Worked 316:

$$\frac{\Delta V}{V} = 9.4 \times 10^{-33} (\phi t)^{1.48} \left[e^{-\frac{5600}{RT}} - (1.78 \times 10^5)\, e^{-\frac{30{,}000}{RT}} \right] \text{- - - - (2)}$$

where $\frac{\Delta V}{V}$ = percent volume change

ϕt = neutron fluence, E >0.1 MeV

Q = activation energy in cal/mole - °K

Equation (1) was developed by using regression analysis to fit an equation of the form:

$$\frac{\Delta V}{V} = A(\phi t)^n\, e^{-Q/RT} \qquad \text{- - - - (3)}$$

to 37 data points selected from available bulk density measurements of type 304 stainless steel components and specimens taken from the EBR-II reactor. In the selection of data, only points corresponding to locations within 10 inches of the midplane were used. The analysis resulted in the following equation

$$\frac{\Delta V}{V} = 5.0 \times 10^{-36} (\phi t)^{1.66}\, e^{-\frac{6800}{RT}}$$

The second temperature dependence term in equation (1), $(\alpha e^{-Q2/RT})$, was empirically fit to force the swelling to peak at 625°C and to go to zero at 750°C. The peak temperature of 625°C was chosen primarily because there are indications of such a peak near 625°C in the UK 316 S.T. fuel pin data.

An equation was developed for the solution treated 316 stainless steel by assuming the same fluence dependence as obtained for 304 stainless steel and using the U.K. fuel pin diameter changes to calculate the temperature dependence and pre-exponential factor. It was assumed in this analysis that the pin diameter increase was due entirely to clad swelling. For temperatures above 450 °C, the results of this equation agreed with equation (1) within 10% of the predicted swelling values over all ranges of fluence. It was, therefore, decided that equation (1) could be used for both 304 stainless steel and 316 stainless steel in the solution treated condition. Figure 54 shows the fluence dependency given by equation (1) at 400 °C and 600 °C. Widening of the confidence bands is due to the lack of data beyond about 1×10^{22} n/cm^2. No confidence limits may be placed on this equation above about 600 °C.

Equation (2) for cold worked 316 stainless steel has been agreed upon by BNW and Westinghouse up to a total volume change of 1% or temperatures less than 500 °C. In the development of equation (2), U.K. data on fuel pin diameter increases and void volume based on electron microscopy were used. In a preliminary analysis, all of the data available were fit to an equation of the form given by equation (3). However, inspection of the results indicated that at high temperatures and fluences (density changes in excess of about 1%) the swelling behavior departed from that predicted from lower temperature data. A change in mechanism apparently occurred at

304, 316 STAINLESS STEEL

$$\Delta V/V = 5.0 \times 10^{-36} (\phi t)^{1.66} \left\{ e^{-6800/RT} - 1.87 \times 10^{4} e^{-27000/RT} \right\}$$

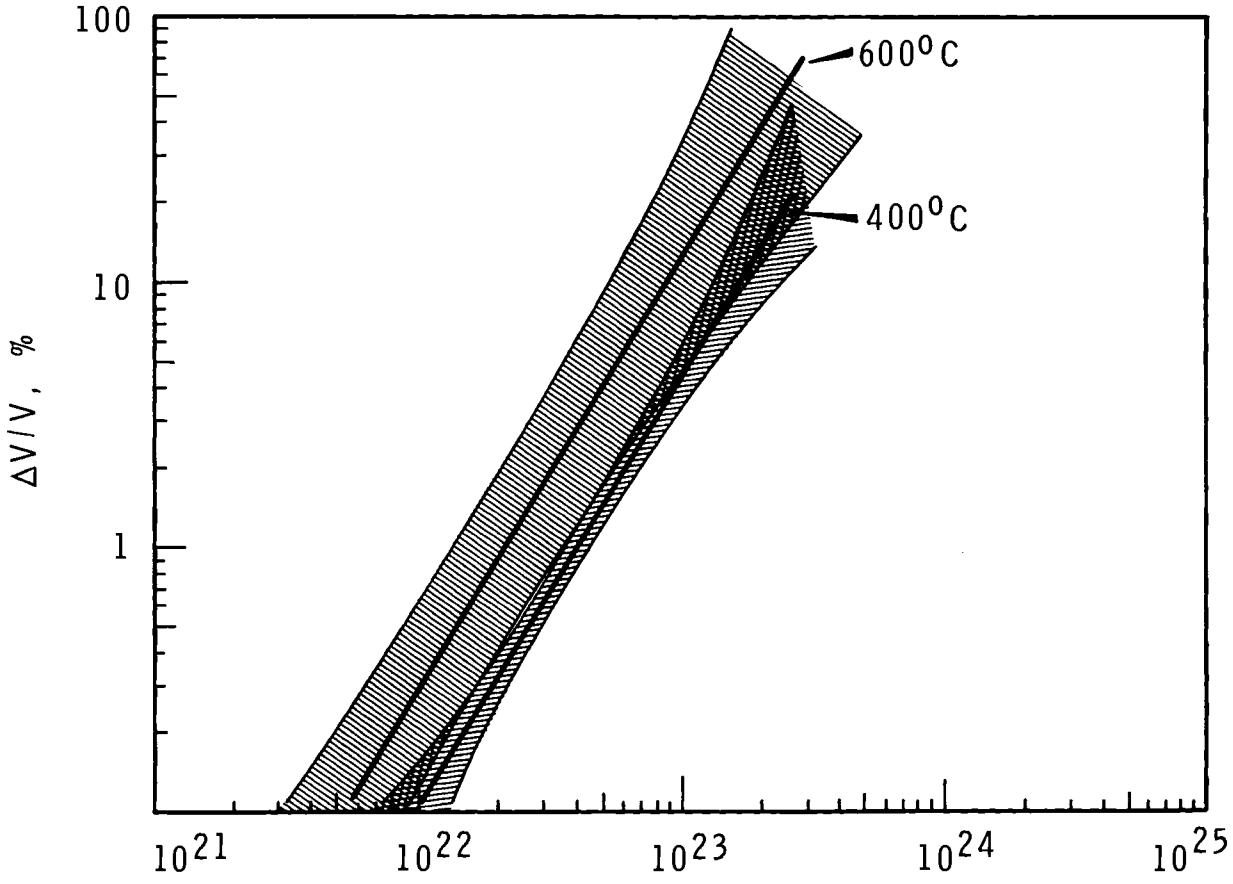

FIGURE 54. Swelling in Solution Treated AISI Types 304 and 316 Stainless Steels

the higher temperatures, which resulted in a much greater increase in pin diameters. It should be noted that all of the data points indicating this increase were associated with the upper sections of U.K. Mark II interior pins.

The data at high temperatures (alternatively at volume changes in excess of 1%) are too fragmentary to allow meaningful analysis. Therefore, equation (2) was developed only from data at temperatures below 530°C.

If the high temperature-high fluence swelling data for cold worked 316 are meaningful, the effect may be due to one of the following mechanisms.

(1) A large portion of the pin diameter increase at high temperatures may be due to fuel swelling. This appears doubtful as the microscopy measurements of void volume appear to agree with the $\Delta D/D$ measurements. There is presently some uncertainty, however, as to whether the microscopy data are representative of the pins in question. Thus one must consider fuel swelling in this region as a possibility, in which case equation (2) represents our best estimate for swelling in cold worked 316 stainless steel at the high as well as low ranges of temperature and fluence. Figure 55 shows the fluence dependency given by equation (2) at 400°C and 600°C.

(2) At high irradiation temperatures the swelling rates may increase with fluence. At the present there is no means of determining if this is the case.

316 STAINLESS STEEL
20% COLD WORKED

$$\Delta V/V = 9.4 \times 10^{-33} (\Phi t)^{1.48} \left\{ e^{-5600/RT} - 1.78 \times 10^{5} \, e^{-30000/RT} \right\}$$

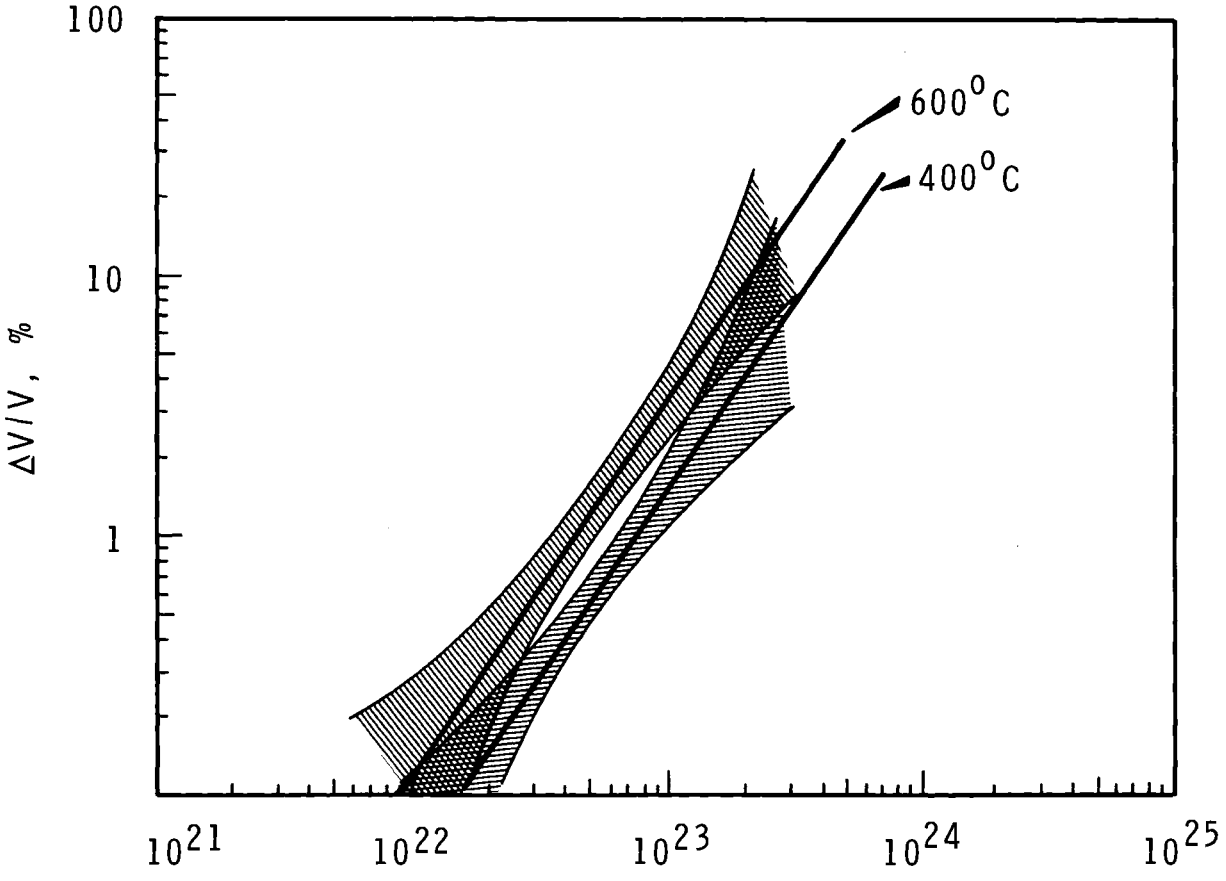

Neg 0692163-2

FIGURE 55. Swelling in 20% Cold Worked M316 Stainless Steel. Refer to text for Limitations on the Use of this Curve

(3) Recovery of cold work may occur in the pins during long exposures at high temperatures (above 500-550°C). If this is the case, one may expect cold worked 316 swelling behavior to be asymptotic to equation (1). Both pin diameter data and microscopy data for temperatures above about 530°C and fluences greater than 3.5×10^{22} n/cm^2 (E >0.1 MeV) indicate swelling close to that given by equation (1).

In view of the few data available for developing equations for swelling in cold work 316 stainless steel it appears that for the present, the best design procedure is to use equation (2) for situations in which the temperature is 500°C or less and predicted swelling is less than 1%, and assume that the swelling will be between the limits of equation (1) and equation (2) at higher fluences and temperatures.

A linear regression technique was used to determine if there is any significant flux rate effect indicated in the PNL swelling data for 304 stainless steel. The data in Table XVIII was fit, using linear regression analysis, to an equation of the form:

$$\frac{\Delta\rho}{\rho} = A\ \phi^x t^y e^{-Q/RT}$$

where ρ is the density, ϕ is the flux (n/cm^2 sec. E >0.1 MeV), t is the time (sec.), and Q, R, and T have their usual meanings.

The effective time for each of the components in Table XVIII was determined by dividing the fluence by the flux. Only the points representing positions 10 inches or less from the reactor midplane were used. The exponents were found to be x = 1.56 (σ=0.40) and y = 1.78 (σ=0.46) where σ is the standard deviation. The small difference between the two exponents, in comparison with the standard deviations, indicates that there is no significant difference between the two exponents.

TABLE XVIII

PNL SWELLING DATA FOR 304 STAINLESS STEEL

Component	Vertical distance from midplane (inches)	Radial distance from centerline (inches)	Calculated Flux E >0.1 MeV (n/cm^2 sec. x 10^{-15})	Calculated Fluence E >0.1 MeV (n/cm^2 x 10^{-22})	Irrad. Temp. °C	$\Delta\rho/\rho$ %
Experiment	- 5	2.5	1.4	1.92	400	0.13
Capsule	- 2		1.66	2.25	420	0.27
X-011	+ 2		1.66	2.25	440	0.33
(2F1)	+ 6		0.81	1.10	450	0.34
	+ 9		0.99	0.66	450	0.13
EBR-II	-17.7	4.6	0.19	0.83	370	0.14
Safety	-12.0		0.52	2.33	370	0.41
Rod Thimble	- 7.0		0.98	4.34	370	0.93
(3D1)	- 5		1.20	5.34	370	1.55
	- 2.5		1.40	6.25	380	2.44
	0		1.52	6.75	390	3.09
	+ 2.5		1.40	6.25	400	2.41
	+ 5		1.20	5.33	420	1.53
	+ 7		0.98	4.34	430	0.87
	+12		0.52	2.33	450	0.47
	+17.7		0.20	0.92	460	0.27
	+22.7		0.06	0.25	470	0.11
EBR-II	-13.9	9.0	0.22	0.88	370	0.12
Control	-11.4		0.31	1.25	370	0.29
Rod Thimble	-10.2		0.37	1.50	370	0.24
(5C3)	- 4.7		0.72	2.92	370	0.51
	+ 1.7		0.87	3.50	400	1.15
	+ 6.7		0.56	2.26	430	0.88
	+10.0		0.39	1.58	440	0.31
	+14.8		0.18	0.73	460	0.19
	+19.1		0.12	0.51	460	0.06
	+20.3		0.07	0.29	460	0.05
	+22.3		0.04	0.18	460	0.05
	+25.7		0.01	0.07	460	0.05
EBR-II Fuel	-12	6.1	0.44	1.08	370	0.29
Subassembly	- 7		0.82	2.00	370	0.37
Thimble	- 5		1.09	2.66	370	0.54
X-G05	- 2.5		1.30	3.16	380	0.80
(4C2)	0		1.40	3.41	390	1.27
	+ 2.5		1.30	3.16	400	1.35
	+ 5		1.09	2.66	420	0.92
	+ 7		0.82	2.00	430	0.47
	+12		0.44	1.08	450	0.22
	+17.7		0.18	0.45	460	0.15
	+22.7		0.07	0.19	470	0.05
	+27.7		0.02	0.05	470	0.06
	+31		0.002	0.006	470	0.04

Transmission electron microscopy studies on austenitic stainless steels are being conducted to provide information for interpreting fast reactor irradiation effects and to assist in both the formulation of material irradiation behavior models and the improvement of the performance of austenitic stainless steel in reactor environments.

The microstructure of solution-treated type 316 stainless steel Figure 56, irradiated in the EBR-II at 900 °F t a fast fluence of 0.8×10^{22} n/cm^2 (E >0.1 MeV), appears to be quite different from the previously reported microstructure of type 304 stainless steel. Figure 57 at comparable irradiation conditions. These microstructure features can be divided into three types; cavities with a density of 5×10^{13}/cm^3, faulted loops, and small polyhedral ($M_{23}C_6$) carbide precipitates.

The 316 stainless steel specimen contained fewer cavities (about 2×10^{12}/cm^3, based on stereoscopic examination) and the cavities did not have the usual sharp border observed in micrographs of voids in irradiated 304 stainless steel. The cavities in the 316 stainless steel ranged in diameter from 100 to 1000 Å and occupied about 0.1% void volume. The fluence is too low to quantitatively determine if there is a significant difference in irradiation swelling between annealed 304 and 316 stainless steel.

In addition, the 316 stainless steel contained smaller and fewer faulted loops than did 304 stainless steel and a low density dislocation network (about 3×10^8/cm^2 was evident. The dislocations were usually curved and formed either partial or a complete loops.

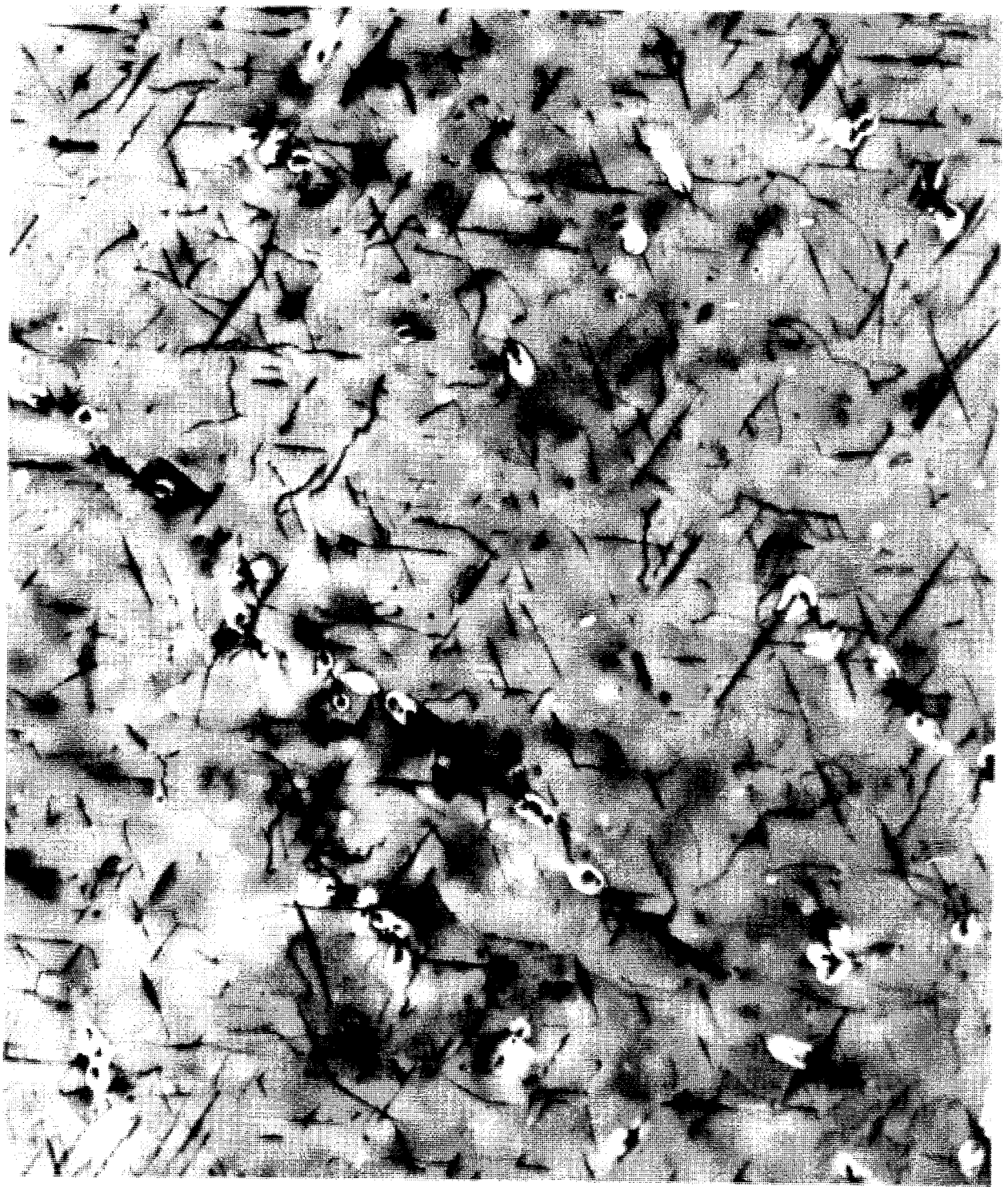

Neg 6487-B

FIGURE 56. Bright Field Micrograph of Solution Treated Type 316 Stainless Steel Irradiated in the EBR-II at 900 °F to 0.8 × 10^{22} n/cm^2 (E > 0.1 MeV)

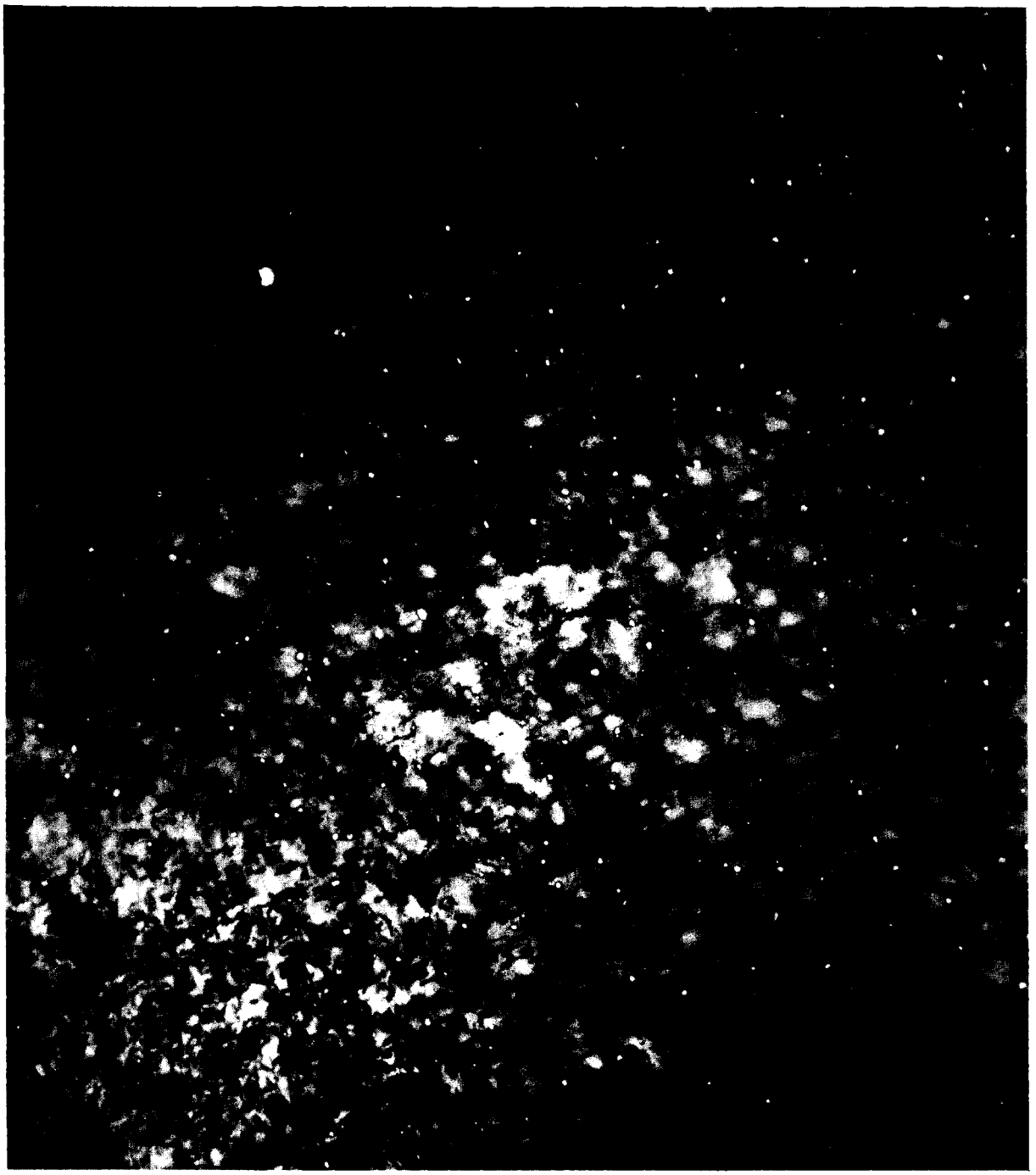

Neg 6020B

FIGURE 57. Bright Field Micrograph of Type 304 Stainless Steel Irradiated in the EBR-II at 860 °F to 0.7×10^{22} n/cm^2 (E > 0.1 MeV)

The most significant difference between the microstructure of the irradiated type 316 stainless steel and the type 304 stainless steel was the formation of rod- or needle-shaped precipitates in the 316 stainless steel. The precipitates were nearly uniformly distributed throughout the matrix, with the long axis of the precipitate parallel to the <111> direction of the matrix. The precipitates were analyzed by X-ray diffraction and electron diffraction of extraction replicas. Both the polyhedral and needle shaped precipitates were $M_{23}C_6$. The morphology of both precipitates is clearly shown by the micrograph of the extraction replica, Figure 58.

It appears that the fast neutron irradiation at 900°F induced the carbide precipitation in the type 316 stainless steel. An unirradiated thermal control sample of the same heat of material was annealed for 3050 hours at 900°F, a time equal to that experienced by the irradiated material in the reactor. The unirradiated thermal control specimens did not contain visible precipitates either at grain boundaries or in the matrix, except for a few large inclusions normally found in commercial steels Figure 59. This absence of precipitates in the unirradiated material is consistent with previously published information.[9]

$M_{23}C_6$ carbides with the same morphology have been reported in the literature[10-13] to occur in unirradiated 316 stainless steel after annealing at higher temperatures. Thus, increased mobility, due to the neutron flux, may have facilitated the formation of a more stable carbide morphology in the irradiated specimens. In order to determine if a similar carbide distribution could be created in our control material, an unirradiated 316 stainless steel control sample, annealed 3050 hours at 1400°F was examined.

Neg 6779-B

FIGURE 59. Extraction Replica Showing Needle and Cuboid Morphology of $M_{23}C_6$ Precipitates from the Same Type 316 Stainless Steel Shown in Figure 1

Neg 6668-A

FIGURE 59. Bright Field Micrograph of Unirradiated Solution Treated Type 316 Stainless Steel Annealed 3050 hr at 900 °F in Static Sodium. Thermal Control Sample of Irradiated Material Shown in Figure 1

This specimen contained only a small concentration ($\sim 10^{10}$ to 10^{11}/cc) of polyhedral precipitates within the matrix. There were essentially no precipitates within the grain boundaries. The relatively low amount of carbides, as compared to the irradiated specimen and results reported in the literature for non-irradiated specimens after similar anneals, indicates that the unirradiated thermal control sample may have been decarborized during the anneal. Chemical analyses are presently being made on irradiated and unirradiated specimens with various thermal treatments to determine if this is the case. Microscopy was initiated on a section of the 3D1 safety rod thimble that was irradiated in the EBR-II at 730°F to the peak fluence of 6.7 x 10^{22} n/cm^2 (E >0.1 MeV), Figure 60. The microstructure consisted of a high concentration of polyhedral voids and precipitates. Preliminary analysis indicated a void density of about 8 x 10^{15} /cm^3 and a lineal averaged void diameter of 170 Å. The volume occupied by the voids was calculated to be about 2.7%. This value is in good agreement with the 3.09% decrease in bulk density measured on the same sample. The precipitates have not yet been identified, but, based on previous examinations of fast reactor-irradiated type 304 stainless steel, they are expected to be $M_{23}C_6$ carbides.

The peak fluence section (4.1 x 10^{22} n/cm^2(E >0.1 MeV)] of the X-G05 thimble irradiated in the EBR-II at 790°F was also examined. Dark field microscopy of the irradiated steel revealed three types of precipitates. The first, Figure 61, is polyhedral in shape and, based on electron diffraction, has a diffracting plane spacing of 2.11 Å. This value is quite close to the 2.13 Å of (Fe-Cr)σ-phase. However, based on the morphology of previously examined specimens, the precipitate is expected to be $M_{23}C_6$ which has a peak intensity plane spacing at 2.05 Å. The second precipitate structure is rod shape Figure 62 and has a diffracting plane spacing of 1.91 Å. This value is

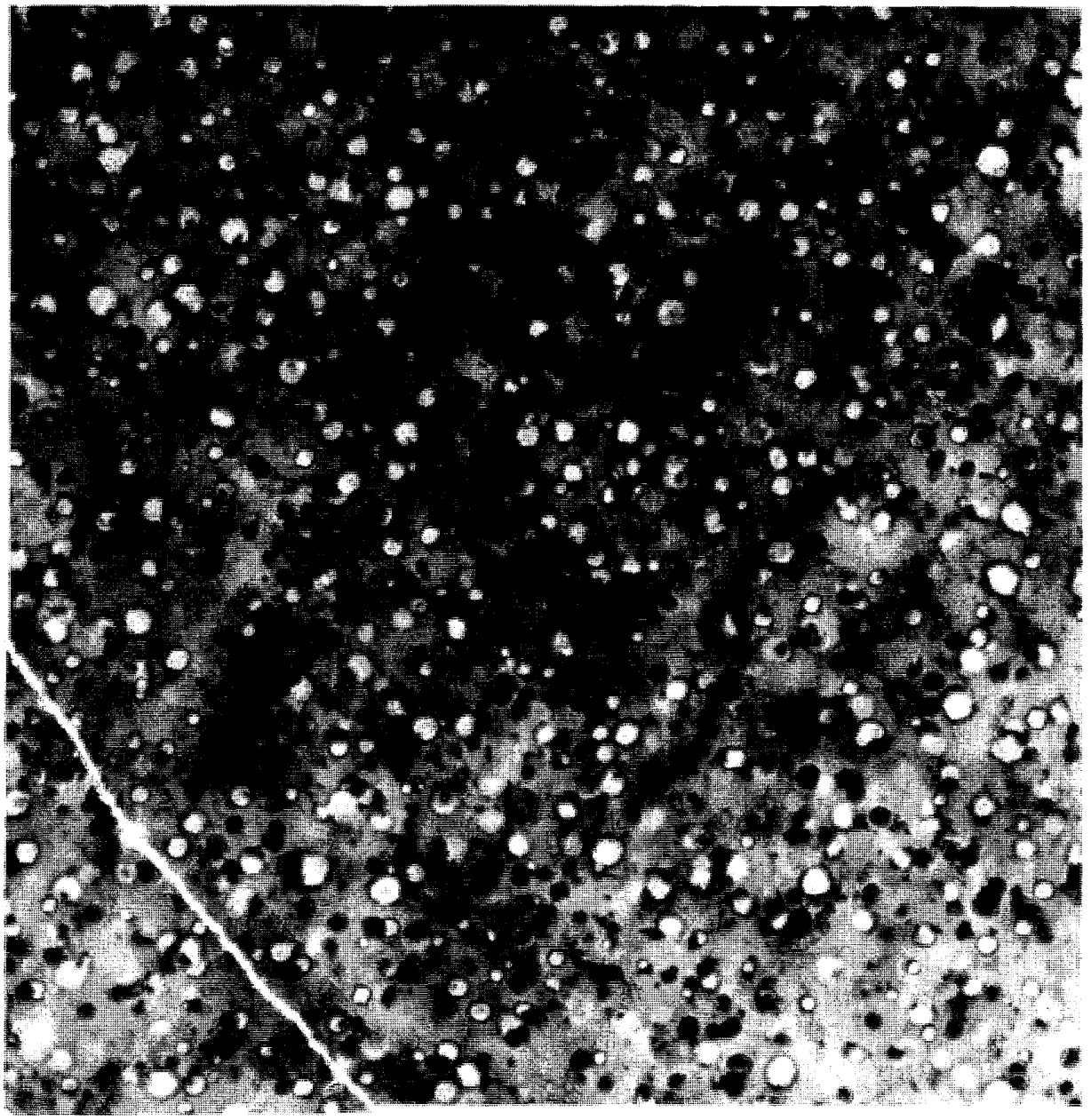

Neg 6802B

FIGURE 60. Bright Field Micrograph of Type 304 Stainless Steel Irradiated in EBR-II at 730 °F to 8.1 $\times 10^{22}$ n/cm^2 (E > 0.1 MeV). Sample 3E of the safety rod thimble EBR-II 3D1.

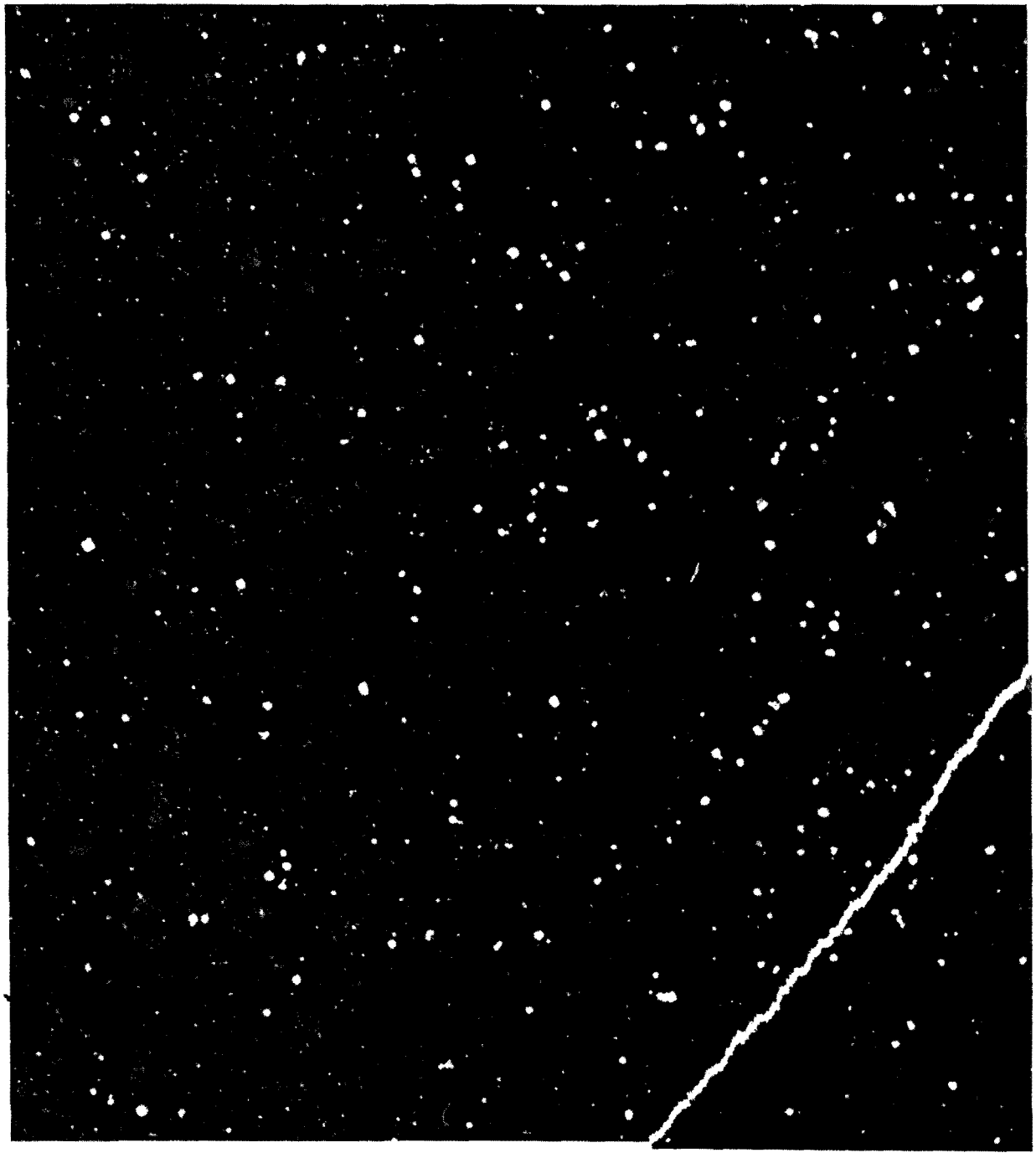

Neg 6563-B

FIGURE 61. Dark Field Micrograph of Polyhedral Precipitates in Type 304 Stainless Steel Irradiated at 790 °F to 4.1 × 10^{22} n/cm^2 (E > 0.1 MeV)

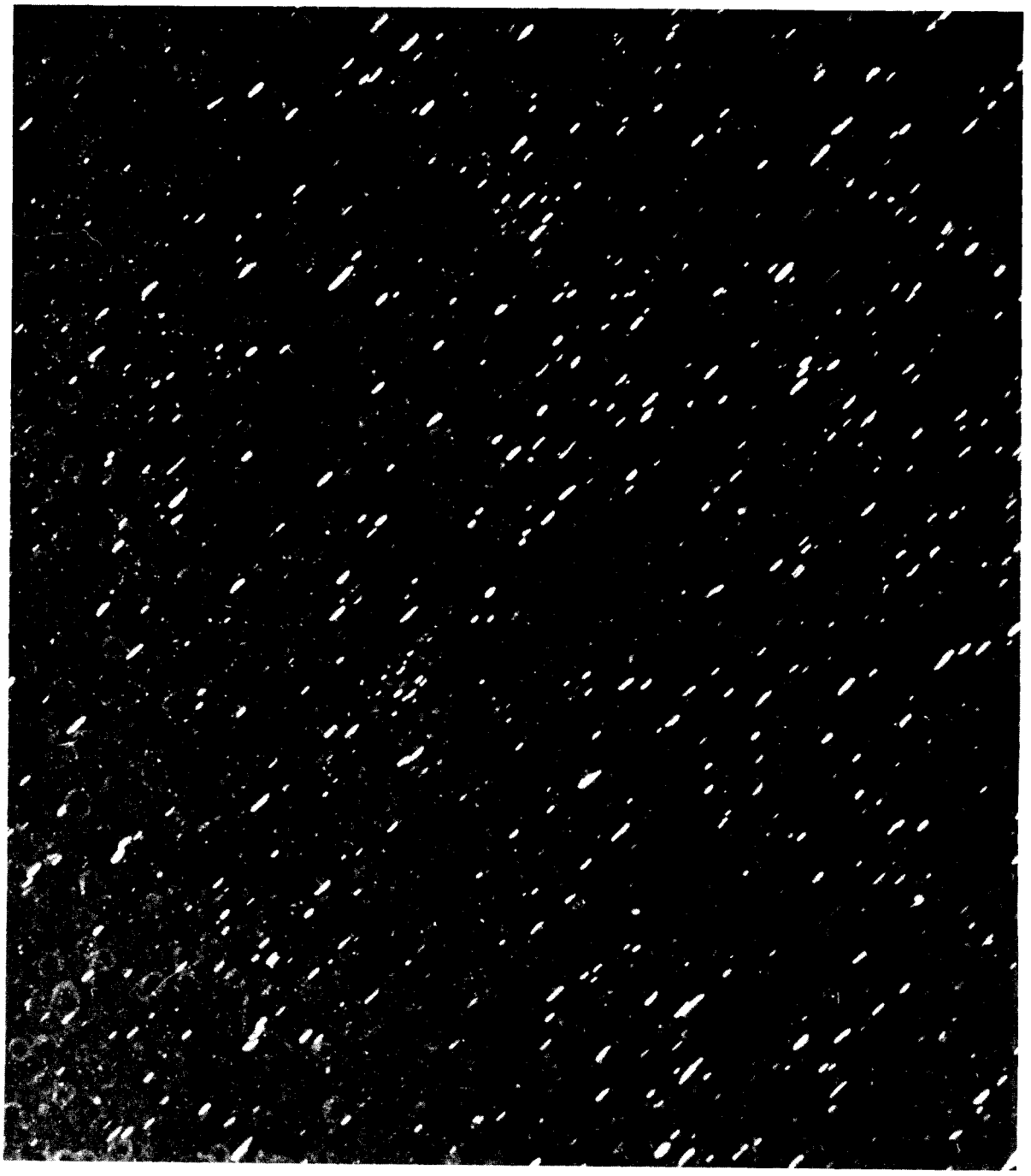

Neg 6559-C

FIGURE 62. Dark Field Micrograph of Rod Precipitates in Same Region of Thin Foil of Irradiated Steel Shown in Figure 6.

very similar to the other (Fe-Cr) σ-phase high intensity diffracting plane spacing of 1.93 Å. This precipitate might also be the 2.05 Å {511} $M_{23}C_6$ carbide. The third precipitate (Figure 63), has a three-fold symmetric diffraction pattern that is consistent with a bcc structure with a 3.57 Å lattice spacing. However, there is no phase of iron, chromium, or nickel that is consistent with the electron diffraction information.(14) A positive identification of this and the other two precipitates in the irradiated steel will be initiated by X-ray and electron diffraction using extraction techniques.

A review of PNL transmission electron microscopy data for 304 stainless steel irradiated in the EBR-II has indicated that the nucleation rate of cavities may increase with accumulated exposure. A summary of the essential features of the void distributions observed to date is given in Table XIX. The void number density has been plotted as a function of fluence, using logrithmic coordinates, in Figure 64. A regression analysis of the data indicates that the void density is related to the fluence by a power law in fluence with the exponent being 1.2 ± 0.3. If the exponent is greater than 1.0, an increase in nucleation rate with accumulated exposure is indicated. It is possible that a continuously increasing helium concentration, due to transmutation reactions, could contribute to an increasing nucleation rate by stabilizing cavity nuclei. No consistent trends relating void number density to irradiation temperature were found. The correlation between void volume based upon microscopy, and immersion density results is indicated in Figure 65. In this figure, microscopy volume changes from Table XIX are superimposed on immersion density values. Except for the point at 5×10^{21} n/cm^2, all microscopy data are in agreement with the bulk density values.

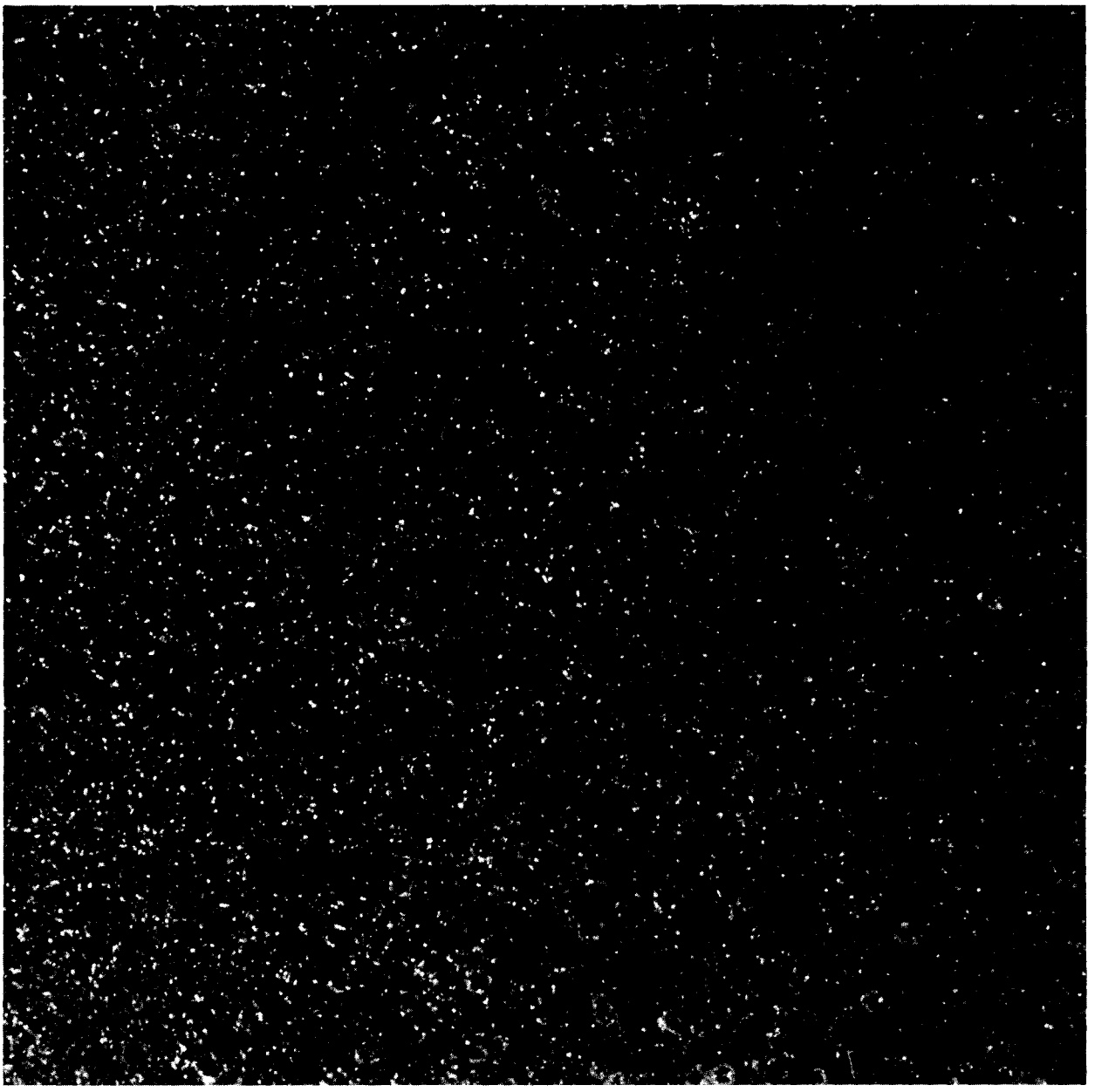

Neg 6554B

FIGURE 63. Dark Field Micrograph of Finely Dispersed bcc Phase in Same Region of Thin Foil of Irradiated Steel Shown in Figure 6.

TABLE XIX

TRANSMISSION ELECTRON MICROSCOPY
OF IRRADIATED TYPE 304 STAINLESS STEEL

Component	Fast Fluence E 0.1 MeV (n/cm^2 sec. x 10^{-22})	Fast Flux E 0.1 MeV (n/cm^2 sec. x 10^{-15})	Irrad. Temp. °C	Cavity Density (cm^{-3})	Lineal Average Cavity Diameter	Swelling
EBR-II Control Rod Thimble	0.5	0.1	460	0.3	245	0.3
	0.9	0.3	370	0.7	125	0.08
	1.5	0.5	370	1.9	145	0.3
	2.2	0.7	430	1.7	210	0.95
	2.4	0.8	420	2.0	200	1.0
	3.3	1.1	380	6.5	150	1.2
EBR-II X-G 5	3.4	1.5	390	2.3	210	1.4
EBR-II Safety Rod Thimble	6.7	1.6	390	8.2	170	2.7

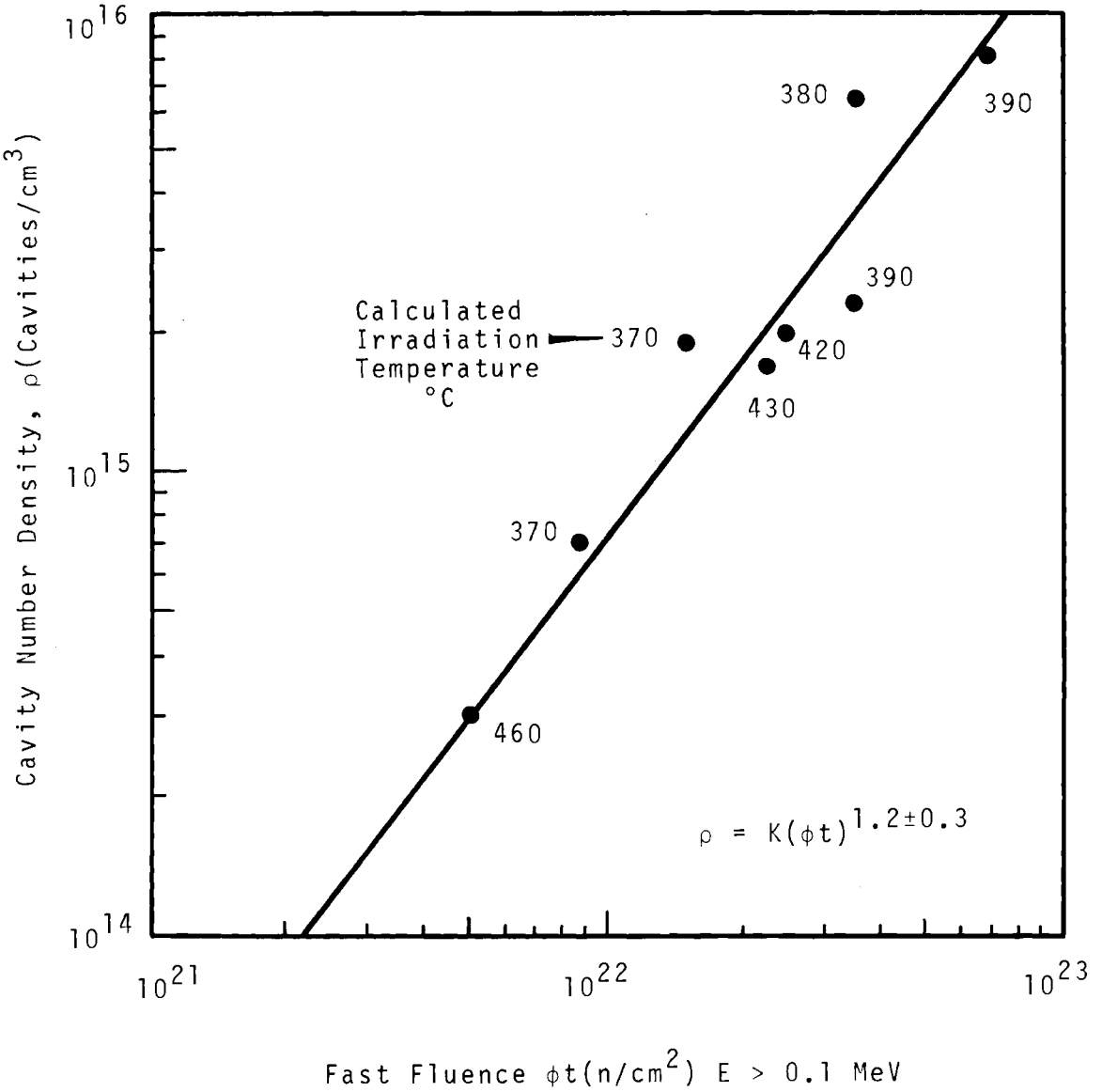

0692070-1

FIGURE 64. Cavity Number Density as a Function of Fluence

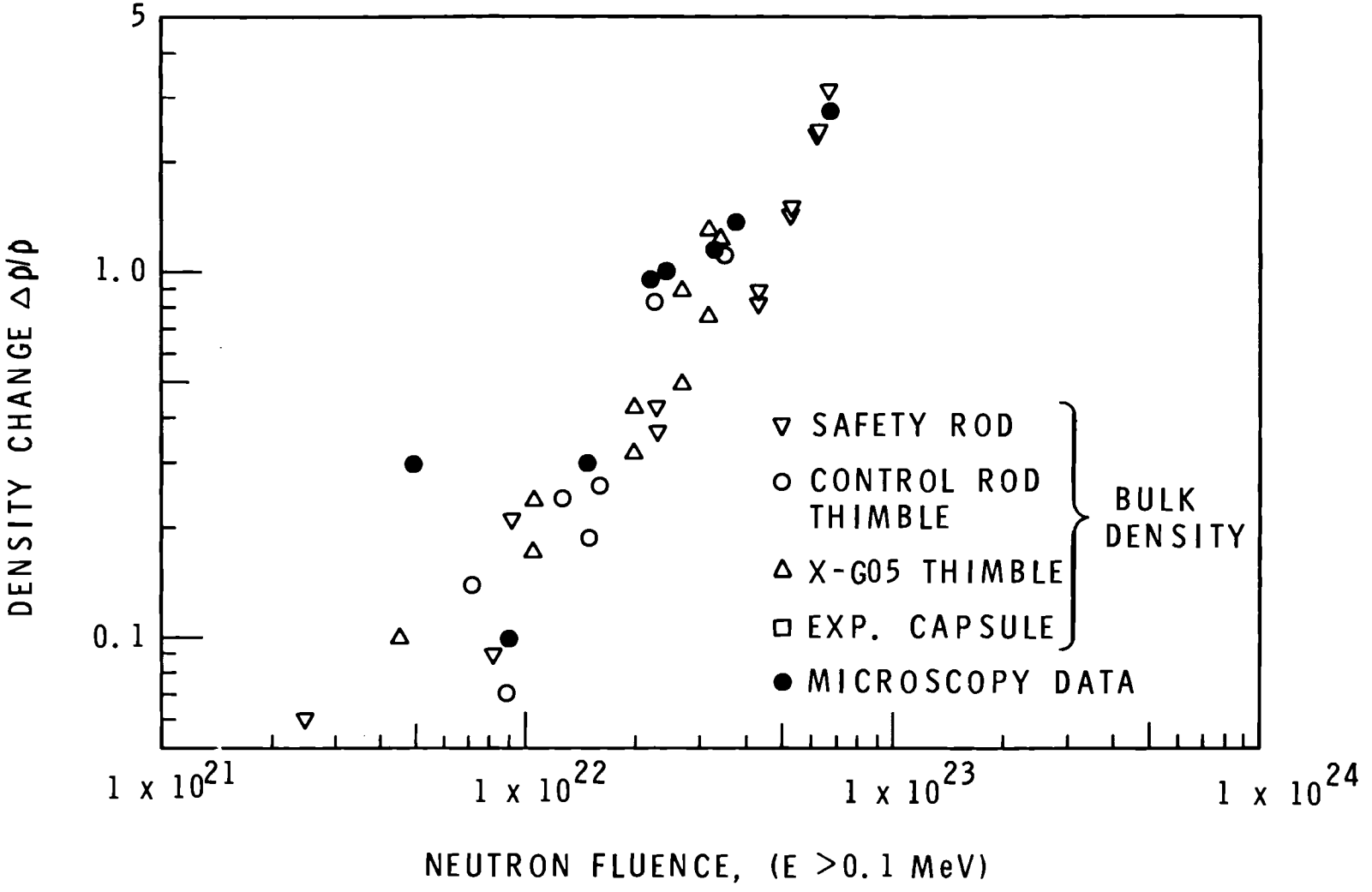

FIGURE 65. Swelling as a Function of Fluence for Various EBR-II Components

A specimen of type 347 stainless steel that was irradiated under conditions essentially identical to the 316 stainless steel test [900 °F to 0.8 x 10^{22} n/cm^2 (E >0.1 MeV)] was examined. The cavity density was low (about $10^{12}/cm^3$). A high concentration (about 7 x $10^{15}/cm^3$) of precipitates, about 100 Å in diameter, were identified by electron diffraction to be NbC. These are shown in Figure 66. The white regions are surface pits where the carbides were preferentially attacked during the electro-polishing. The precipitates normally appeared as beads on a string, either singly or in the form of a curtain strecching from one edge of the foil to the other Figure 67. Most of the single strings of precipitates appeared to be associated with dislocations. The curtains of precipitates did not appear to be related to dislocations. However, the regular alignment of the curtain of NbC precipitates indicates that the NbC may have formed on a dislocation that was still able to climb.

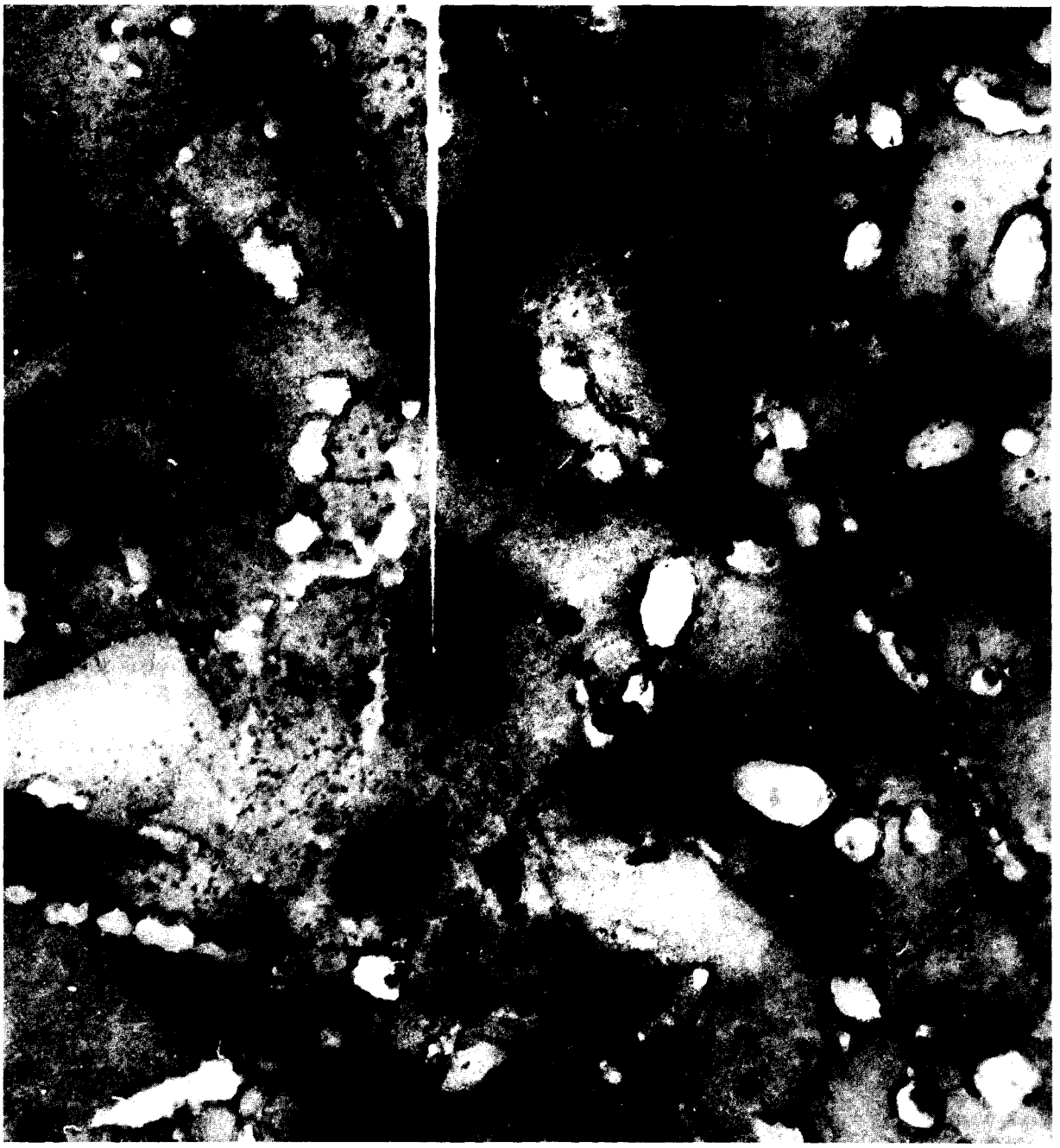

Neg 6444-E

FIGURE 66. Bright Field Electron Micrograph of Type 347 Stainless Steel Irradiated in the EBR-II at 900 °F to 0.8×10^{22} (E > 0.1 MeV). Large white regions are surface pits caused by preferential extraction of NbC during electropolishing.

Neg 6445-C

FIGURE 67. Dark Field Micrograph of Figure 9 Showing High Concentration of Finely Dispersed NbC Precipitates

REFERENCES

1. FFTF Monthly Report, April, 1969
2. Stone, D. H., "Some High Temperature Mechanical Properties of Zircaloy-2, Type 304 Stainless Steel, and AM 350 Stainless Steel", NAA-SR-11047, June 15, 1965.
3. Johnson, G. D., "The effect of Variations in Chemical Composition on the Creep Rupture Behavior of Austenitic Stainless Steels", NAA-SR-11788, December 15, 1965.
4. Monkman, F. C., Price, P. E., and Grant, N. J., "The Effect of Composition and Structure on the Creep Properties of 18-8 Stainless Steel", Transactions of the ASM, 1956, Vol. 48, pg. 418-445.
5. Garofalo, F., "Fundamentals of Creep and Creep-Rupture in Metals", Macmillian Series in Materials Science, 1965, pg. 29.
6. F. W. Woodfield, FFTF Development Monthly Progress Report, March, 1969.
7. F. W. Woodfield, FFTF Development Monthly Progress Report.
8. C. Cawthorne, E. Fulton, "Voids in Irradiated Stainless Steel", Nature, Vol. 216 (1967) 575.
9. J. A. Mazza and G. Willoughby, "Structural Changes and Creep Mechanisms in Type 316 Steel at 600 °C", JISI, 204, 718, (1966).
10. E. M. Mahla and N. A. Nielsen, "Carbide Precipitation in Type 304 Stainless Steel - An Electron Microscopy Study", Trans. ASM, 43, 292, (1951).
11. A. B. Kinsel, "Chromium Carbide in Stainless Steel", J. Metals, 4, 469 (1952)
12. P. W. Teare and N. T. Williams, "Structural Features of Isothermal Aging at Elevated Temperatures of Four Austenitic Steels', JISI, 201, 125 (1963).

13. J. T. Barnby and E. Smith, "The Deformation of An Austenitic Steel Containing a Distribution of Coarse Precipitates", Acta Met. 12, 1353 (1964).

14. W. B. Pearson, "Handbook of Lattice Spacings and Structure of Metals", Pergamon Press, 1967.

3. LMFBR Fuel and Cladding Information Center - F. R. Shober

An information center was established to document and to record all qualitative and quantitative information relating to the irradiation performance of LMFBR fuel pins. Those areas of materials information included in the system are melting process, fabrication techniques, heat treatments, mechanical properties, physical properties, quality inspection results, and performance records of individual lots of material. The system is a computerized information storage, retrieval, and data analysis system consisting of six sections; cladding fabrication; fuel fabrication; fuel pin fabrication; fuel subassembly fabrication; irradiating history; and postirradiation examination. The sectional nature of the system permits analysis and evaluation of data from each section independent of others or, if preferred a multisection analysis.

Activities of the information center presently include:

(1) Identification of terms and fields related to the expansion of the system;

(2) Preparation of a format for storage of data available on fabricated fuel pins and experimental subassemblies.

(3) Identification of and formation of interfaces with data sources and information needs;

(4) Storage of data from stainless steel cladding procured by:

   (a) BNW, lots G and H

   (b) Argonne National Laboratory

(5) Evaluation of data logging systems for reactor operation pertinent to the irradiation history section of system.

It appears that the major problem confronting the staff is to identify on and offsite sources of data and to interface with these sources.

C. FUELS QUALITY ASSURANCE -

H. G. Powers

1. Development and Control of Inspection and Testing

a. Ultrasonic Cladding Test

A. C. Callen, W. F. Stevenson

Development of ultrasonic equipment and application techniques for inspecting fuel pin cladding was continued. The objective of this work is to improve the state of the art to permit reliable detection of defects of smaller relative size than can be determined by now conventional practice Current FFTF specifications require testing based on a 0.001 inch deep x 0.030 inch long notch in the axial and circumferential orientations on both the outer and inner surfaces of 0.250 inch OD x 0.015 inch wall cladding.

The pulse-echo technique was used to inspect approximately 2700 feet of type 316 SS tubing. The tester was maintained in a state of statistical control by making multiple check tests on the standard and using $\bar{x}$ and R control charts. A standard with several sets of artificial notches spark-machined to different moninal depths was used. Tester response equivalent to exact 1 x 30 mil notches was then obtained from the calibration curve for each group of notches of the same surface location and orientation. Metallographic examination of tubing defects is in progress to establish the approximate confidence limits for the tester-response to natural defect size correlation, which are larger than for the artificial notches because of the spectrum of natural defect location, orientation, and shape. Further work being done in this area to assure valid testing of 0.230 inch OD tubing.

The effect of noise, i.e., high tester background, and its source are being studied in conjunction with the cladding inspection effort. Excessive noise accounts for more cladding rejection than actual verified rejects because the defect status is indeterminate when the tester background is greater than the acceptable response to defect signal. Preliminary evaluation indicates that larger than normal grain size is a significant factor. For the cladding tested, most of the noise is associated with cladding having a grain size of about ASTM 7; very little noise is associated with cladding having a grain size of between ASTM 8 and ASTM 9.

b. Eddy Current Cladding Test

A. C. Callen

Development of the eddy current technique was continued to provide a potential complementary test to the ultrasonic method of defect detection in tubing. The encircling coil method has not been sensitive enough to meet this goal. Development of alternate methods is planned with emphasis on pancake-type search coils located between the driver coils. Encouraging results were obtained using two to four search coils in one tube sector. An eighteen-coil search unit was then fabricated to allow testing in one tubing pass.

The technique utilizes two encircling coils as drivers and multiple pancake coils as pickups. The coil configuration consists of two encircling coils wound in 0.030 inch wide slots spaced 0.050 inch apart. Eighteen 0.040 inch diameter pancake coils are positioned between these slots around the coil form circumference. This number of pancake coils provides 100% inspection coverage of 0.250 inch OD tubing in one pass.

The advantages of this technique are:

- 100% inspection of the tubing for defects can be made in one translation of the tubing through the coil form;
- The sensitivities to both axial and transverse defects are nearly equal.
- The sensitivity to EDM notches is much better than either the ultrasonic system now in use or the encircling coil eddy current system. Only the new encircling coil-pancake coil technique can detect all of the notches in a 0.250 inch OD 316 SS standard, H-3, which has axial and circumferential 0.030 inch long EDM notches ranging in depth from 0.00051 inch to 0.00193 inch.

The prototype coil system was used to inspect about 500 feet of tubing with excellent results. The technique for fabricating both the coils and the coil forms is being improved. A coil form and coils for use in inspecting 0.230 inch OD tubing were fabricated and successfully used for evaluating the smaller diameter tubing.

c. Ultrasonic Testing of Fuel Pin Seal Welds

A. C. Callen

The feasibility of using the ultrasonic technique for detecting defects in fuel pin welds in being studied. A reliable nondestructive test is highly desirable for supplementing process control, visual inspection, and radiographic examination of the very critical fuel pin closure weld.

The high incident angle, pulse-echo ultrasonic test demonstrated exceedingly good sensitivity to a small region of the weld which includes the original tubing inner surface-to-end cap interface. It shows great sensitivity to defects in this region, such as lack of penetration, while rejecting to a large degree surface signals resulting from such causes as weld puddle, ripple, or shoulder. The surface conditions mentioned here rendered all more conventional test approaches invalid because of confusing echos or poor transmission of ultrasound.

A preliminary experiment was performed to determine the feasibility of employing acoustic emission as another nondestructive test technique for the end closure weld. The defects formed were of gross nature, but significant acoustic emission was detected.

d. Alpha-Autoradiography

D. A. Stranik

Alpha-autoradiographs were made of a sample pellet (0.25 Pu, 0.75 U)O_2 using platinum foil as a filter. Platinum filters out the alpha tracks coming off the PuO_2 at shallow angles to decrease the blossoming effect of the alpha tracks. These preliminary samples showed the blossoming effect to be nearly eliminated. More work will be continued using platinum foil and thicker Mylar.

e. Fuel Pellet Micro-Homogeneity

D. A. Stranik

Scanning electron microprobe studies are being conducted on 75 wt % UO_2-25 wt % PuO_2 fuel pellets to determine: (1) the PuO_2 concentration gradients across a pellet, and (2) the size of PuO_2 enriched areas versus the PuO_2 concentration. From the size of PuO_2 enriched areas and PuO_2 concentration versus the frequency that each concentration appears, a three-dimensional distribution will be calculated. This distribution will be used to form probability statements about: (1) the distribution of these areas within the pellet, and (2) the size of these areas in relationship to the processing parameters under which the pellets were fabricated.

These studies will show the distributions for pellet-to-pellet variation within a batch, and batch to batch variation. All of these results will be correlated to the processing parameters of the batches in order to explain the differences in the calculated distributions from each of the various batches. The microprobe is standardized by the use of a polished PuO_2 microsphere.

f. Evaluation of Offsite Test Equipment

W. F. Stevenson

Experiments were designed and conducted to evaluate the adequacy (for tube testing) of ultrasonic test equipments submitted by various equipment manufacturers. Plans are presently underway to evaluate pulsed eddy current tube testing equipment at Aerojet General Corporation.

g. Visual Standards

D. A. Stranik

Visual standards were drawn using graphic art as required in the FTR specifications. Standards were prepared for pellet cracking, acceptable welds, weld concavity, lack of fusion in welds, weld penetration, weld cracking and weld porosity. These visual standards will be used both for the PNL fuel fabrication and for the fuel vendor prequalification program.

2. Quality Systems and Procedures

a. Follower and Data Card System

D. A. Stranik

Establishment of a system to provide traceability, documentation and quality status of components from the raw materials through final fuel pin fabrication is essential for quality control, development activities and manufacturing activities. Storage of these records for a number of years is also of importance because of the long time cycle from start of fabrication of the fuel pins to completion of postirradiation examination.

The card system consists of two main types of data: (1) the follower cards, and (2) the inspection data cards. The follower cards physically follow the materials through the process and include a summary of the quality status of the material. These cards also cross reference material and process specifications and the backup inspection data which is

given in detail on the inspection data cards. The inspection data cards and the follower cards are cross referenced in order to obtain complete traceability.

The system has been incorporated into all the fuel pin fabrication, both in the demonstration facility and the irradiation test pin fabrication line. The card system will be revised and upgraded in the near future and at that time the forms used will be finalized with only periodic upgradings anticipated.

b. Calibration Program

W. F. Stevenson

The calibration program to assure accuracy and traceability to NBS of all measuring and test equipment and standards used in the fabrication (at BNW) of FFTF fuels was implemented. All such equipment and standards were initially certified by BNW Standards Laboratory and will be entered on a computer recall program to assure periodic recall and recertification at prescribed intervals of time. The procedures document covering this activity is ready for management concurrence and signature.

c. Receiving Inspection

W. F. Stevenson

General policy and procedures governing this activity were documented and implemented. Detailed inspection procedures are being formalized and documented. Inspection data forms were designed and committed to use.

d. In-Process (at BNW) Inspection Plans

W. F. Stevenson

Acceptance sampling plans and accompanying acceptance criteria were developed for all specified irradiation test fuel pellet characteristics. The operating characteristic curves for each of these plans were calculated and are being reviewed with design and fabrication personnel to obtain agreement on producer and consumer risks.

D. FUELS EVALUATION

J. E. Hanson

1. Fast reactor Irradiations

LA Pember, EO Ballard, RD Leggett, JW Weber,
SH Christensen, MK Millhollen

An irradiation testing program is being conducted in EBR-II to confirm as well as possible the adequacy of the FTR driver fuel pin design. this program is characterized by the emphasis placed on testing statistically significant numbers of carefully characterized fuel pins in geometries approximating that of the FTR driver fuel design.

a. Status of Fast Flux Irradiation Tests

A summary of the status of fast flux, steady-state irradiation experiments is presented in Table XX

Irradiation of two nonencapsulated 37-pin subassemblies, PNL-4 and PNL-5, was begun in EBR-II at the beginning of run 34 and 33, respectively. PNL-4 is designed to operate at 9.5 kW/ft and PNL-5 is designed to operate at 14 kW/ft to exposures of 50,000 MWd/MTM.

Irradiation of subassemblies PNL-2 and PNL-3 continues satisfactorily in EBR-II. The estimated accumulated exposure on these subassemblies at the end of run 33 (4/22/69) is:

Subassembly	Estimated Burnup MWd/MTM, peak
PNL-2 (X032)	30,000
PNL-3 (X051)	3,130
PNL-4 (X059)	--
PNL-5 (X054)	2,736

TABLE XX

SUMMARY OF STATUS OF STEADY STATE IRRADIATION EXPERIMENTS FOR TASK FP-7

Test No.	Test Objective	Description	Goal Expos. Peak Power	Facility	Status: Est. Exp. (MWd/MTM)	Status: Discharge Date	Status
PNL-1	Obtain steady state fast flux irrad. data on candidate FFTF fuel forms. Irradiate fuel materials for subsequent transient (TREAT) testing.	Encapsulated 25% PuO_2 - 75% UO_2 fuel pins, 304 SS cladding. 12 pins 0.250" OD w/0.016" wall. 7 pins 0.238 OD w/0.010" wall. Smeared density 85 - 88% TD.	10,000 MWd/MTM (Est.) 10 kW/ft	EBR-II X031 Position 6C1	8000	6-15-68	S/A discharged. Pins 1-3 and 1-6 exam. completed at BNW. Pins 1-15, 1-16, 1-17, 1-18, 1-19 at LASL for exam. Remaining 12 pins held at BNW for subsequent exam. or transient testing. Test chgd. 11-22-67
PNL-X	Provide information on kinetics of fuel-cladding gap closure. Effect of initial gap size on the fuel radial temp. profile. Fission gas release as a function of temperature. Extent of fuel restructuring which will take place at low linear power levels.	5 encapsulated 25% PuO_2 - 75% UO_2 fuel pins, 304 S/S cladding. 0.250" OD x 0.016" wall. ρ_s - 88% TD Gap - 0.004, 0.006, and 0.008".	7500 MWD Est. 6 kW/ft and 10.4 kW/ft	EBR-II X039 Reconstituted X011 Position 3C2	Est. 8500 for 10.4 kW/ft	12-24-68	S/A discharged, shipped to LASL for exam. in January, 1969.

TABLE XX (Continued- 2)

Test No.	Test Objective	Description	Goal Expos. Peak Power	Facility	Status: Est. Exp. (MWd/MTM)	Status: Discharge Date	Status:
PNL-2	Same as PNL-1	Same as PNL-1	50,000 MWd/MT (Est.) 10 kW/ft	EBR-II X032 Position 6F1	(Est.) 30,000	Est. 2-70*	In reactor (Chgd. 11-22-67).
PNL-3	Obtain statistically significant data on swelling behavior, gas release rates, and general irradiation performance of pins fabricated w/typical FTR fuel pin parameters irradiated under approx. FTR conditions.	37-bare fuel pins, 25% PuO_2 - 75% UO_2. 304 S/S cladding, 0.250" OD x 0.016" thick wall. 19 pins-solid pellets 0.212 OD. ρ_p - 93% TD ρ_s - 88% TD. Gap 0.006". 6 pins-annular pellets 0.212 OD x 0.054 ID. ρ_p 96% TD, ρ_s - 85% TD Gap 0.006". 6 pins-solid pellets 0.212" OD. ρ_p - 89.9% TD, ρ_s - 85% TD., Gap 0.006". 6 pins-solid pellets 0.212" OD. ρ_p - 91.6% TD, ρ_s - 85% TD, Gap 0.008".	Interim exam. at 30,000 MWd/MTM 6 kW/ft. Goal of 50,000 MWd/MTM	EBR-II X051 Position 3A2	(Est.) 3,200	Est. 6-71* Est. 2-73*	S/A in reactor charged 12-12-68.
PNL-4	Same as PNL-3	Same as PNL-3	Same as PNL-3 9 1/2 kW/ft	EBR-II X059 Position 4A1	--	Est. 9-71*	S/A in reactor. Charged 4/23/69.
PNL-5	Same as PNL-3	Same as PNL-3	Same as PNL-3 14 kW/ft.	EBR-II X054 Position 4E1	--	Est.* 1-71	S/A in reactor. Charged 3/31/69.

*Based on est. 35% EBR-II operating efficiency.

TABLE XX (Continued - 3)

Test No.	Test Objective	Description	Goal Expos. Peak Power	Facility	Status Est. Exp. (MWd/MTM)	Status Discharge Date	
PNL-6,7,8	Obtain statistically significant data on the behavior of fuel pins fabricated using typical dimensional tolerances and fuels fabricated by typical processes.	Each 37-bare pin S/A. 25% PuO_2 - 75% UO_2. 316 S/S cladding, 0.250" x 0.016" thick wall.	50,000 MWd/MTM 6, 10, 14 kW/ft.	EBR-II	--	Est.* 4-7 10-71 2-71	Final fab. procedure development being completed. Est. chg. date 6-69.
PNL-9,10 11	Provide confirmation of reliable performance of fuel pins fabricated to the reference FTR design through in-reactor statistical testing.	Each, 61-bare pin S/A. 25% PuO_2 - 75% UO_2. 316 S/S cladding 0.230" OD x ∿0.015" thick wall.	50,000 MWd/MTM 6, 10, 14 kW/ft.	EBR-II	--	Est.* 12-72 7-71 12-70	Conceptual design completed. Est. charge date 8-69.
PNL-14,15 16	To obtain statistically significant data on the performance of the reference design FTR fuel pin as a function of cladding cold work state through in-reactor testing.	Each, 61-bare pin S/A 25% PuO_2 - 75% UO_2 316 cladding, 0.230 in. OD x ∿0.015" thick wall. Cladding to be 0,5,10, and 20% cold work.	50,000 MWd/MTM 6, 10 14 kW/ft.	EBR-II	--	Est.* 3-73 10-71 3-71	Conceptual design completed. Cladding procurement initiated. Est. charge date 11-69.
PNL-17	Proof testing of S/A hardware & design & instrumentation. Confirm design parameter assumptions for subsequent instrumented S/A irrad.	Instrumented S/A. Coolant temperature & flow measurement in 37 bare pins S/A of 25% PuO_2 - 75% UO_2.	Approx. 4 reactor cycles	EBR-II	--	Est.* 10-69	Est. charge date 7-69.

b. Postirradiation Examination of Fast Flux Irradiated Fuel Pins

(1) Postirradiation Examination of PNL-1 Pins

Examination of sections from PNL-1-15, 17 and 19 was completed at LASL. The negatives were sent to BNW for printing, laying up of mosaics and detailed review and analysis. Two sections from each of pins PNL-1-16 and 18 are scheduled for examination in August, 1969.

(2) Postirradiation Examination of PNL-X Fuel Pins

The five PNL-X series capsules which were irradiated in EBR-II subassembly X039 were opened at LASL and the pins successfully recovered. Two of these pins, PNL-X-6 and 7, operated at an estimated 10.6 kW/ft to a burnup of 8500 MWd/MTM, while the other three, PNL-X-1, 3 and 4, operated at an estimated 6 kW/ft to 4800 MWd/MTM. After cleaning in Dowanol and water, the pins were photographed at three axial orientations with and without the wire wrap. Each capsule was gross gamma scanned, radiographed with the betatron, and punctured for gas collection and analysis. As expected, all pins were intact and appeared to be in excellent condition. The pins are presently being measured with a profilometer after which they will be punctured to collect the internal gas for analyses.

Pin PNL-X-1 showed some peculiar markings in the plenum region which are not completely explained but are not believed to have influenced the performance of the pin in any deleterious way. Figure 68 is a photograph taken of the pin while immersed in Dowanol. The network of dark lines appear reddish-brown when viewed in air at low

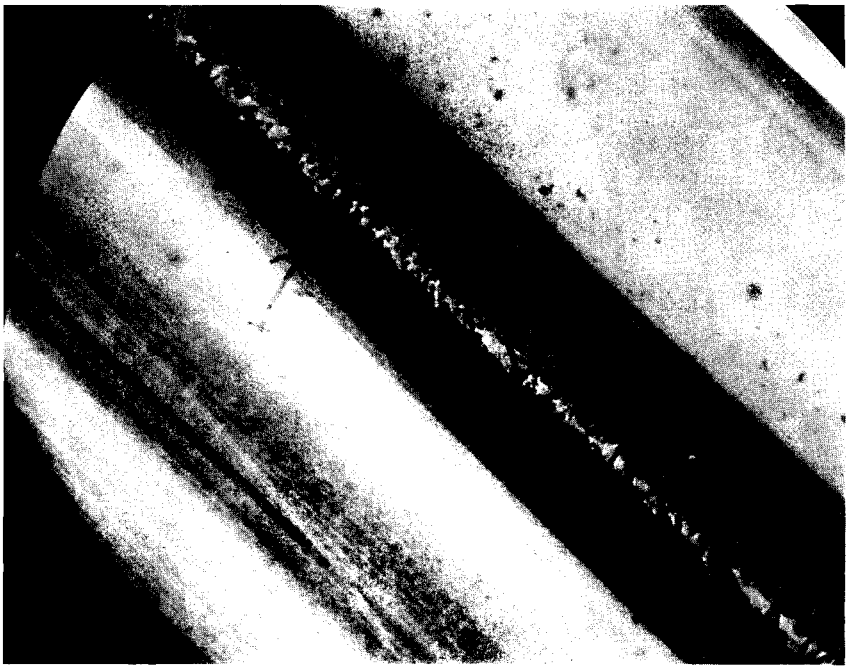

FIGURE 68. Appearance Under Dowanol of the Pin PNL-X-1 in the Plenum Region Above the Sodium Level

magnification with a microscope. These are probably sites of preferential oxidation at light scratches placed on the surface of the pin during fabrication. These streaks are neither protrusions nor indentations but appear more like stains. It was not possible to verify with the microscope on dry pins what appeared to be pits when viewed under Dowanol. Isolated areas of a fine, crystalline deposit could be seen, but it was impossible to establish whether this was debris from handling in the cells or a deposit that had formed during irradiation. The inner surface of the capsule tubing had features similar to those seen on the pin. A portion of the crystalline deposit was removed from the tube for analysis.

c. EBR-II Instrumented Fueled Subassembly (PNL-17)

An instrumented subassembly is to be irradiated in EBR-II to measure subchannel coolant temperatures. The magnitude of the forced interchannel mixing of the coolant due to the wire wrap can be determined from the measured temperature profiles.

The proposed EBR-II instrumented fueled subassembly consists of thirty-six 0.230 inch diameter, fuel pins separated by 0.054 inch wire wrap and one empty fuel pin used as an instrument lead conduit. Some of the wire wraps will comprise sheathed thermocouples, some will be hypodermic needle tubing containing flux monitor wire and the rest will be solid wire.

Preliminary calculations based on a 50 MW reactor power level show that the maximum linear heat generation rate in a fuel pin is 11.84 kW/ft. This rate is achieved with 93% TD, 75 wt % UO_2-25 wt % PuO_2, pressed and sintered pellets in which the UO_2 is fully enriched. Since an increase

in EBR-II power level to 62.5 MW is anticipated in the near future, it will be necessary to decrease the UO_2 enrichment to approximately 65%, to maintain the same linear heat generation rate. At a proposed inlet temperature of 700°F and an outlet temperature of 930°F, pressure drop across the subassembly will be approximately 26 psi. A maximum mean cladding temperature calculated for the hottest pin (11.84 kW/ft) is 1089°F, including uncertainty factors. The calculated maximum centerline temperature of the hottest fuel pin is 4157°F.

Approval-in-principle for this test was requested from RDT.

An analytical comparison of the thermal hydraulics of 19 and 37 pin subassemblies with a prototypic FTR 61-pin subassembly was completed. The purpose of the study was to determine which subassembly more closely approximated the coolant flow characteristics of the prototypic FTR subassembly in order to establish the design for the instrumented subassembly.

The flow characteristics of the subassemblies were calculated using the COBRA computer code. Results from this were used in the HAZAN computer code to obtain cladding temperatures. The flow distribution model is shown in Figure 69 . Figure 70 shows the subassembly dimensions.

The coolant inlet temperature was assumed to be 700°F. The inlet flow rates were divided among the channels to give equal pressure gradients over the length of the bundles.

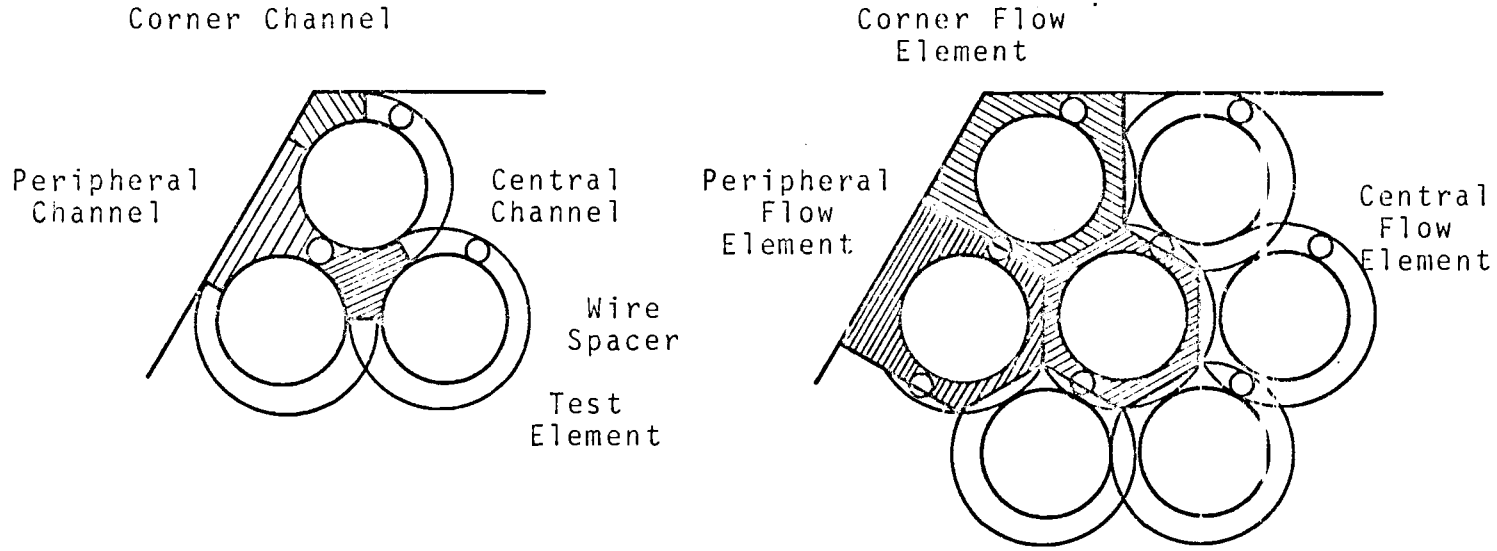

FIGURE 69. Flow Distribution Model

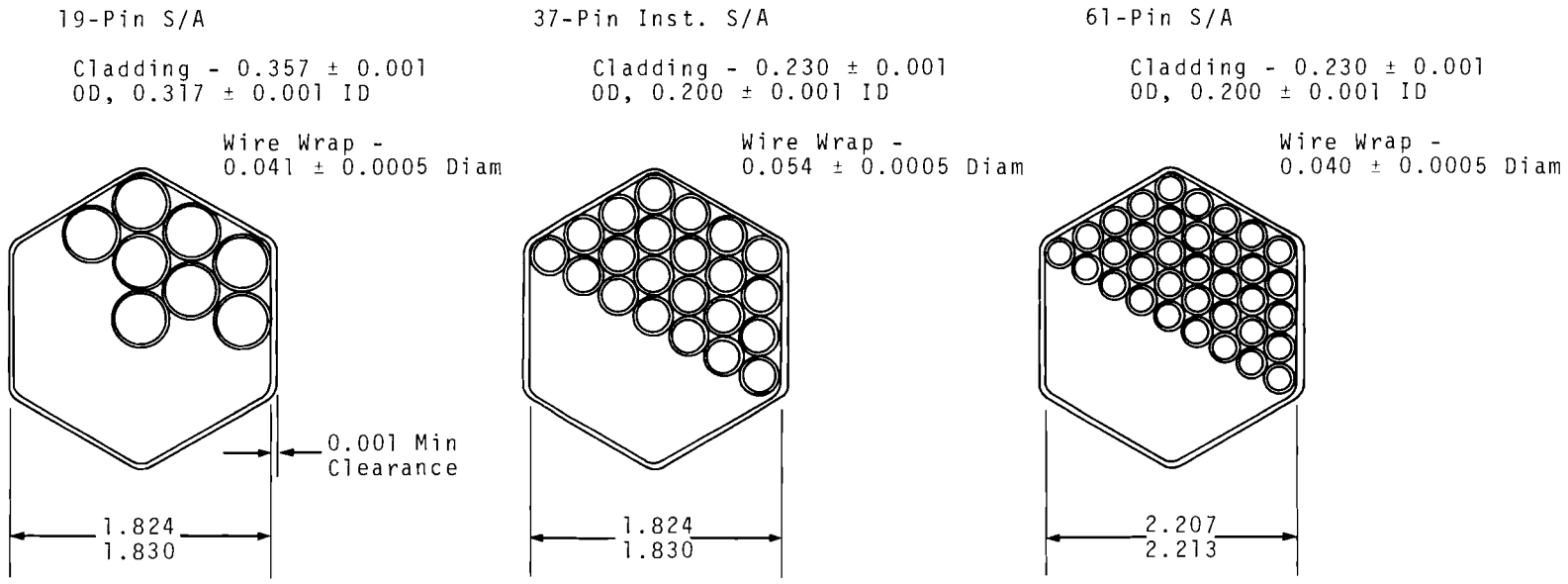

FIGURE 70. Subassembly Dimensions

A comparison of the velocity and flow distributions is given in Table XXI . It is seen that the 37-pin bundle correlates more closely with the prototypic FTR bundle than does the 19-pin bundle. This result is also true when considering turbulent interchannel mixing (forced mixing) as shown in Table XXII.

Figures 71 - 73 show the coolant temperature profiles at the top of the fuel columns.

It was found that the flow characteristics were largely dependent upon the geometry rather than the power generation of the subassemblies. Since the purpose of the proposed instrumented subassembly experiment is to determine more accurately the coolant flow characteristics of the FTR subassembly and, more specifically, the forced interchannel mixing, it is concluded that the 37-pin bundle will yield the most applicable data.

2. Thermal Reactor Irradiations - R.D. Leggett, L.A. Pember, J.W. Weber

a. Thermal Irradiations of UO_2 + PuO_2 Fuel Pins

This task is devoted to the steady state and transient testing of prototypic FTR length fuel pins. The activities involved in this study include design of irradiation capsules, steady state irradiation of prototypic length fuel pins to average burnups of 10,000 and 50,000 MWd/MTM, postirradiation examination of these fuel pins to characterize the pre and post transient fuel pin condition, and transient irradiations in the TREAT facility.

Work during this report period was directed toward all four activities. Progress was made on the capsule designs for irradiations to be initiated in FY-1970. These capsules include the Mark-II GETR/TREAT

TABLE XXI

VELOCITY AND FLOW DISTRIBUTION

Type	Velocity, % of Average Central Channel	Peripheral Channel	Corner Channel
61-pin	90.6	116.0	106.4
37-pin	97.6	115.8	105.6
19-pin	89.2	112.1	86.3

Type	Flow, % of Average Central Element	Peripheral Element	Corner Element
61-pin	69.4	140.0	166.3
37-pin	70.6	124.0	144.0
19-pin	63.1	116.7	127.0

TABLE XXII.

Peripheral-Central Interchannel Mixing

Peripheral-Peripheral Interchannel Mixing

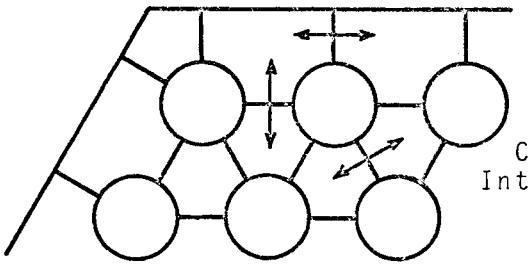

Central-Central Interchannel Mixing

Percent of Turbulent Interchannel Mixing To Average Flow Rate Per Channel (lb/hr)

	Central-Central	Peripheral-Central	Peripheral-Pheripher
		For A = 0.0062	
61-Pin[1]	17.0%	25.3%	30.2%
37-Pin[2]	17.3%	22.5%	26.0%
19-Pin[3]	11.3%	16.1%	17.8%
	11.5%	16.0%	17.5%
	11.9%	17.0%	18.5%
	11.4%	16.5%	18.0%
		For A = 0.0124	
61-Pin	34.4%	50.8%	60.5%
37-Pin	34.2%	45.0%	51.6%
19-Pin	22.8%	32.4%	35.5%
	22.5%	32.2%	35.0%
	23.8%	33.3%	36.7%
	23.0%	32.9%	36.1%

1. Corresponds to a flow rate of 108 gal/min
2. Corresponds to a flow rate of 53 gal/min.
3. Corresponds to a flow rate of 55 gal/min, 49 gal/min, 29 gal/min and 39 gal/min, respectively.

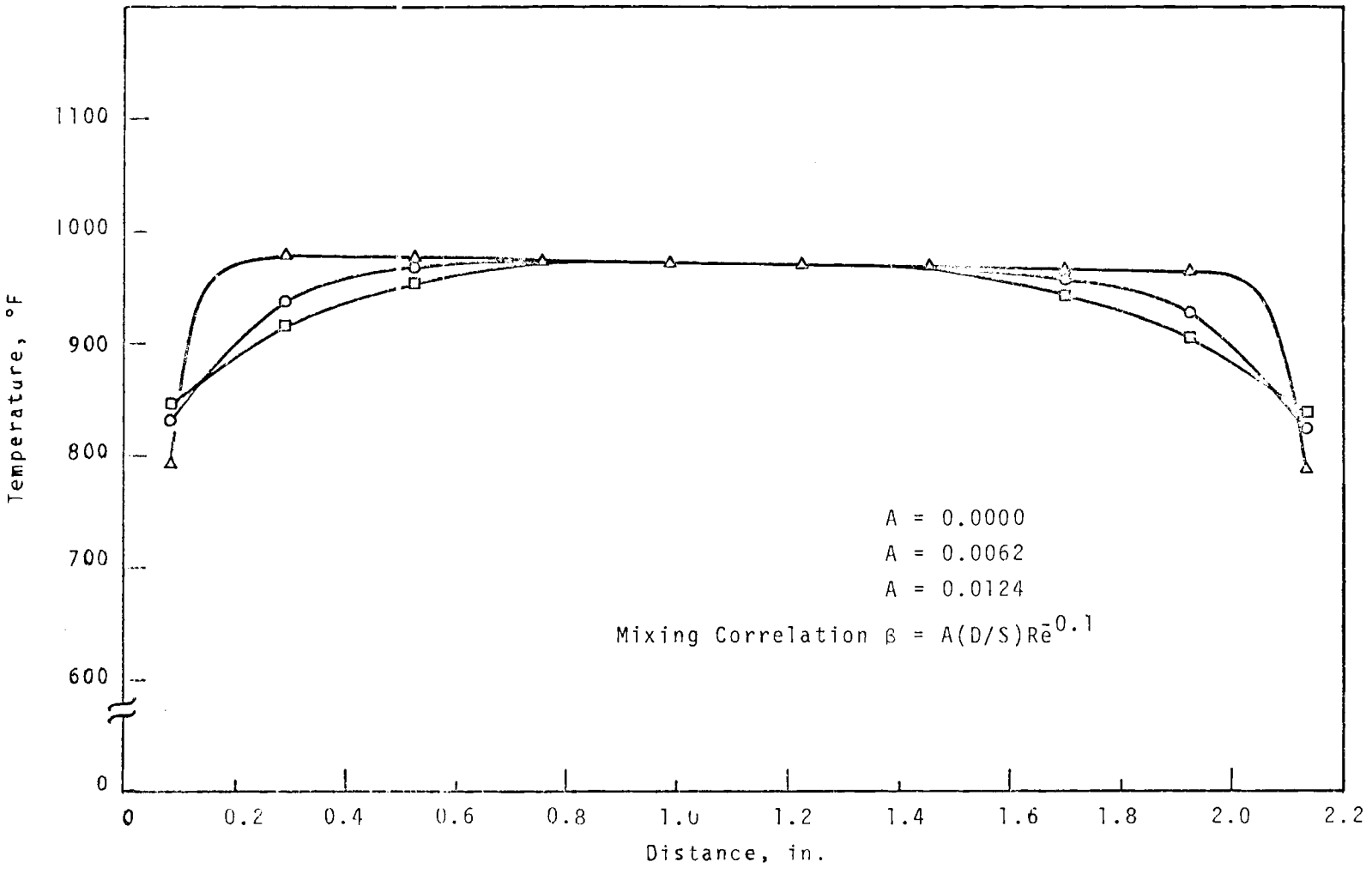

FIGURE 71. Coolant Temperature Profile of 61-Pin Subassembly at Top of Fuel Column for Fully Enriched Fuel for Position 3N1 in EBR-II; Mixing Correlation $\beta = A(D/S)Re^{0.1}$

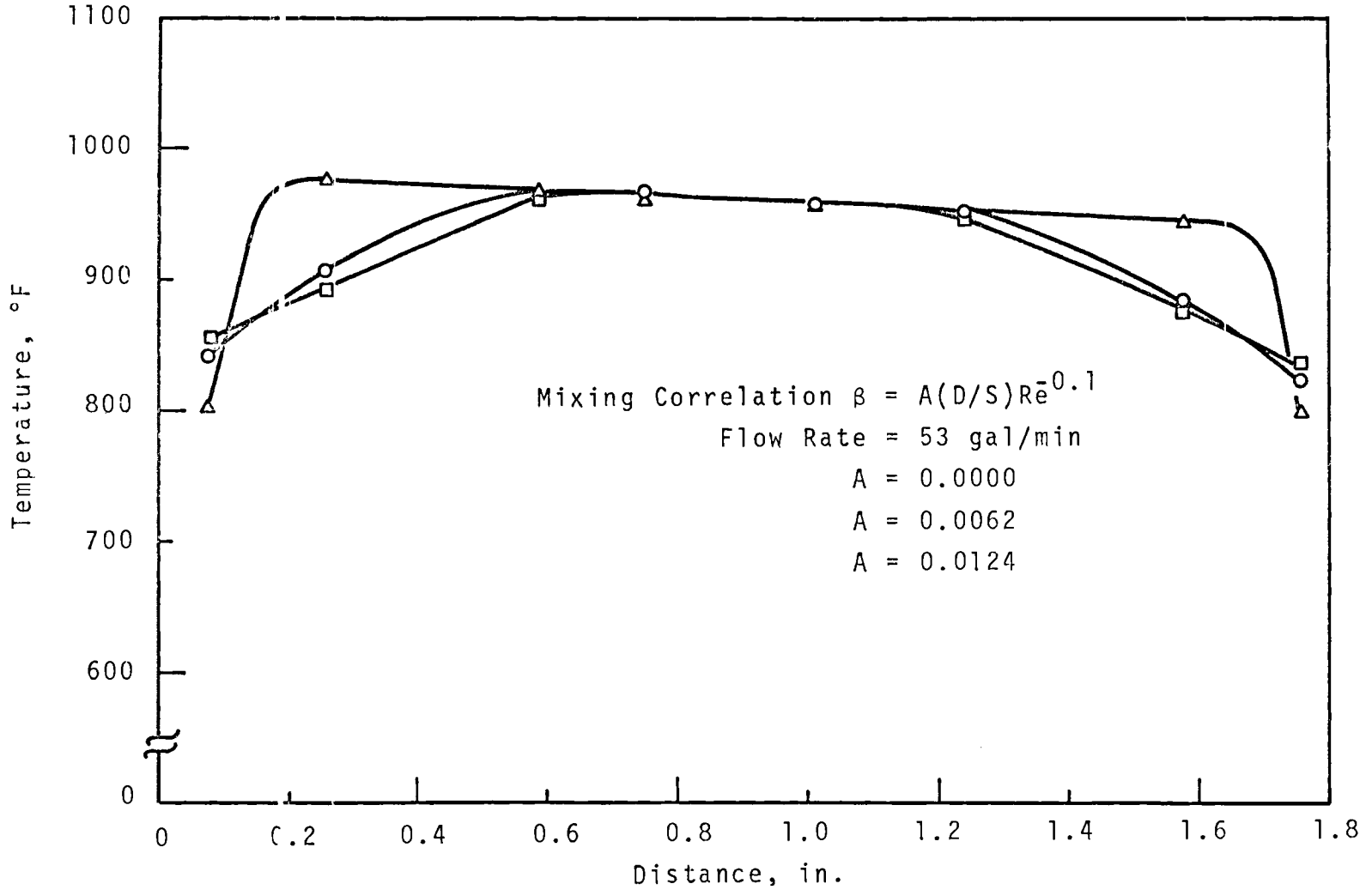

FIGURE 72. Coolant Temperature Profile of 37-Pin Inst. Subassembly at Top of Fuel Column for Fully Enriched Fuel for Position C6 in EBR-II

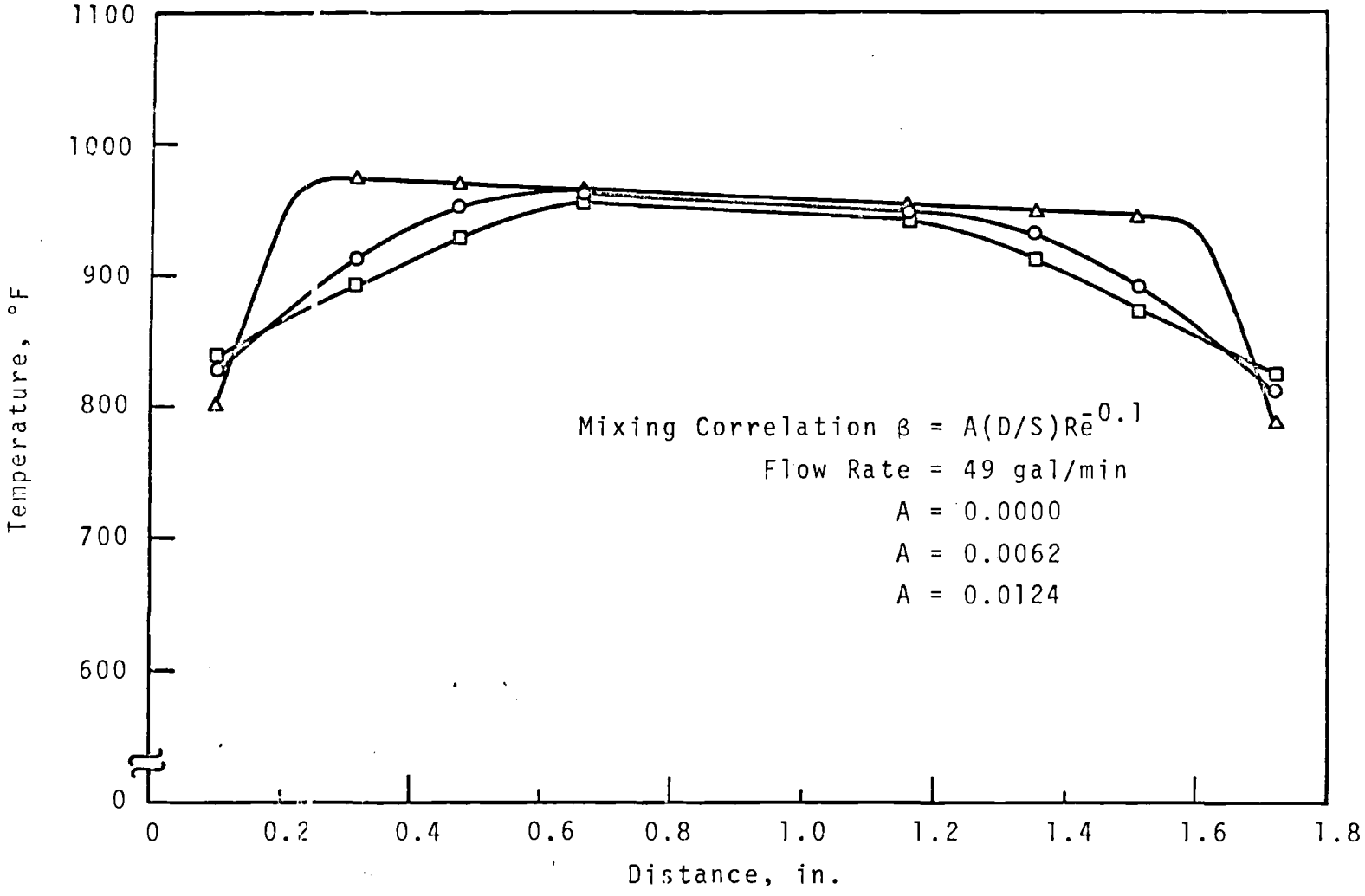

FIGURE 73. Coolant Temperature Profile of 19-Pin Subassembly at Top of Fuel Column for Fully Enriched Fuel for Position C6 in EBR-II

capsule which contains a fuel pin of the current FTR conceptual design, i.e., type 316 stainless steel cladding and 0.230 inch diameter. The other capsule design will provide the necessary containment to perform run-to-failure irradiations in the GETR.

The status of the steady state irradiations in FETR is shown in Table XXIII. These capsules contain fuel pins clad in 0.250 inch diameter type 304 SS. Capsules PNL-59-7 and 8 reached their goal exposure of 50,000 MWd/MTM. Neutrography indicates that the fuel pins are in excellent condition and suitable for transient testing.

Postirradiation examination of capsule PNL-59-5 (10,000 MWd/MTM) was begun. The fuel pin was recovered from the NaK filled, instrumented capsule without incident, gamma scanned, photographed and profilometered. The gamma scan indicated a reasonably symmetrical average power profile with a peak to average ratio of 1.34. Preliminary profilometer data indicate no measurable increase in fuel pin diameter. The fuel pin is being sectioned for metallographic and burnup analyses.

Preparations for transient testing are in progress. A calibration capsule to measure the power relationship between the TREAT reactor and the fuel pin was fabricated. Approvals to perform the experiment are being obtained. Hazards analysis and data packages for the first preirradiated pin transient tests are being prepared and hot cell facilities to handle these experiments are being completed.

TABLE XXIII

GETR/TREAT CAPSULE STATUS

MAY, 1969

Capsule	Goal Burnup MWd/MTM	Status
PNL-59-1	10,000	Completed irradiation, awaiting transient testing.
PNL-59-2	10,000	Completed irradiation, awaiting transient testing.
PNL-59-3	10,000	Completed irradiation, awaiting transient testing.
PNL-59-4	10,000	Completed irradiation, awaiting transient testing.
PNL-59-5	10,000	Completed irradiation, undergoing postirradiaton examination.
PNL-59-6	10,000	Completed irradiation, scheduled for pellet separations evaluation.
PNL-59-7	50,000	Completed irradiation, scheduled for destructive examination.
PNL-59-8	50,000	Completed irradiation, awaiting transient testing.
PNL-59-9	50,000	40,000 MWd/MTM
PNL-59-10	50,000	40,000 MWd/MTM
PNL-59-11	50,000	Capsule re-inserted at 8,000 MWd/MTM after eight month hold.
PNL-59-12	50,000	Capsule re-inserted at 8,000 MWd/MTM after eight month hold.

b. Thermal Flux Irradiations of Hypostoichiometric UO_2 - PuO_2 Materials

This task includes irradiation testing of mixed oxide fuel specimens of different stoichiometries to high burnups in a thermal neutron flux. The apparent effective thermal conductivity during irradiation of hypostoichiometric mixed oxide fuel, relative to that of stoichiometric fuel, offers the potential for reactor operation at higher power densities and for lower fuel temperatures. The swelling and gas release characteristics of UO_2 - PuO_2 fuel as a function of stoichiometry and fuel form must be determined at high burnup before a maximum performance fuel can be selected.

The general status of the fuel pins being irradiated and examined under this task (FP-6) is summarized in Table XXIV. The reported burnup values were derived from ^{148}Nd analyses of sections removed from the center of the fuel pins. The burnup values for those pins not yet examined were estimated from the reported fluence, assuming a linear relationship between fluence and burnup.

Detailed examination of the neutron radiographs prepared from the capsules discharged from the reactor in February, 1969 (BNW-1-1, 2, 3, 5, 10 and 12) indicates that all pins are intact and in excellent condition. Two capsules (BNW-1-10 and 12) were returned to the ETR to complete their irradiation to 100,000 MWd/MTM. Although the thermocouples have now failed in these two capsules, the lead tubes will be sealed and the capsules will be returned to the same irradiation positions as before. Thus, the previous temperature data should apply, provided ETR conditions remain unchanged.

TABLE XXIV

SUMMARY STATUS OF HYPOSTIOCHIOMETRIC UO_2 - PuO_2 FUEL IRRADIATIONS

Issue Date: 5/15/69

Test Designation	Description(1) Fuel Form	O/M	Facility	Status: Goal Exposure MWd/MTM	Actual Exposure MWd/MTM	Discharge Date	
BNW 1-1	Solid	1.93	MTR	100,000	(Est)120,000	2-69	Stored at the reactor.
BNW 1-2	Solid	1.93	ETR	50,000	(Est) 70,000	2-69	Stored at the reactor.
BNW 1-3	Solid	1.96	MTR	100,000	(Est)150,000	2-69	Stored at the reactor.
BNW 1-4	Solid	1.96	MTR	50,000	71,000	6-68	Exam. completed at BNW.
BNW 1-5	Solid	2.00	MTR	100,000	(Est)160,000	2-69	Stored at the reactor.
BNW 1-6	Solid	2.00	MTR	50,000	75,200	10-68	Exam. completed at BNW.
BNW 1-7	Annular	1.93	MTR	50,000	<1,000		Lead tube failed. Exam. at BNW.
BNW 1-8	Annular	1.93	MTR	100,000	29,000	1-68	Failed. Exam. at BNW.
BNW 1-9	Annular	1.96	MTR	50,000	81,800	6-68	Exam. completed at LASL.
BNW 1-10	Annular	1.96	ETR	100,000	(Est) 55,000	(Est)2-70	Discharged 2-69 for interim exam. Recharged 5/69.
BNW 1-11	Annular	2.00	MTR	50,000	87,400	8-68	Exam. completed at LASL.
BNW 1-12	Annular	2.00	ETR	100,000	(Est) 55,000	(Est)2-70	Discharged 2-69 for interim exam. Recharged 5/69.

(1) Fuel
25% PuO_2 - 75% UO_2
Pellets 0.212 in. OD (0.052 in. ID for annular pellets)
Smeared density - 87.5% TD
Pellet density - solid pellet 93% TD, annular pellet 95% TD
Fuel column length 13.5 inch

Cladding
OD - 0.250 in.
Wall thickness - .016 in.
304 SS

(1) Postirradiation Examination of BNW-1 Fuel Pins

Pins BNW-1-4 and 6 were examined at BNW, and pins BNW-1-9 and -11 were examined at LASL. The bulk of the data, including ceramography, was reported last quarter for the BNW-1-4 and 6 pins, and all available data except ceramography was reported for BNW-1-9 and -11. Ceramography has now been completed on the latter at LASL and the film was sent to BNW for printing, laying up of mosaics, detailed review and analysis.

Specimens of BNW-1-4 and -6, and of BNW-1-7 and -8 that had been examined previously are being prepared for examination on the BNW shielded electron microprobe. Special attention will be given to the interaction between the fuel and cladding and to the stringers of metallic material that were observed in BNW-1-4 and 6 fuel. The samples also will be studied for segregation of U and Pu, for composition of second phase metallic inclusions and ingots, and for variations in inclusion composition at specific locations in the pin.

A specimen from BNW-1-7 was examined with the BNW shielded electron microprobe for redistribution of plutonium or uranium and fission product segregation. Since this is a low burnup specimen (1000 MWd/MTM), it will serve as a base case for comparison with higher burnup samples, BNW-1-8, 4 and 6. No gross redistribution was found in BNW-1-7, but some homogenization on a micro scale was observed in the sintered regions of the fuel. Particles of UO_2 and PuO_2 were encountered in non-restructured areas.

When preparing specimens for microprobe examination, it is mandatory that water be avoided because water reacts with some of the fission products, such as cesium, causing

erroneous results. This is of particular concern with the BNW-1-4 and -6 specimens because other sites[1,2] have reported high cesium concentrations at the grain boundaries near the inner surface of the stainless steel cladding. Since the usual ceramographic techniques at BNW employ water and dilute chromic acid on the final polishing wheels, alternate means of preparing the specimens were explored. Figure 74 compares the appearance of the specimen from BNW-1-4 at the edge of the fuel when polished with water and with kerosene on the wheels. Retention of the broad reaction layer is much better when kerosene is used. This reaction layer is only observed in fuel pins that have failed, which leads us to believe that it is due to NaK-fuel interaction. ANL[3] has reported similar reaction layers in failed fuel pins operating in sodium. Although unirradiated hypostoichiometric UO_2-PuO_2 is compatible with Na or NaK, it is possible that the chemical reactivity of the fuel is altered by the preferential accumulation of certain fission products at the edge of the fuel or by the migration of oxygen to the relatively cold regions of the fuel, or both. Oxygen migration would lead to a hyperstoichiometric fuel composition near the fuel surface which would tend to react with Na or NaK.

Although using kerosene instead of water on the grinding and polishing wheels is useful in retaining certain constituents, it can produce artifacts in the fuel structure. Figure 75 compares the edge region of a specimen from BNW-1-6 for the two preparation techniques. The ordinary method using water and chromic acid produces much the better structure at the edge of the fuel. Both methods produced similar results in the center of the fuel where restructuring had occurred and the amount of small porosity was considerably less. This exaggeration of the fine porosity in the edge regions is even more pronounced when Freon is used

Fuel Reaction Layer Clad

(a)

Fuel Reaction Layer Clad

(b)

FIGURE 74. Comparison of the Relative Retention of a Reaction Layer in BNW-1-4 (pin failed at ~19.5 kW/ft) When Polished with Water on the Wheels (a) and with Kerosene on the Wheels (b)

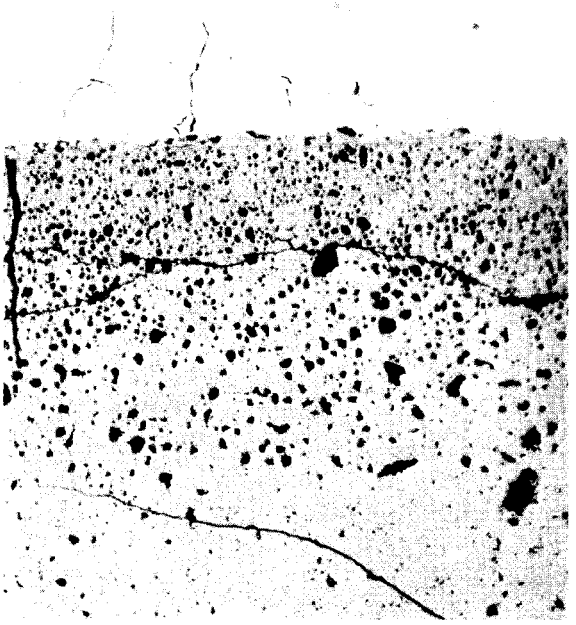

Cladding

Fuel

Water

Cladding

Fuel

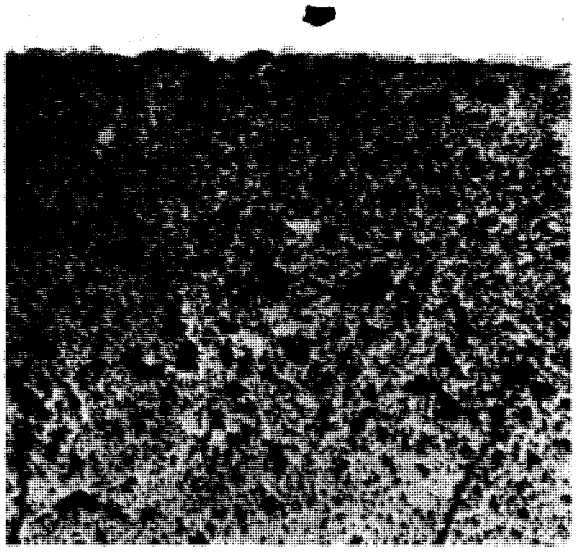

Kerosene

250X

FIGURE 75. Effect of Polishing Procedure on Fuel Structure in BNW-1-6 (75,000 MWd/MTM, 16 kW/ft)

as the coolant lubricant on the grinding and polishing wheels. Figure 76, the edge region of specimens from BNW-1-9 and 11, illustrates this point.

Detailed heat transfer calculations are underway for this series of BNW-1 capsules using the TIGER-V computer code. The burnup analysis, time in reactor and gamma scan data were used to obtain pin axial power profiles for input to TIGER-V. Detailed physics calculations are also being made to provide estimates of the radial power profiles which will be checked with burnup analyses made from radial micro-drill samples. This information will be assimilated with the ceramography and microprobe analyses to best define the nature and cause of the fuel-cladding interaction and to establish the conditions under which it occurs. Sections of the fuel pins will also be burst tested at approximately 900 ^{o}F to determine the consequences of this interaction on the strength and ductility of the cladding.

3. Out-of-Reactor Tests - M.K. Millhollen

a. 7-Pin Cluster Sodium Flow Test

Additional metallographic examination of a fuel pin cladding tube from the 7-pin cluster sodium flow test revealed no visible increase in surface damage to that section of the cladding located under the wire wrap. The cladding, which was exposed to flowing, 1060^{o}F sodium for 9000 hours, was metallographically examined to compare surface damage under the wire wrap to surface damage at other locations on the cladding. Three cross sections of the cladding were mounted and polished and the location of the wire wrap on each

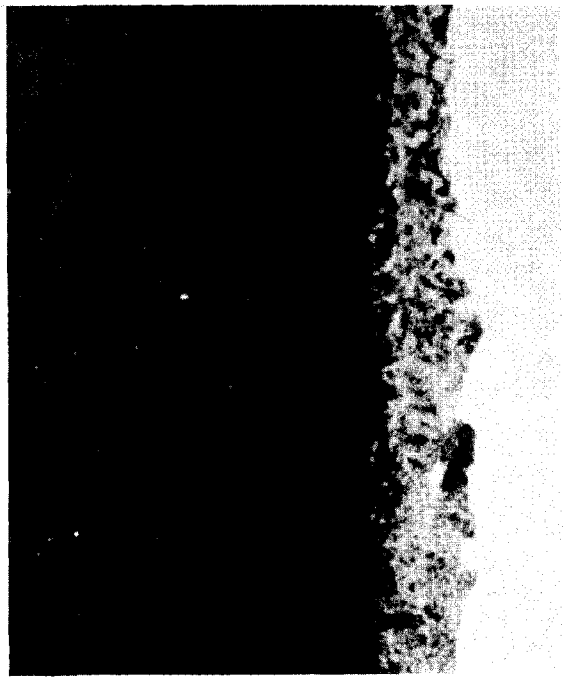

Fuel Clad

a) BNW-1-9

Fuel Clad

b) BNW-1-11

FIGURE 76. Specimens from BNW-1-9 (82,000 MWd/MTM, 16 kW/ft) and BNW-1-11 (87,000 MWd/MTM, 16 kW/ft). Prepared at LASL Using Freon TF on the Wheels

cross section carefully marked. These cross-sections were visually examined under a microscope and though slight surface damage was visible on all surfaces exposed to sodium, no particular damage oriented to the wire wrap location could be detected.

One typical cross section was photomicrographed. The section of cladding directly under the wire wrap is shown in Figure 77 . Three other surface locations are shown in Figures 78 , 79 and 80 . In each case the sample is shown both etched and unetched. Typical surface damage by penetration along grain boundaries is evident in all the photomicrographs, but there is no preferentially located damage area visible at the wire wrap location.

4. Fuel Performance Prediction and Analysis - R.D. Leggett, R.L. Fish K.R. Merckx, F.E. Bard

This work is directed toward development of empirical and theoretical formulations for predicting mixed oxide fuel behavior during irradiation.

a. Hybrid Computer Simulation

As a tool for development of fuel behavior models, a hybrid computer is being used. The main advantage of this type of computer is the output mode. A visual display of simulated fuel microstructural features is possible in addition to the normal tabular printout. A significant cost savings is also possible after initial set up. Instantaneous output is achieved with control of input variables accomplished by merely turning knobs.

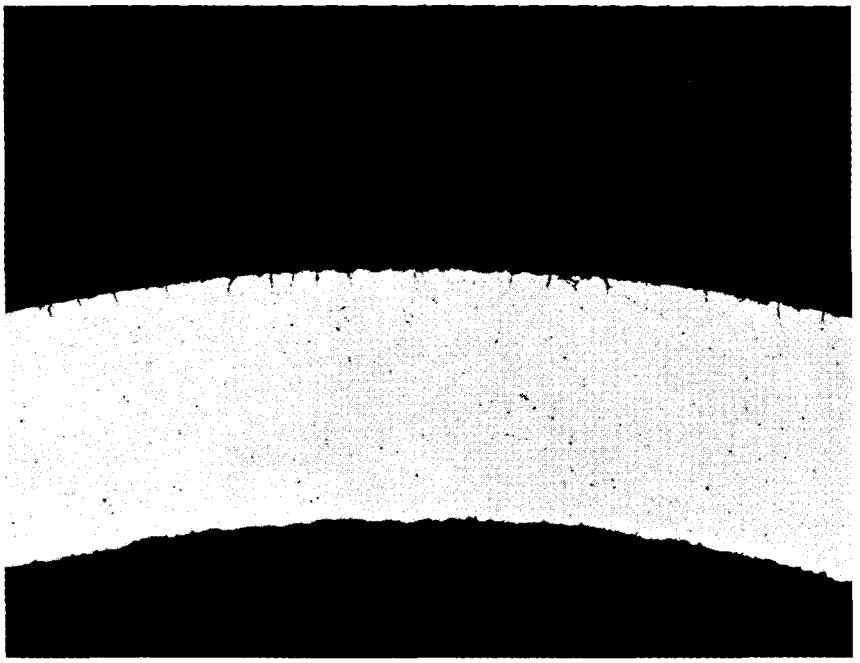

100X
As-polished

Neg 469165A

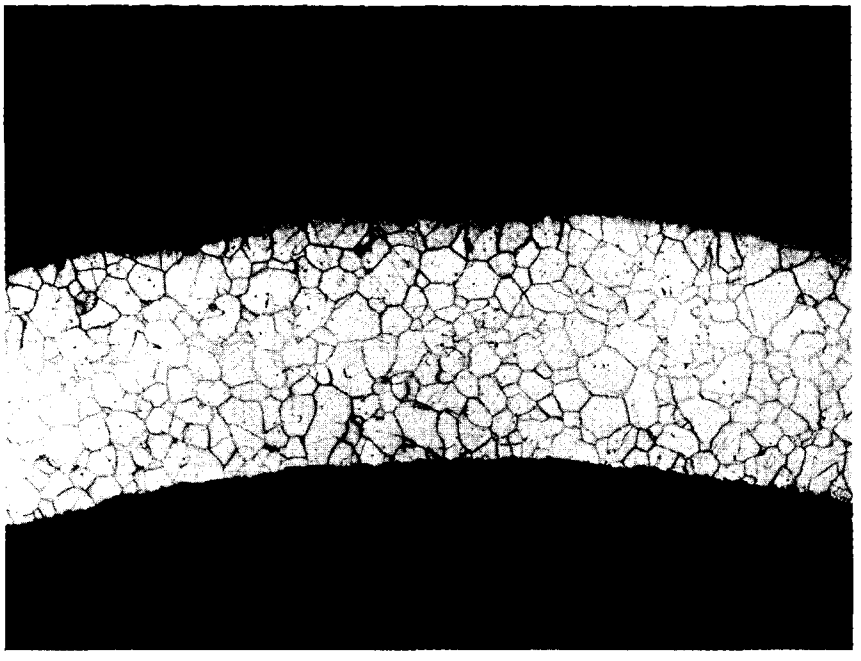

100X
Etched

Neg 469165B

FIGURE 77. Cladding Directly Under Wire Wrap After 9000 hr in Flowing 1060 °F Sodium

100X
As polished

Neg 469165C

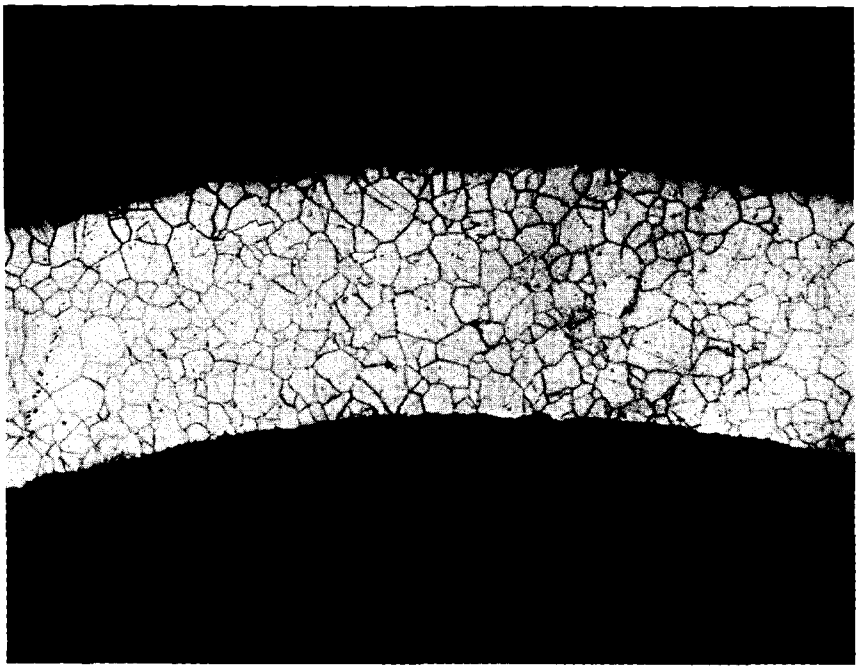

100X
Etched

Neg 469165D

FIGURE 78. First Random Cladding Surface Location After 9000 hr in Flowing 1060 °F Sodium

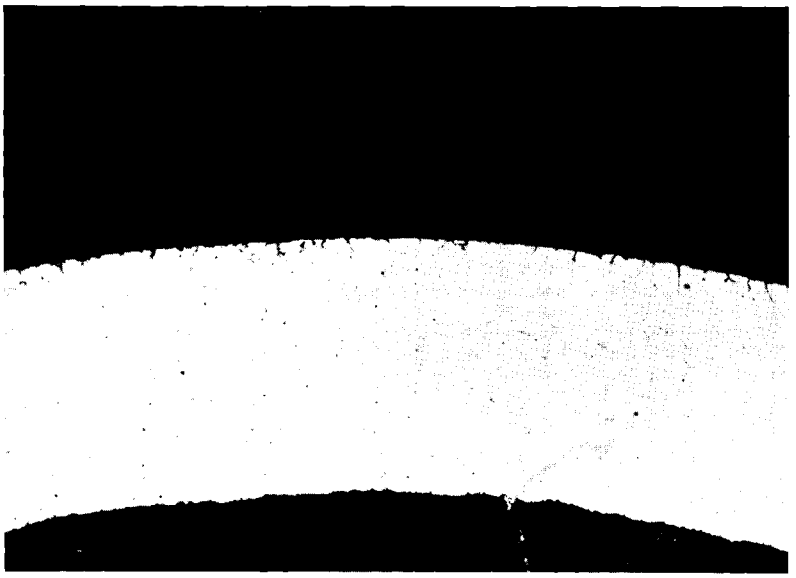

100X
As polished

Neg 46965E

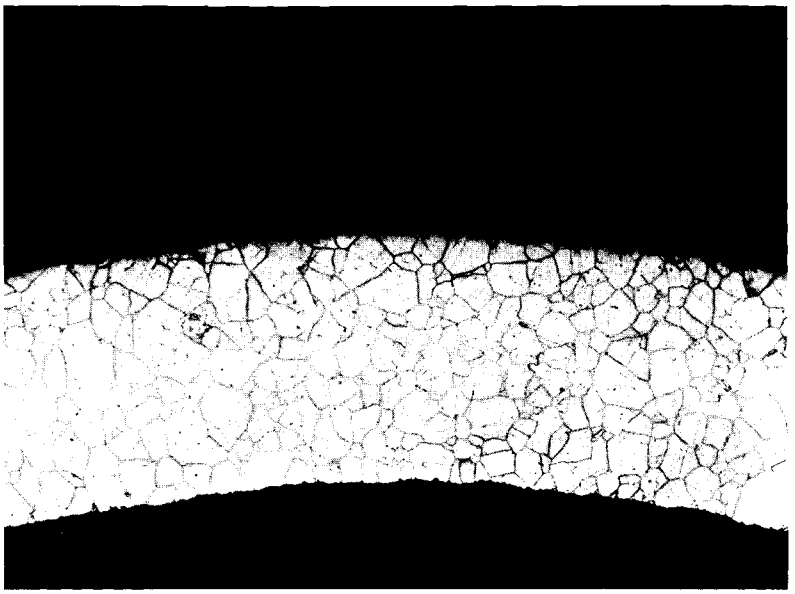

100X
As polished

Neg 46965F

FIGURE 79. Second Random Cladding Surface Location After 9000 hr in Flowing 1060 °F Sodium

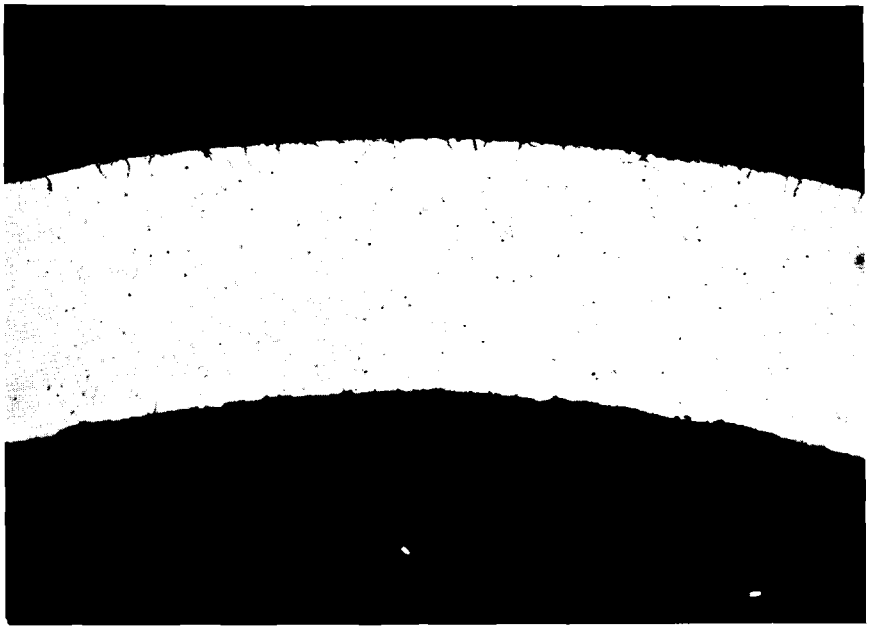

100X
As polished

Neg 469165G

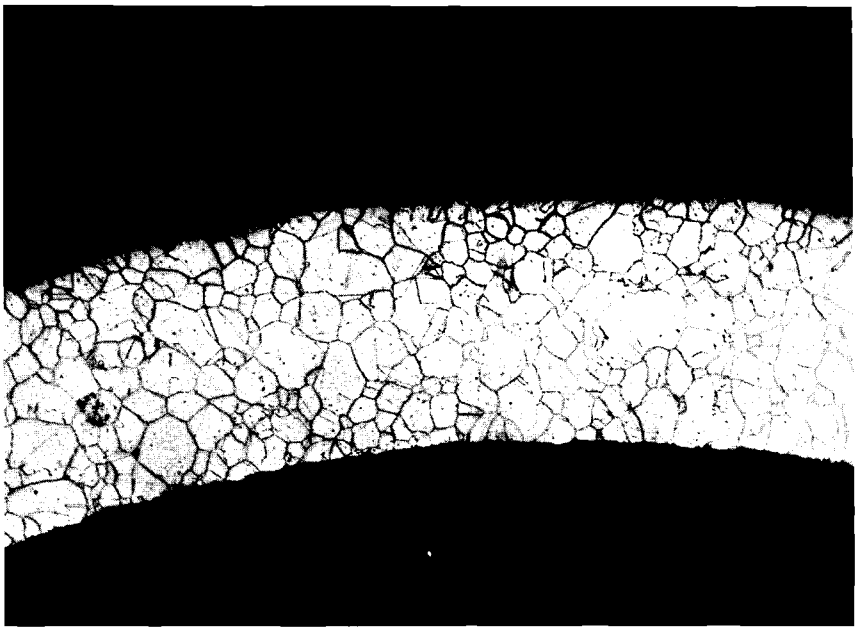

100X
Etched

Neg 469165H

FIGURE 80. Third Random Cladding Surface Location After 9000 hr in Flowing 1060 °F Sodium

The initial mathematical model being programmed into the hybrid is that of the program SINTER (a fuel restructuring code). A few variations will be incorporated into this program to allow for the analyses of either fast or thermal neutron flux irradiation tests. The program will provide both axial and radial fuel temperature profiles, central void size, and restructured fuel diameter. Variation of certain input parameters will allow correlation of the computer output with observed fuel microstructures. In this way determination can be made of the correct combination of input parameters for the particular pin fabrication and irradiation data. The dependence of these parameters on fuel burnup and other pertinent variables will be determined in refining of the model.

Additional refinements which may be made in the fuel behavior model include additional fuel restructuring zones (e.g., columnar and equiaxed grain growth zones), release and retention of fission gases and resultant pin pressures, fuel and cladding swelling, and transient effects. These refinements can come only with careful step by step correlation of computer output with fuel pin postirradiation examination results as they become available.

The initial case considered with hybrid-SINTER was the expected structure in typical FTR, 0.230 inch diameter, fuel pins operating at 6 kW/ft (low), 10 kW/ft (average), 14.5 kW/ft (peak) and 18.2 kW/ft (25% overpower), respectively. The output from the hybrid was displayed on a polychromatic C.R.T. to produce cross-sections color coded to correspond to the expected structure at a given fuel radius. A cross section at each of approximately 1600 axial segments per power level was generated, photographed and assembled on 16 mm film to provide a visual

simulation of the change in structure from one end of a pin to the other at the four power levels considered.

b. General Fuel Pin Data Analysis

A concerted effort was continued to assemble all available data involving irradiation experiments with stainless steel clad, oxide fuel pins in order to critically analyze the fuel pin performance. Our best estimates of the physical and mechanical properties of the fuel pin system, the reactor environment, and the pre- and postirradiation measurements are being combined with the best mathematical models available to develop a rationale of fuel pin performance. In addition to the data available from BNW experiments, data are being collected and analyzed from ANL, GE's PA-10, NUMEC, and DFR. We are emphasizing the detailed analysis of existing data in order to calibrate and refine the various mathematical models that exist, using the expertise available in materials, stress analysis, physics, reactor engineering and thermal hydraulics.

A general system for predicting failure rates and deformations of fuel pins is being developed. A schematic diagram showing the inter-relationship among components of this system is given in Figure 81. The computer programs being used as the components of this system are given in Table XXV. All of these programs are individually operable, but interlocking of them into a general system is still in development Within the last quarter the REM file (Radiation Effects on Materials) was searched for tensile data of irradiated 316 and 304 stainless steel.

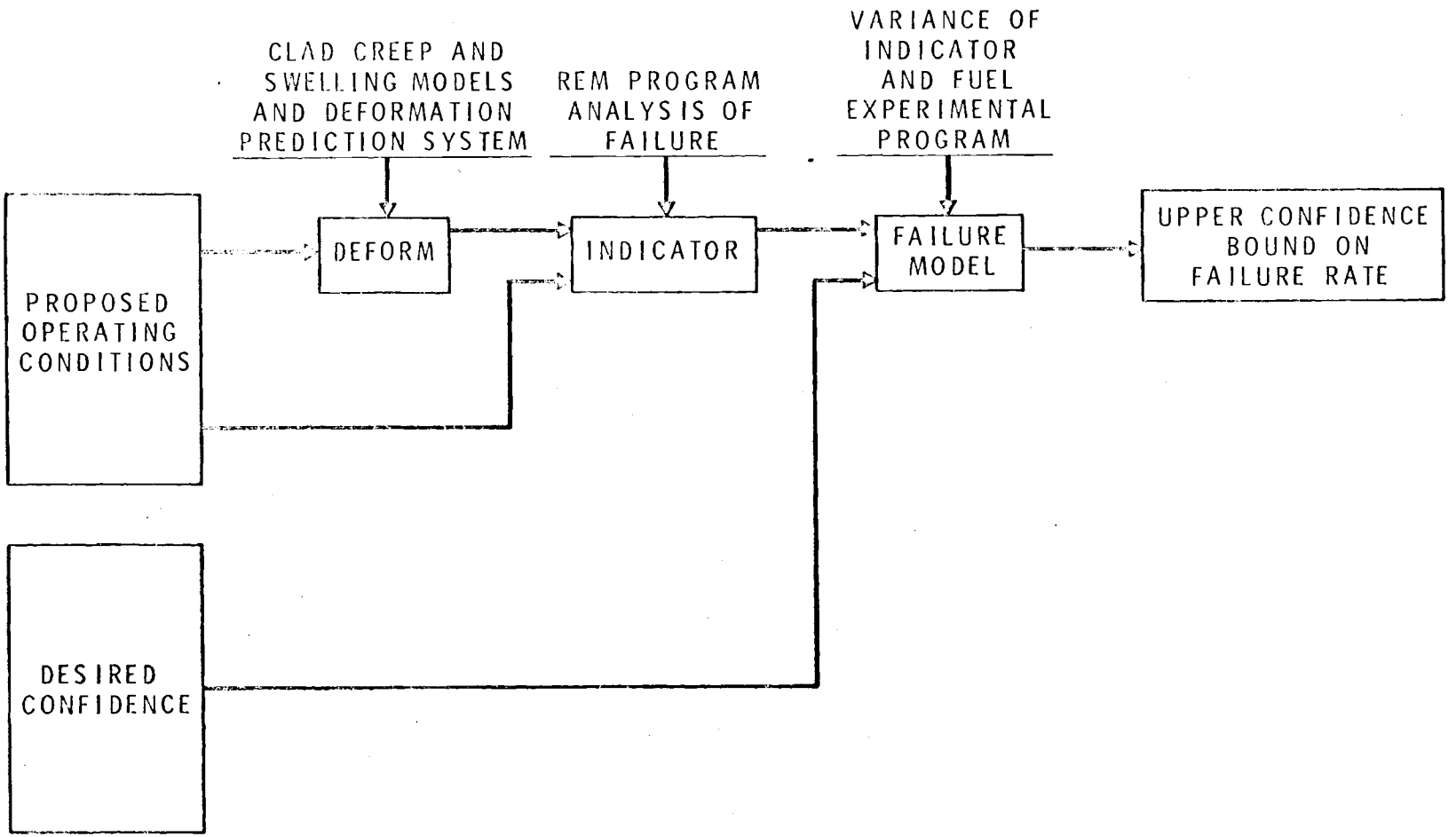

FIGURE 81. Model for Fuel-Clad Interaction Failure Mode

TABLE XXV. Programs Used in Fuel Pin Performance Estimation

PROGRAM	PURPOSE
SINTER	THERMAL ANALYSIS AND FUEL REDISTRIBUTION
DEFORM	MECHANICAL ANALYSIS FOR DEFORMATIONS
SIMPLEX	EVALUATION PROCEDURE FOR PARAMETERS IN DEFORM
R.E.M.	DATA FILE ON IRRADIATED CLADDING PROPERTIES
GEORGE	MULTIPLE REGRESSION ANALYSIS
WISER	PARAMETER EVALUATION FOR WEIBULL DISTRIBUTION

The GEORGE multiple regression analysis program was used to analyze this tensile data so that the shape of the failure surface could be established for the indicator function to be used in the failure model. (Reference Figure 81). The actual coefficients obtained from this analysis for linear and quadratic fits of the data are given in Table XXVI . A plot of these data for a fluence of 10^{22} nvt is given in Figure 82 . The data for the 316 stainless steel was for irradiations below fluence levels of 2×10^{21} and thus the extrapolation to the higher irradiation conditions may be unrealistic.

Most of the effort during the last quarter was directed toward establishing the interrelationships between the various programs in the Deformation Prediction System (Figure 83). DFR data had been previously analyzed with the DEFORM program and parameters in this steady-state model adjusted manually. The tie-in of the DEFORM program with the SIMPLEX program (automated search routine) and the addition of a model for estimating the total cladding deformations including both the clad swelling during an incubation period and a fuel-clad interaction after restructuring (Figure 84) was included within this prediction system. Estimates were made with this prediction system using eight experimental values for cladding deformation of DFR pins. Adjustment of the parameters with this system reduced the difference between predicted and measured values, but to obtain a minimum variance between the predicted and measured values, the adjustments of the parameters assumed unrealistic values. The parameters which are being adjusted by the deformational prediction system are given in Table XXVII. All of these parameters have physical significance and can be independently determined from material tests. Small variations

TABLE XXVI

REGRESSION ANALYSIS OF TENSILE FAILURE DATA

Material	b_o	b_1	b_2	b_3	b_4	b_5
Linear*						
304 SS	0.1129	-0.2208	-0.05925			
316 SS	0.2656	-0.2015	0.05710			
Quadratic**						
304 SS	0.1568	-0.1977	-0.01487	-0.4528	0.04107	0.02242
316 SS	0.2808	-0.2137	0.01940	-0.5344	-0.02574	-0.01439

* Linear fit: $E_f = b_o + b_1 \left(\frac{T}{1000} - 1\right) + b_2 \left(\log_{10} \frac{\phi t}{10^{22}}\right)$

** Quadratic fit: $E_f = b_o + b_1 \left(\frac{T}{1000} - 1\right) + b_2 \left(\log_{10} \frac{\phi t}{10^{22}}\right) + b_3 \left(\frac{T}{1000} - 1\right)^2 + b_4 \left(\frac{T}{1000} - 1\right)\left(\log_{10} \frac{\phi t}{10^{22}}\right) + b_5 \left(\log_{10} \frac{\phi t}{10^{22}}\right)^2$

Where: E_f - Strain of failure

T - Temperature, ^oK

ϕ - Flux, neutrons cm^{-2} sec^{-1}

t - Time, secs

b_o, b_1, b_2, b_3, b_4 and b_5 - constants

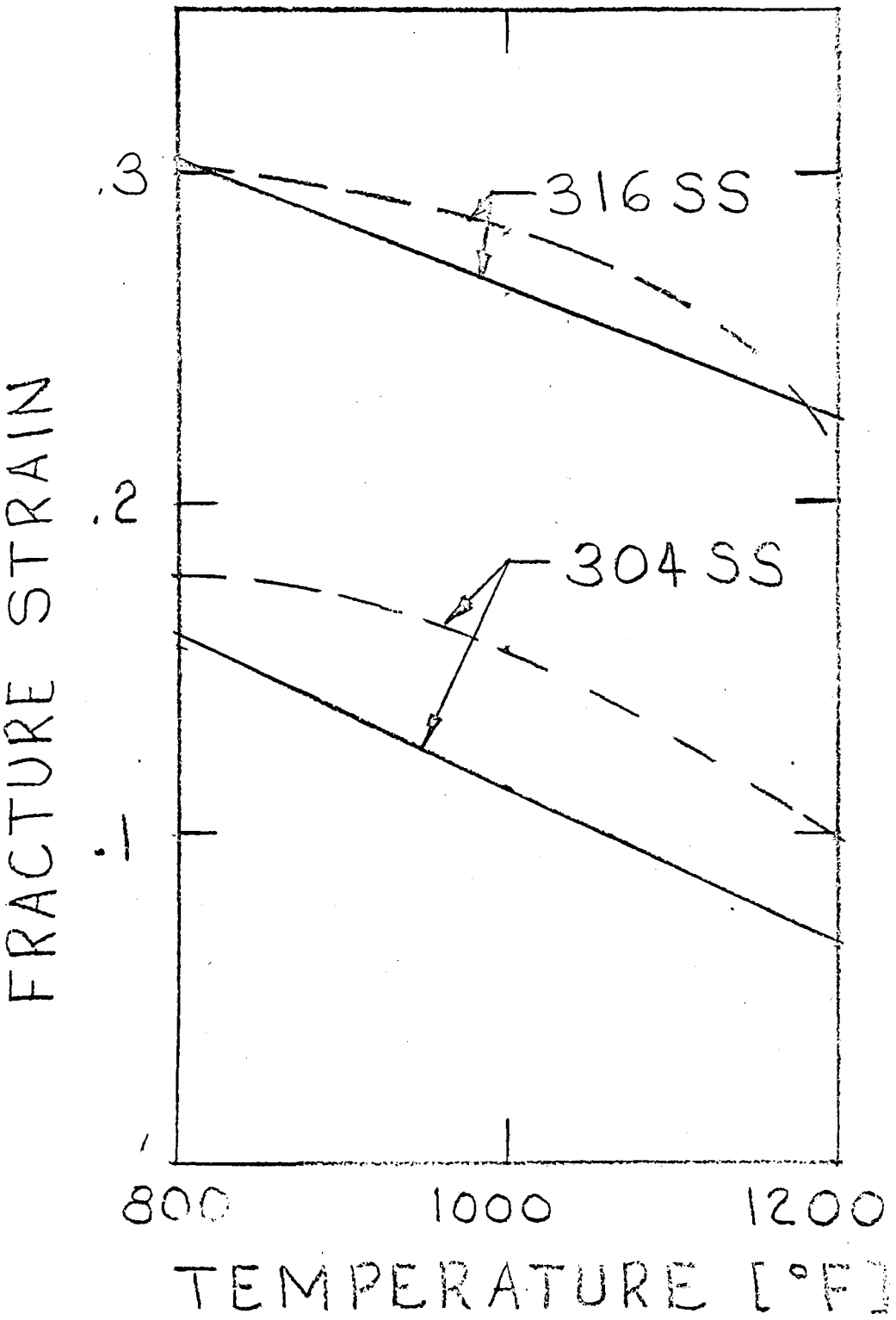

FIGURE 82. Predicted Fracture Behavior for $\phi t = 10^{22}$ from Regression Analysis

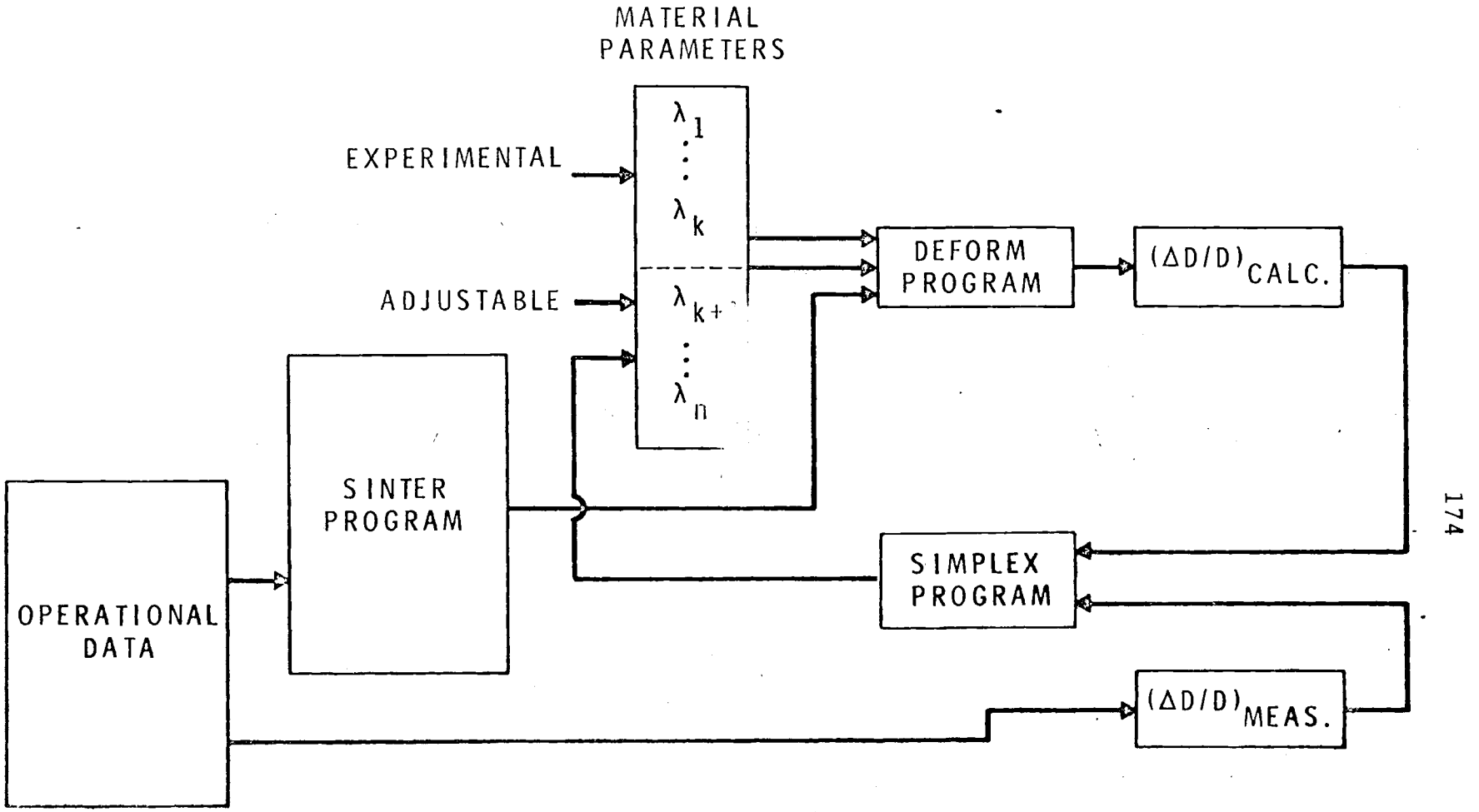

FIGURE 83. Deformation Prediction System

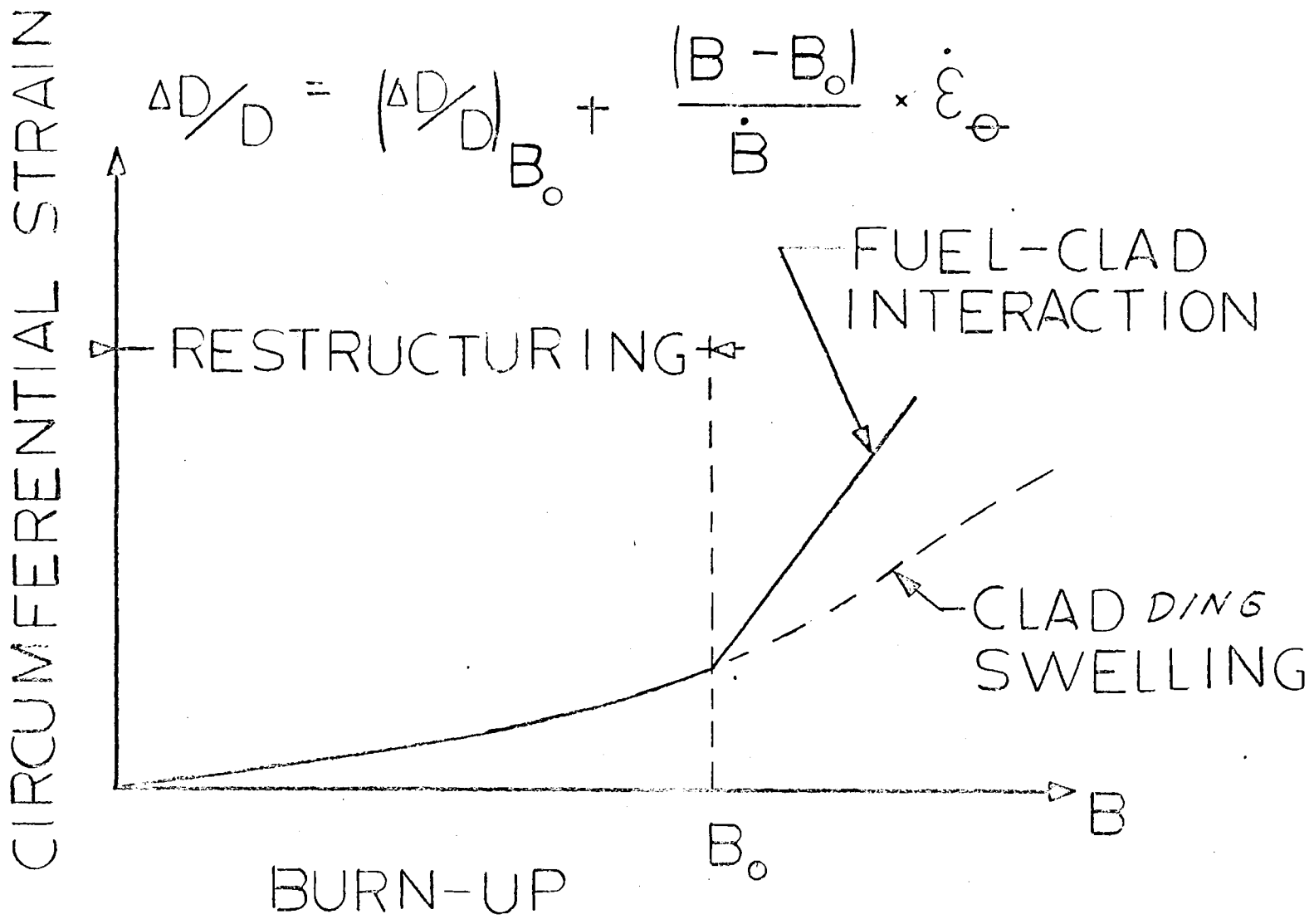

FIGURE 84. Prediction Relation Between Strain and Burnup for Stainless Steel Clad Mixed Oxide Fuel Pins

from reference values are expected, but if the prediction system requires major adjustments of the parameters, then reformulation of the models will be required. Data from GE fuel pin irradiations have recently been collected and punched into the card formats necessary to the prediction system. Analysis of this data is begun; thus, the values of the parameters which best fit this data are not yet available. Besides the SIMPLEX search routine, a gradient search technique is being programmed into the Deformation Prediction System since some runs using the DFR data did not efficiently search the parameter space.

1. RESTRUCTURING PERIOD
2. RADIATION FUEL CREEP
3. CLAD CREEP
4. FUEL SWELLING RATE
5. CLAD SWELLING
6. CLAD SWELLING RATE

E. OFFSITE FUEL PROGRAMS

G. A. Last

1. LMFBR Fuel Development

B. R. Hayward, F. M. Smith

Contract negotiations with all participating external sites (AI, GE. B&W, UNC, and NUMEC) for Phase II of the Analytical Chemistry Program were completed and the work started. The Phase II work is based on the needs shown by the Phase I analytical round and by discussions held at the individual sites. In Phase I, about 50% of the methods and standards were found to be satisfactory and 50% needed more development work. The following analyses are being made in Phase II:

Uranium assay	Carbon
Plutonium assay	Nitrogen
Spectrographic impurities	Density (geometric)
O/M ratio	H_2O content
Gas evolution	Homogeneity
Tungsten	

Agreement in the isotopic analyses was good among the labs during Phase I and is not repeated in Phase II. Tungsten was added for Phase II because of potential process contamination with this element. Analytical methods were recommended for Phase II, but it has been made clear that the use of these methods is not mandatory. However, if the individual sites use other methods, each site must show that the substitute procedures are equivalent to the recommended ones.

A special batch of 3000 UO_2-25 wt % PuO_2, designated as PL-10, was prepared by the Fuel Element Development Section for use in Phase II. Preliminary analyses show these pellets have uniform density, O/M, carbon content and spectrographic impurities. One hundred of these pellets were centerless ground for the Phase II density determination, and 200 more were specially processed to reduce the O/M value below the approximate 1.99 obtained on the parent batch. Portions of these different types of pellets were shipped to the individual sites per their needs.

To establish uniformity in the emission spectrographic impurity procedure, each laboratory received from LASL high purity PuO_2 to be used as matrix material for preparing working standards. Two sets of "primary" standards were also supplied for comparison with the working standards. These materials will contribute a great deal to the success of the spectrographic analysis.

To assure having mixed oxide samples with measurable amounts of chloride, fluoride, carbon and nitrogen, Los Alamis with BNW cooperation supplied the laboratories with powder spiked with these impurities. This was considered necessary since the ME-21 pelelts used in Phase I were quite pure, and in many cases the impurity contents were at or below the detection limits of many procedures used.

The Lyons method for determination of O/M was suggested for Phase II, and almost all the laboratories are familiar with it. This method involves oxidation above 750°C in air followed by reduction in dry He-6% H_2 at 700°C. The O/M is calculated from the accompanying weight change. Precision is generally good, but inconsistencies occur if whole pellets are used and not

allowed to come to equilibrium during the oxidation step. Some sites are evaluating at 800-900°C temperature range for more consistent results. Two other methods are being evaluated and compared with the Lyons method at LASL and BNW. One of these methods resorts to ultimate analysis for oxygen combined with uranium and plutonium assay. The other, developed by Chikalla at BNW, is a single step procedure where the sample is heated at 800°C for six hours in a flowing Ar-8% H_2 bas saturated with water at 0°C. From this work conclusions will be drawn and a standard method designated.

Homogeneity determination remains a problem. It will be evaluated in Phase II by making determinations of the chemical homogeneity by assay methods and of particle size by alpha-autoradiography. Restrictions on particle size in the homogeneity specifications have been based on discrete particles present in the pellet when, in actuality, the conditions in the sintered pellet are vastly more complex. In the sintered pellet interdiffusion has occurred between the PuO_2 and the UO_2, resulting in PuO_2 concentration gradients. Additional work is planned on homogeneity using electron microprobe scans of pellets and relating these to alpha autoradiographs.

The recommended gas evolution method involves measuring the gas evolved at 1600°C after trapping out the water. Although this method will be used in Phase II, some question exists as to whether or not all of the gas in the pellets is released at 1600°C. LASL has set up inert gas extrationn equipment capable of heating samples up to 2600°C to explore this problem.

Plutonium assay by controlled potential coulometry is well established, but americium may interfere with this analysis. It is not yet clear what role americium plays in the interference, but it is suspected

that it either is reduced with the Pu to bias results, or that it contributes to formation of a peroxide, giving erratic results. Work at Los Alamos is being directed to solving this problem.

Substantial progress was made at United Nuclear on the elimination of the need for pellet grinding. Between 90 and 100% of the pellets in large batches meet the present dimensional specifications in the as-sintered condition. The principal variables influencing pellet properties are original powder and press characteristics. Additional work is being started during this quarter at NUMEC and UNC on characterizing weight per length of both pellets and fuel pin columns. These data will be useful in establishing the desirability of modifying fuel specifications to eliminate specific and parallelism and end flatness requirements.

Two irradiation test subassemblies are being fabricated by NUMEC. These tests are based on FFTF conceptual pin design and development program requirements to test the performance of fuel pins prepared by a typical fuel supplier using FFTF specifications. The status of the test assemblies is as follows:

(a) The request for Approval in Principle was submitted to ANL, RDT, and BNW for comment. Minor comments by BNW were returned to NUMEC.

(b) Design drawings and the Engineering Test Plan were reviewed by BNW and returned with comments. Two primary design problems are being reviewed with RDT: (1) fuel pin smeared density and (2) pin design for an EBR-II power level of

either 50 or 62.5 MW. The design power level affects the enrichment of uranium used in the pins and the core lo-ation and/or relocation of the test subassembly.

(c) The Hazards Analysis Report is being prepared by NUMEC with assistance from BNW in areas of commonality with BNW irradiations.

(d) Fuel pin hardware stock and components are being sent to NUMEC as available. Three components have been sent to date. The cladding schedule is tight due to the extra cleaning required and evaluation of the NDT standards being used for defect detection.

(e) NUMEC has taken the mixed oxide preparation as far as possible prior to the final decision on pellet density and fuel enrichment.

2. Fuel Manufacturing Development Program

J. F. Williams

Responses to the request for proposal for the prequalification of LMFBR fuel suppliers were received from eight potential suppliers. Proposals were evaluated in depth and an evaluation report with recommendations was submitted to the AEC. Following a detailed review with both RDT and RL, approval was received to negotiate with the recommended suppliers and negotiations were begun.

The statement of work was reviewed and revised to include variables data for quality assurance purposes. Relaxation of some

dimensional tolerances was also incorporated in the revised statement of work.

All materials to be supplied by BNW are on hand except the end plug stock and plenum springs. The end plug stock was received but was improperly annealed. This was returned to the supplier to be annealed per the original specification. The plenum springs were ordered made from Inconel 750 X per the specification but the supplier has been unable to perform. An emergency order was placed for 300 series stainless springs for prequalification. Cladding tubes are currently being cut to length and a cleaning process is being activated to remove an unidentified foreign material discovered during inspection. Other components are being inspected and packaged.

DISTRIBUTION

I. Deliver 2 review copies to FFTF TPO, 703 Building.

II. Deliver 114 copies to FFTF DMSS, 703 Building for Distribution as follows:

No. of Copies	
12	U.S. Atomic Energy Commission Division of Reactor Dev & Tech Washington, D.C. 20545 Asst Director for Project Mgmt., A Giambusso FFTF project Office, JJ Morabito Asst Director for Plant Engineering, MA Rosen Asst Director for Engineering Standards, JW Crawford Asst Director for Reactor Engineering (5), EE Kintner, CE Weber, DK Magnus, AC Millunzi, EA Wright Asst Director for Reactor Technology (3), EE Sinclair, JM Simmons, GW Cunningham Asst Director for Nuclear Safety, AJ Pressesky
2	AEC Richland Operations Office FFTF Program JM Shivley
3	AEC Site Representatives - BNW PG Holsted
1	LMFBR Program Office
2	Liquid Metal Information Center JJ Droher
1	Los Alamos Scientific Laboratory University of California RD Baker
2	Bechtel Corporation JJ Teachnor DH Weiss (Richland)

No. of Copies

2 Westinghouse Electric Corporation

JCR Kelley
RS Strzelecki (Richland)

89 BNW/FFTF On Site

ER Astley
FJ Arrotta
JC Cochran
DL Condotta
EA Evans
PL Hofmann
FC Gronemeyer
WB McDonald
JC McMahon
WE Roake (60)
RJ Squires
RC Walker
Tech Files (5)
FFTF Files (2)
BNW-Tech Publications
BNW-Tech Information (5)
FFTF-TPO-703 (3)
Legal-703
Legal-ROB